DEVELOPMENT AND MECHANICAL CHARACTERIZATION OF ANTI-BLAST SANDWICH COMPOSITES FOR EXPLOSIVE EFFECT

A Thesis Submitted to
the Graduate School of Engineering and Sciences of
İzmir Institute of Technology
in Partial Fulfillment of the Requirements for the Degree of

DOCTOR OF PHILOSOPHY

in Mechanical Engineering

by
Suat Bahar BAŞTÜRK

December 2011
İZMİR

We approve the thesis of **Suat Bahar BAŞTÜRK**

_____
Prof. Dr. Metin TANOĞLU
Supervisor

_____
Prof. Dr. Ramazan KARAKUZU
Committee Member

_____
Assist. Prof. Dr. H. Seçil ARTEM
Committee Member

_____
Assist. Prof. Dr. Engin AKTAŞ
Committee Member

_____
Assist. Prof. Dr. Selçuk SAATÇİ
Committee Member

26 December 2011

_____   _____
Prof.Dr. Metin TANOĞLU   **Prof.Dr. R. Tuğrul SENGER**
Head of the Department of   Dean of the Graduate School of
Mechanical Engineering   Engineering and Sciences

ACKNOWLEDGEMENTS

ABSTRACT

DEVELOPMENT AND MECHANICAL CHARACTERIZATION OF ANTI-BLAST SANDWICH COMPOSITES FOR EXPLOSIVE EFFECT

Composite sandwich structures have high potential to be used in anti-blast armour systems due to their lightweight and resistance to explosive effects. This study focuses on the production and mechanical characterization of sandwich structures with aluminium (Al) foams of various thicknesses in conjunction with skins composed of Al/GFPP fibre/metal laminates. The bonding between the components of the sandwich was achieved by various surface modification techniques such as silane surface treatment, polypropylene (PP) adhesive film addition and their combination. The Al sheet/Al foam sandwiches were also prepared to investigate the effect of GFPP addition on the performance of sandwich structures. The energy absorption capacities together with compressive and flexural behaviour of both Al foams and FML/Al foam sandwiches were evaluated by flatwise compression and three point bending tests. The samples with higher elastic modulus usually exhibited higher collapse strength for each thickness set of foam and foam based sandwiches. Also, the core thickness increase led to the increase of overall flexural collapse load and GFPP presence promoted the strength of the sandwiches and dissipated energy values. In order to investigate the blast response of the sandwich panels, the quasi-static sandwich panel analysis was related to dynamic blast loadings. For this purpose, the sandwich composites were subjected to compression loading with a specially designed loading fixture and the corresponding test method is called as "simulated blast test". The sandwiches were assumed as single degree of freedom mass-spring systems to include the dynamic effect. The peak deflections and survivability of the panels under blast loading were predicted based on the formulations reported in the literature. To evaluate the blast response of the monolithic materials, composites and sandwich panels, blast testing was performed using specially designed blast test frame system and 0.5 to 6 kg TNT explosives. Test results revealed that composites such as GFPP exhibited successful results against blast explosions.

ÖZET

PATLAMA ETKİSİNE KARŞI ANTİ-BLAST SANDVİÇ KOMPOZİTLERİN GELİŞTİRİLMESİ VE MEKANİK KARAKTERİZASYONU

Kompozit sandviç yapılar düşük ağırlıkları ve patlama etkisine karşı yüksek dirençlerinden dolayı anti-blast zırh sistemlerde kullanılmak için yüksek potansiyele sahiptir. Bu çalışma, cam elyaf takviyeli polipropilen (CETPP) kompozit ve aluminyum (Al) levhadan oluşan fiber/metal lamina (FML) sistemlere farklı kalınlıklardaki aluminyum köpük malzeme entegre edilmesiyle hazırlanan sandviç panellerin üretim ve mekanik karakterizasyonuna odaklanmıştır. Bahsedilen laminant yapı bileşenleri arasındaki bağlanma, amino bazlı silane bağlayıcı ajan ve/veya polipropilen (PP) bazlı film eklenmesi ile sağlanmıştır. Al levha/Al köpük sandviç örnekler de CETPP kompozitin sandviç yapıdaki etkisini incelemek amacıyla hazırlanmıştır. Monolitik Al köpüklerin ve tabakalı sandviç malzemelerin enerji absorpsiyon karakteristikleri ile beraber basma ve eğme davranışları, yüzeysel basma testi ve üç nokta eğme testi ile incelenmiştir. Basma testi sonuçlarına göre, her köpük kalınlığı için en yüksek elastik modül değerine sahip örnek genellikle en yüksek çökme mukavemet değerini göstermiştir. Ara tabaka kalınlığı arttıkça, hibrid sistemin taşıdığı yük miktarı artmış ve CETPP varlığı da hem eğme mukavemeti hem de enerji absorpsiyon kapasitesi açısından pozitif bir etki göstermiştir. Sandviç malzemelerin patlama yükü altındaki davranışlarının anlaşılması kuasi-statik sandviç panel analizi ve dinamik patlama yüklemeleriyle ilişkilendirilmiştir. Bu amaçla, sandviç kompozitler özel olarak tasarlanmış bir yükleme fikstürü ile basma yüküne tabi tutulmuş ve bahsedilen bu test yöntemi "simüle edilmiş patlama testi" olarak adlandırılmıştır. Dinamik etkiyi ilave etmek için sistemdeki numuneler tek serbestlik dereceli kütle-yay sistemi gibi kabul edilmiştir. Literatürdeki mevcut formüller kullanılarak sandviç panellerin maksimum deformasyon değerleri tahmin edilmiştir. Monolitik metallerin, kompozit malzemelerin ve sandviç panellerin patlama etkisi karşısında tepkisini açığa çıkarmak için, özel olarak tasarlanmış test çerçeve sistemleri ve 0.5 ile 6 kg TNT patlaması ile patlama testleri gerçekleştirilmiştir. Test sonuçları özellikle CETPP tip kompozitlerin patlama etkisi karşısında oldukça başarılı sonuçlar verdiğini göstermiştir.

TABLE OF CONTENTS

LIST OF FIGURES

LIST OF TABLES

CHAPTER 1

INTRODUCTION

1.1. Background

In the recent days, the strength of structures under blast loading has vital importance due to the presence of explosions and terrorist attacks. Drastic damages take place where the explosions produces high pressure and loading rate such as structural failure, progressive collapse and extensive plastic deformation as shown in Figure 1.1 (Zhu, 2008).

(a)

(b)

Figure 1.1. Structural damage type examples: (a) HSBC explosion, Istanbul (Source: AP, 2003) (b) a military vehicle was subjected to blast attack, Hakkari (Source: National Ministry of Defence, 2011).

In case of dynamic loading, huge amount of kinetic energy arises during the large plastic deformation and leads to the failure of structures. Many energy absorbers made of ductile materials are improved and utilized for the anti-blast applications such as automotive, aero-space and military industries. Apart from traditional structures which subjected to small elastic deformation, energy absorbers have to maintain their stability under intense blast loads. Thus, their deformation and failure include large geometry changes, strain-hardening effects, strain-rate effects and various deformation mechanisms such as bending and stretching. The performance of structural components under blast loading has attracted great interest by many researchers. Traditionally, ductile metals like low carbon steel and aluminum (Al) alloys are commonly employed materials as energy absorbers (Zhu, 2008). There are several studies related with the response of monolithic materials under impulsive loads. However, the application of hybrid material systems as blast resistant structures opens a new perspective in the academic area. As it is known that, the integration of separate components using an appropriate technique has critical importance to manufacture the composite structures. Various material systems have been experienced by the researchers to obtain the best configuration for the performance increase under blast loading conditions. Due to the light weight and energy absorption capabilities of fiber-metal laminates (FML) containing thermoplastic/thermoset composite layers offers great potential in many applications such as automotive industry, anti-blast armor systems, aerospace transportation industry and etc. (Cantwell, 2000). ARALL$^®$ (aramid fiber reinforced epoxy with Al laminates) and GLARE$^®$ (glass fiber reinforced epoxy with Al sheets) laminates are first generation FML systems and they showed highly better impact resistance as compared to monolithic aluminum plates and carbon/epoxy composites (Vlot, 1996). Fat et al. (2003) investigated the ballistic limit and energy absorption capacity of GLARE$^®$ laminates with different thickneeses and revealed different absorption mechanisms after impact loading. McCharty et al. (2004) examined the impact response of aluminum/glass fiber reinforced epoxy FMLs and carried out high strain rate tests. The authors revealed the positive strain rate sensitivity. In spite of the advantages of thermoset based FMLs, such as excellent fatigue and impact properties, some disadvantages of these systems limited their application. Unlike from thermoset type FML systems, thermoplastic based FML hybrid structures showed low interlaminar fracture resistance and low processing cycles. Specifically, polypropylene based FMLs have been developed and tested under different static and dynamic conditions. Langdon

et al. (2005) revealed the front and back face damage characteristics of FML systems with various thicknesses. They found that the magnitude of impulse (produced from the ballistic pendulum set up) significantly affected the damage shapes and zones of the test structures. Matrix cracking, delamination/debonding and perforation of panels increased the energy absorption levels of the FMLs. Based on the test results, bending and stretching of glass fibers also provided energy absorption during dynamic loading.

The foams are widely used in different applications including marine and automotive industry. In recent years, due to their high energy absorption capability and light weight, these cellular structures have been used as structural components in the anti-blast material systems.

Numerous studies were carried out in terms of the quasi-static mechanical characterization of foams and foam based sandwiches. However, the combination of metallic foams and FML systems has created a novel research area. The sandwich panels manufactured using thermoplastic fiber/metal laminate (FML) skins and an aluminum foam core was considered as an alternative configuration for the blast applications. Cantwell and colleagues (2007) studied about the applications of aluminum foam sandwiches with fiber-metal laminates. Both quasi-static and dynamical behavior of GFPP/Al foam sandwich panels were investigated and characterized. Reyes et al. (2007) examined the flexural and low velocity impact behavior of the FML reinforced sandwich panels with aluminum foam core. It was found that the failure mechanisms of the sandwich components contributed to the energy absorption capability of the system and the proposed energy balance model explained in their study was in good agreement with the experimental results. Zhu et al. (2008) investigated the structural performance of sandwich panels under blast loading. Based on his study, the samples with thicker skins and high density core exhibited localizded inelastic front face deformation while thinner skin and sparse core displayed lower deformation. Pitting and indenting were the failure modes observed in the central parts of the panels and dome shaped deformation was also seen on the back face of the sandwich panels.

1.2. Objectives

The objective of this study is to contribute to the development of FML/Al foam sandwich structures for anti-blast applications. The FML system consists of glass

fiber/PP fabrics (GFPP) and aluminum (Al) metal sheet act as the skin component and closed cell Al foams with various thicknesses act as core in the sandwich panels. The integration of separate constituents using an appropriate technique has vital importance to manufacture the hybrid systems. In the present study, another objective is manufacturing of the sandwich structures with various surface modification techniques and examining their quasi-static mechanical properties in depth. Prediction of the blast response of the prepared sandwich systems by applying "simulated blast tests" is another objective. In this test, compressive quasi-static loading was carried out and the sandwiches were assumed as single degree of freedom mass-spring systems in order to include the dynamic effect. The blast performances of hybrid material systems was predicted based on the modified formulations presented by Baker et al. (1983) and Andrews et al. (2009). Evaluation of the blast response of the monolithic and sandwich composites is also among the aim of the work.

The specific objectives of this work are as follows;

- Preparation of FML/Al foam sandwich structures with various integration techniques such as silane surface modification, PP based film introduction and combination of silane treatment with PP based film addition.
- Determination of the interfacial bonding properties of FML systems.
- Determination of the energy absorption capacities together with compressive and flexural behavior of FML/Al foam sandwiches.
- Prediction of the blast response of prepared sandwich panels by the establishment of special test apparatus that loads the sandwiches by compressive forces.
- Evaluation and comparison of various materials´ (monolithic metals, composite structures, FML systems and sandwich panels) blast performances under TNT explosions.

1.3. Dissertation Outline

The brief background information given in this present chapter implies the importance of hybrid materials under blast/impact loading conditions. Both interfacial and mechanical properties of these systems should be taken into consideration to increase their performance under dynamic effects. Relevant literature regarding Al

foams, FMLs and Al foam based sandwich composites as well as surface pretreatment techniques are presented in Chapter 2.

In Chapter 3, the blast characteristics of materials against blast loading were investigated and compared. The literature review on the response of monolithic materials, composite structures, FML systems and sandwich panels was provided within details.

The materials used in this thesis were introduced and the integration techniques for the preparation of hybrid systems were explained in depth in Chapter 4. The mechanical characterization of Al foams, Al sheet and GFPP composite was carried out. Lap shear and peel test application to the Al/GFPP system was described. Flexural and compression test parameters were identified for the Al foam core sandwich structures. The design of test apparatus under real air blast loading was introduced and the relevant materials were given in the mentioned chapter. Finally, the principles of simulated blast was described and establishment of its test apparatus was presented.

In Chapter 5, results of the tests explained in the experimental section were reported. The mechanical properties of sandwich panels manufactured with various integration techniques were determined and compared. Also, both simulated blast test and real air blast test results were presented with the deformation images of sandwich panels.

Finally in Chapter 6, conclusions of these studies and overall outlook are given.

1.4. Unique Contributions

This dissertation aims to develop sandwich composites including fiber/metal laminate (FML) face-sheet and metallic foam core for anti-blast applications. Glass fiber reinforced polypropylene composite (GFPP) and aluminum (Al) metal layer constituted the FML component and integrated with aluminum foam of various thicknesses. The bonding among the sandwich components were achieved by various surface modification techniques. To our knowledge, there is a very limited work in the literature on the fabrication and testing of described material system. In addition, this study is the first in the literature on the preparation of FML/Al foam sandwich panels bonded with various surface modification approaches (silane treatment and combination of silane treatment with PP based film addition). Although the compressive and energy

absorption behavior of Al foams are extensively examined in the literature, the studies for the investigation of the compressive mechanical behavior and energy absorption characteristics of the studied sandwich systems are very limited. This work has analyzed the energy absorption capacities of sandwich structures together with flexural and compression properties. This has original contributions to the literature.

In this thesis, the "simulated blast test" was performed in order to evaluate the blast response of sandwich panels. This test method relates the quasi-static sandwich panel analysis with dynamic blast loading and very few studies are present in the literature. The specially designed loading fixture was manufactured for the application of simulated blast test and the sandwiches bonded with PP based film addition were tested. The new findings based on this approach will be original contribution to the literature. In addition, there is very limited results on the blast response of composites and their constituents in the literature. The real blast explosion test results are new findings that will contribute to this area.

CHAPTER 2

FIBER/METAL LAMINATE SYSTEMS AND SANDWICH COMPOSITE STRUCTURES

2.1. Fiber/Metal Laminate (FML) Systems

Recently, there has been a growing interest for the fabrication of fiber/metal laminate (FMLs) systems which have great offeringss to various application areas such as automative, electronics and aerospace industries (Ryes, 2007). The combination of metals and polymer composites constitute the FMLs and their synergistic properties provide superiorities over traditional materials. Thin layers of aluminum alloys (Al) constitute the hybrid system with thermoset or thermoplastic type of composites as seen in Figure 2.1. Excellent impact resistance, high fatigue life and damage tolerance capacities with the improved strength and stiffness properties are the main advantages of FMLs compared to the other material systems. Particularly, because of the crack briding mechanisms developed by the fibers, both fatigue life and residual strength of cracked FMLs are greater than bulk metals.

The first generation of fiber/metal laminate systems were composed of epoxy thermoset matrices with glass fibers (glass reinforced Al laminates-GLARE[®]) or aramid fibers (aramid reinforced Al laminates-ARALL[®]). Krishnakumar focused on the mechanical properties of the ARALL hybrid system and he found that the strength of FMLs showed better performance compared to the monolithic Al alloy (Compston, 2001). Asundi and Choi et al. (1997) evaluated the similar parameters for the same FMLs and provided general information about these novel hybrid materials. Vlot et al. (2000) investigated the quasi-static and impact properties of ARALL and GLARE systems with their components and according to the test results, the FMLs showed smaller post-impact zone compared to the polymer composites. Vogelesang and Vlot (2000) concantrated on the tension-tension fatigue performance of GLARE systems and they found that the crack growth rates of FMLs were between one tenth and one hundredth of those measured in a monolithic aluminum.

alternating layers of metal

fibre-reinforced polymer (FRP) composite
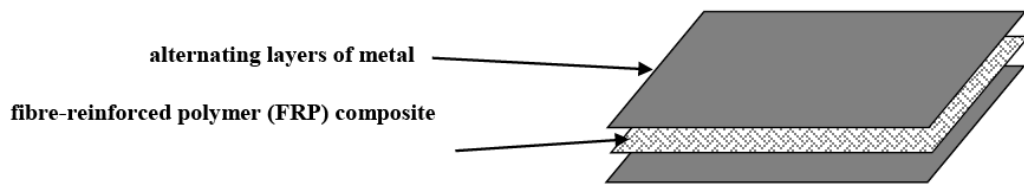
Figure 2.1. Schematic representation of FML system

Thermosetting based FMLs were quite brittle and they required longer processing times which was not cost effective. Therefore, the thermoplastic based composite materials have been developed which offer relatively shorter processing times, high interfacial fracture toughness and post-impact properties (Compston, 2001). Kulkarni et al. (2008) investigated the mechanical behaviors of long fiber thermoplastic (LFT) composite and Al alloy hybrid system. The nylon was used as the thermoplastic component and the glass fiber acted as the reinforcement phase of the composite material. The elastic modulus of LFT/Al system was found to be lower and ultimate tensile strength was higher than monolithic Al metal, as expected. Delamination among the plies, fiber pull-out and inelastic deformation of metallic layer were the major failure mechanisms observed during quasi-static testis. The flexural test results showed that the failure started with the cracking of metallic layer on the tensile side without any ply delamination. Low velocity impact test revealed the impact resistance of the structures and specific perforation energy value of the LFT/Al system was considerably higher than the LFT composite. The increase of perforation energy was attributed to the formation of different failure types such as bending and shear fracture of aluminum plies, ply delaminations and fracture of composite. In 2004, Cortes and Cantwell attempted to use carbon fiber-reinforced polyether-etherketone (PEEK) and titanium alloy as the constituents of FMLs and they investigated the tensile and fatigue properties this hybrid system. The mechanical properties of PEEK/Ti system could be calculated by using rule of mixtures approach. They also showed that the fatigue life performance of notched unidirectional FMLs were 50 times greater than the notched monolithic titanium alloy. In the light of experimental results, the delamination was observed more commonly in FMLs consisted of thick composite layers than in laminates including thin layers. Polyropylene (PP) and polyamide thermoplastics were implemented as the components of fiber/metal laminates and according to the experimental results, PP showed high toughness and polyamide displayed excellent high temperature

performance (Carillo and Cantwell, 2009). A research group with the leadership of Cantwell in the Liverpool University published a number of papers related with the application, production and testing of FML sytems. Reyes and Cantwell focused on the mechanical properties of FMLs based on glass fiber reinforced polypropylene (GFPP) and Al alloy. The surface treatment of Al layer with amorphous chromate coating increased the interfacial adhesion while the introduction of comercial maleic anhydride modified polypopylene (PP-g-MA) provided integration between the components of FML system. The fracture energy values of the FMLs were significantly high over a broad range of loading rates according to the single cantilever beam tests. Tension tests of FMLs showed that the volume fraction of composites considerably affected the tensile properites of the hybrid materials. Low velocity impact tests showed that the FMLs with three different stacking sequence exhibited perfect resistance to dynamic loading. The microscopical images revealed the damaged zones after impact test. It was observed that the incident energy was absorbed with plastic deformation in the Al layer while the localised microcracking developed in the composite plies (Reyes and Cantwell, 2000). Very similar study was conducted by Carrillo and Cantweel in 2009 with self reinforced polypropylene (SRPP) composite and Al alloy. The SRPP included the PP based fiber and PP resin matrix and the interlaminar fracture toughness of the FML was lower than the composite-metal adhesive due to the low consolidation pressure. Tensile properties of SRPP/Al layer system showed better performance compared to the plain thermoplastic composite and the FML plates subjected to impact loading showed high energy absorption. The impact damage formed as thinning in the Al layer and fracture in the composite plies. In addition, the high velocity impact properties of FMLs consisted of SRPP/Al alloy was investigated by Abdullah and Cantwell in 2008. Two types of Al alloys, 2024-O and 2024-T3, were used and it was observed that the former type exhibited superior perforation resistance with the same polymer composite. More than two layers of Al alloy were placed among the composites (multi-layered material systems) and their impact performances were also evaluated. According to the experimental results, the specific perforation energy values of multi-layered FML system based on SRPP/Al alloy were higher than Kevlar based laminates. Ductile tearing, delamination and fiber failure were the failure mechanisms seen within the composite plies while the plastic deformation, thinning and shear fracture observed as the damage types in the Al layer (Abdullah and Cantwell, 2008). Langdon et al. (2006) concenrated on the failure response of FML panels exposed to

localised blast tests. Glass fiber reinforced polypropylene (GFPP) composite and Al alloy were implemented as the components of FML panels and the blast tests were conducted to these panels with different constituent configurations. It was observed that the GFPP increase decreased the mid-point displacement value of FML sample. For the similar impulses, the panels with higher composite content resulted in larger debonding regions for both back and front faces. The thicker FML panels stiffness was higher with small peak displacements for the same impulse magnitude. However, the increase of impulse led to the back face debonding for all of the samples. Extensive plastic deformations due to the multiple debonding and fibre stretching/rupture were observed as the main energy absorbing/damage mechanisms of the FML panels. Another study (Langdon, 2007) comprise the FMLs based on glass fiber reinforced polyamide (GFPA) composite and Al alloy. The polypropylene based adhesive was used for bonding the components and the interfacial fracture characteristic of the composite-metal interface was investigated with single cantilever beam testing. The interfacial fracture toughness value of GFPA/Al system was higher than plain composite but lower than GFPP/Al hybrid structures. Various stacking configurations of GFPA/Al panels were subjected to blast testing and their damage mechanisms were analysed. The back face deformations occured with the shape of diamond or circle while the front face showed pitting, global displacement and tearing type of deformations.

2.2. Sandwich Structures

Sandwich structures are the combination of different materials that provide stiffnes and strength with a lightweight composition compared to the traditional materials. The distinctive properties of the sandwiches are obtained by the contribution of each component's superior feature into the whole system. Characteristicly, sandwiches consist of three main components: the face-sheets (skin), the core and the adhesive for the integration of constituents. Generally, the strong and stiff face-sheets are connected with a less dense core material which show lower strength and stiffness as seen in Figure 2.2 (Sarzynski, 2003).
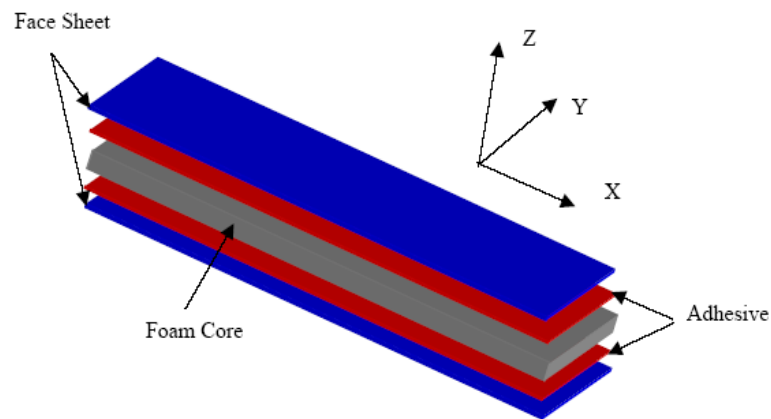
Figure 2.2. Typical geometry of sandwich panel
(Source: Sarzynski, 2003).

The adhesive type that bonds the faces to the core has vital importance in terms of the mechanical performance. The selected adhesive should be strong enough to resist shear and tensile stresses occured between the components. Many types of skin and core materials are available with various combinations. It can be a beam, a panel or any other special shape. The skin can be made of metal, wood, plastic, FRP composites or any other materials. Similarly, the core structures can be classified based on their geometry and/or material. Honeycomb, corrugated or foamed cellular materials show significantly better structural integrity with lesser weight. In terms of structural sandwiches, facesheets are generally identical both in material type and thickness. These structures are referred as symmetric sandwich structures. However, material/thickness variation of the facesheets can be compulsary in some exceptional cases due to the different loading conditions and working environment. This type of constitution is called as asymmetric sandwich structures. The face-sheet materials in the sandwich structures bear the in plane compressive and tensile stresses because of the bending moment presence. By the seperation of thin skins, the second moment of inertia is increased which leads to the increase of sandwich stiffness. Face-sheets are employed to distribute the localized loads and reactions to the softer and weaker core. The essential function of the core material is to withstand deformation perpendicular to the in-plane direction and provide shear rigidity along the planes perpendicular to the skins. Compared to the traditional materials, the sandwich structures exhibit advantages in terms of mechanical properties

such as lower lateral deformations, higher buckling resistance and higher natural frequencies (Sezgin, 2008; Gupta, 2003).

2.2.1. Theory of Sandwich Structures

The configuration of I-beam, which consist of two flanges and a web tying those flanges, exhibit the anology of the sandwich structures (Figure 2.3). In the I beam, the flanges move together and the web shows resistance against shear stresses and buckling. In sandwich composites, the facesheets and the core imitate the roles of flanges and web, respectively. During flexural (bending) test conditions, the laminates act together and one side of the face-sheet is under compression while the other side is under tension. The core material resists to out of plane loading and provides the integrity of the skins against buckling and wrinkling (Sezgin, 2008).
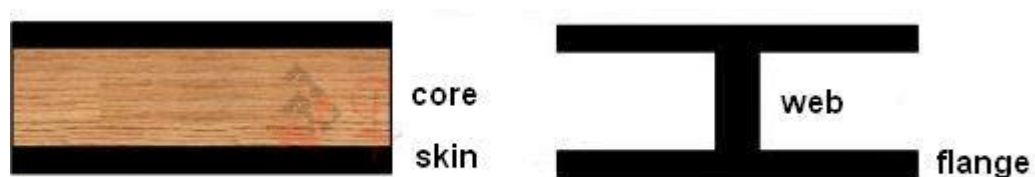
Figure 2.3. Sandwich structure representation with an I beam
(Source: element6composites, 2011)

The mechanical properties of a sandwich structure can be determined by using the known material properties of the components and details of configuration geometry. Specifically, the flexural properties can be calculated using beam bending theory adapted to sandwich structures (Zenkert, 1995). Figure 2.4 shows the geometry of a sandwich beam.
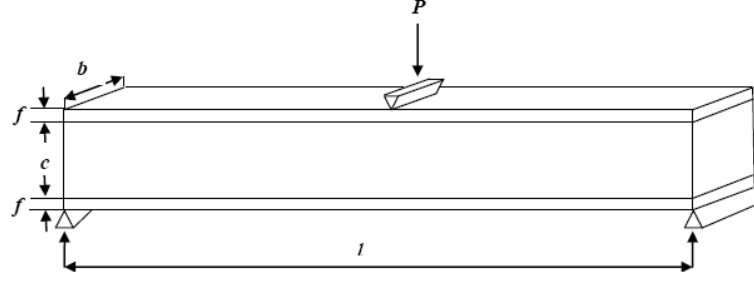
Figure 2.4. Geometrical representation of a sandwich structure.

The flexural rigidity (D) is calculated using the sum of the flexural rigidities of the constituent parts, about the centroidal axis of the sandwich beam, as shown in Equation 2.1. Based on this equation, the E_f is the modulus of the skins Newton per metres squared (N/m^2), E_c the modulus of the core, b is the width of the sandwich beam, f is the skin thickness, d is the distance between the skin centroids and c is the core thickness (Zenkert, 1995).

$$D = E_f \frac{bf^3}{6} + E_f \frac{bfd^2}{2} + E_c \frac{bc^3}{12} \qquad (2.1)$$

$$\tau = \frac{P_{max}}{D} \left(\frac{E_f fd}{2} + \frac{E_c}{2} \frac{c^2}{4} \right) \qquad (2.2)$$

The maximum core shear stress is given by Equation 2.2 where P_{max} is the maximum load on the sample in Newtons (N), and D is the flexural rigidity in Newtons metres squared (Nm^2). The maximum stress in the face-sheets and core are calculated by means of Equation 2.3 and 2.4 respectively. According to those equations, M is the maximum bending moment and h represents the total sandwich thickness (Zenkert, 1995).

$$\sigma_f = \frac{Mz}{D} E_f \text{ and } z = \frac{c}{2} + f \qquad (2.3)$$

$$\sigma_c = \frac{Mz}{D} E_c \text{ and } z = \frac{c}{2} \qquad (2.4)$$

2.2.2. Components of Sandwich Structures

The sandwich components have critical importance in terms of mechanical properties of whole structure. The design of sandwiches as well as individual features of components strongly affects the overall performance of the hybrid systems. Therefore, the constituents should be selected by considering the application area and working environment. Both core and face-sheet types vary with respect to the design requirements and the manufacturing of sandwiches depend on these components.

2.2.2.1. Face-sheets

The face sheets provide the flexural rigidity of the sandwich panel. It should also possess tensile and compressive strength. A broad range of materials are available for the usage as skins. Metals like aluminum, titanium, steel and fiber reinforced plastics (FRP) are some of the common examples of skin materials. Choice of skins is important in terms of the working environment. Corrosion, heat transfer characteristics, thermal expansion characteristics, moisture absorption and other properties of the whole sandwich composite can be controlled by proper choice of skin material. In most cases both skins of the sandwich are of the same type, but could be of different type depending on specific designs. Difference may be in terms of material type, thickness, fiber orientation, fiber volume fraction or in any other design parameter. For the fiber reinforced polymer skins, the material properties can be controlled directionally in order to arrange the properties of the sandwich composite. Fiber reinforced polymers are extensively preferred as skins due to their low density and high specific strength. The choice of proper adhesive for bonding the skin and the core becomes very important and it should have enough compatibility with the components of the sandwich structure. The adhesion must have high strength level and should not be influenced from the working environment (Zenkert, 1995; Gupta, 2003).

2.2.2.2. Cores

The main goal of the core material is to enhance the flexural stiffness of the sandwich structures. Usually, core materials have lower density in order to decrease the total weight of the sandwich panel. Both the stiffness and resistance of the core must be high enough under shear forces. Considering the design requirements, many materials can be used as core and they can be divided into three classes as described below and seen in Figure 2.5. (Gupta, 2003)

- *Low density solid materials:* open and closed cell structured foams, balsa and other types of wood.
- *Expanded high-density materials in cellular form:* honeycomb, web core.
- *Expanded high-density materials in corrugated form:* truss, corrugated sheets.

(a)   (b)
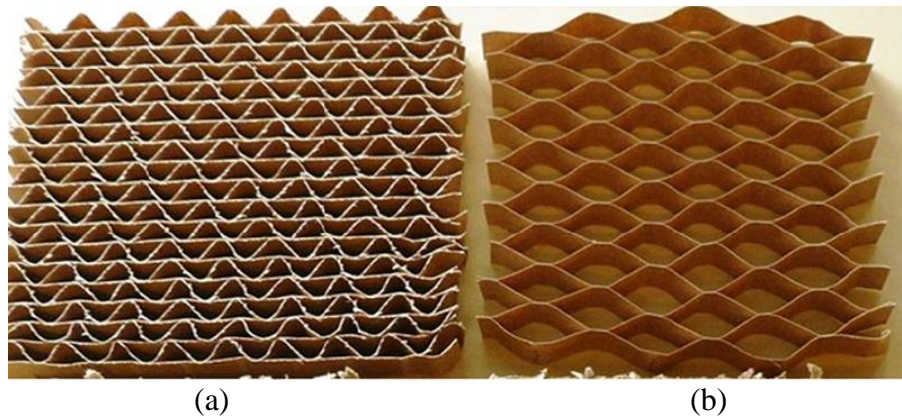
Figure 2.5. Two different types Kraft paper honeycomb: (a) Corrugated honeycomb core (b) Expanded honeycomb core (Source: Chen, 2011).

High-density materials are employed in order to produce cores include aluminum, titanium and different types of polymers. The interfacial properties between the components are greatly influenced by the core material. Generally, expanded high density materials supply smaller contact area as compared to the low density materials. The core should satisfy the requirements according to the design parameters for a sandwich structure given in specifications or service conditions (Gupta, 2003).

Polymeric or metallic type of foam cores is available in the industry and their applications are growing up in a broad range. A very popular type of polymeric core is vinyl sheet foam which is a rigid, closed cell material that resists hydrocarbons, sea

water or gasoline. Vinyl foam based sandwiches are commonly employed in aircraft and automotive industry and thermoforming method is used for the production of these hybrid systems. Polyurethane (PU) type of foam is also preferred due to its perfect thermal insulation property. This core is extensively used in the marine applications and cost-effective when a lower property cored laminate is required. In addition, its compatibility with thermosetting resins provides advantageous over other foam materials. Honeycomb foam is the combination of a group of cells with the same geometry and stacked together to form hexagonal structures. There are numerous studies related with the production, testing and characterization of honeycomb foam panels due to their properties such as fire retardancy, flexibility, lightweight, and high impact resistance (Vinson, 1999; Sezgin, 2008).

The aim for the manufacturing of metallic foams is to eliminate the disadvantageous of polymeric foams especially under impact and shock loading. Metallic foams have various remarkable features for the acting as cores in sandwich structures such as good stiffness and strength to weight ratios, good sound damping, electromagnetic wave absorption, high thermal insulation and non-combustibility. A number of engineering alloys, such as aluminum, iron, nickel or copper can be foamed to relatively densities as low as 3% by different production routes. Some metal foams can be up to an order of magnitude stiffer and stronger than polymer foams. Another characteristic of interest is impact performance. Based on the experimental observations, the main failure mode is progressive crushing of the cells in the foam that leads to significant impact absorption. Among the metallic foams, the popularity of aluminum foams is growing up in transport (aerospace, ship building, etc.), sport and biomedical industries. Relatively recent studies related with aluminum foam have revealed the impact performance of sandwich structures with composite skins. The researchers observed that the significant impact energy is absorbed through buckling and crushing of cells throughout the foam core (Styles, 2008).

The properties of metal foams and cellular metal structures have close relationship with the properties of the parent metal, relative density and cell topology. The foams can be considered in two groups in terms of their cell structure; open and closed-cell foams (Figure 2.6-a and 6-b). Simplest cubic models of open-cell and closed-cell foams are shown in Figures 2.7-a and 2.7-b, respectively. Open cell metallic foams are consisting of cells connected to each other through open faces. The solid material is present in cell edges including struts and rods. This foam type is open to

fluids passing through it; therefore it is useful as a filtering medium. High thermal conductivity and high internal surface area are the main advantages of open cell foams specifically for the heat transfer systems. The closed cell metal foams consist of non-interconnected cells with solid material faces. The properties of these foams are investigated for potential applications. The differences in cell wall thickness, wall material type, cell size and imperfections influence the mechanical properties of the foam. The variations of these parameters referred above can be changed by considering the production route according to the required properties. Open and closed cell structure Al foams can be produced by various manufacturing techniques such as melt gas injection, gas-releasing particle decomposition in the melt or in semi-solids, casting and metal deposition on cellular preforms and etc, according to the different applications (Gibson and Ashby, 2000).

Foams may also be classified into three groups in terms of their mechanical behavior: elastomeric, elastic-plastic and elastic-brittle. Under compressive loads, Al foams show characteristic stress-strain behavior. Compressive stress-strain curve consists of three distinct regions: linear elastic region, collapse region and densification region (Figure 2.8).

| (a) | (b) |
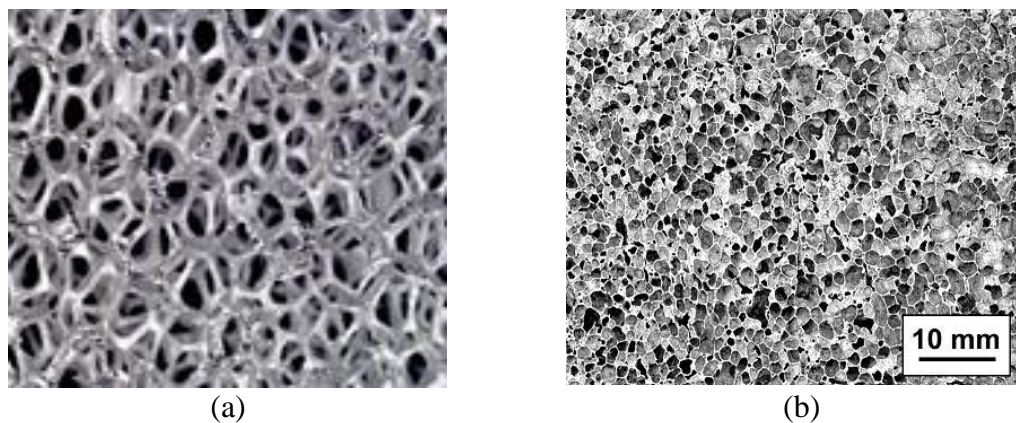
Figure 2.6. Aluminum foam types according to the cell structures: (a) Open cell foam (b) Closed cell foam (Source: Vikipedi, 2011).
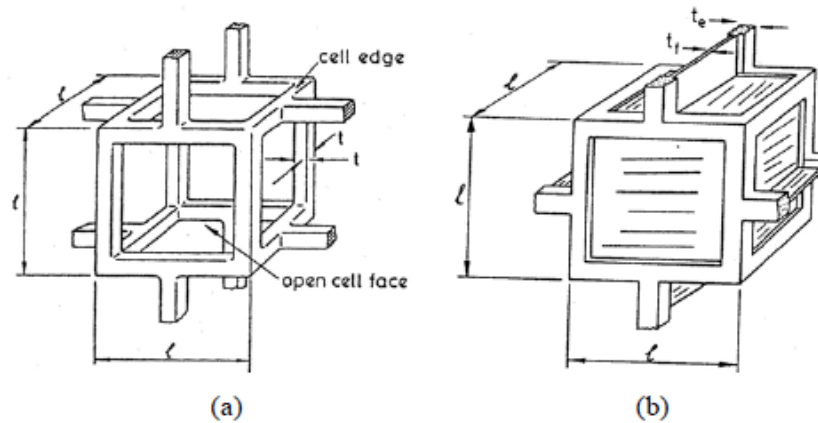
Figure 2.7. Cubic Models of a) Open cell and b) Closed cell foams
(Source: Gibson and Ashby, 2000).

Linear elasticity is a very small region and generally limited to 5% or less strain values. The yield strength of the foam is strongly affected by the mechanical properties of its parent material. If the foam is loaded beyond its linear-elastic limit, the structure will collapse which leads to horizontal plateau in the stress-strain curve with an irreversible deformation. The failure mechanisms such as elastic buckling and plastic failure are localized and a deformation band is usually occurred transverse to the loading axis. This band propagates through the undeformed parts of the foam. By the increase of displacement or strain, the band continues to fill the whole foam structure. As the third zone, after collapsing of cells at a critical strain, the cell walls will be in close contact and start to touch each other. This region is called as densification region and the foam behaves as a dense material which approaches to the strength of the solid foam material. The performance of metallic foams can be enhanced by sandwiching it between two strong and stiff face sheets to produce a lightweight structure. Under static loading conditions, the face sheets carry the axial load or resist against bending, whereas the core carries the shear deformation (Gibson and Ashby, 2000).
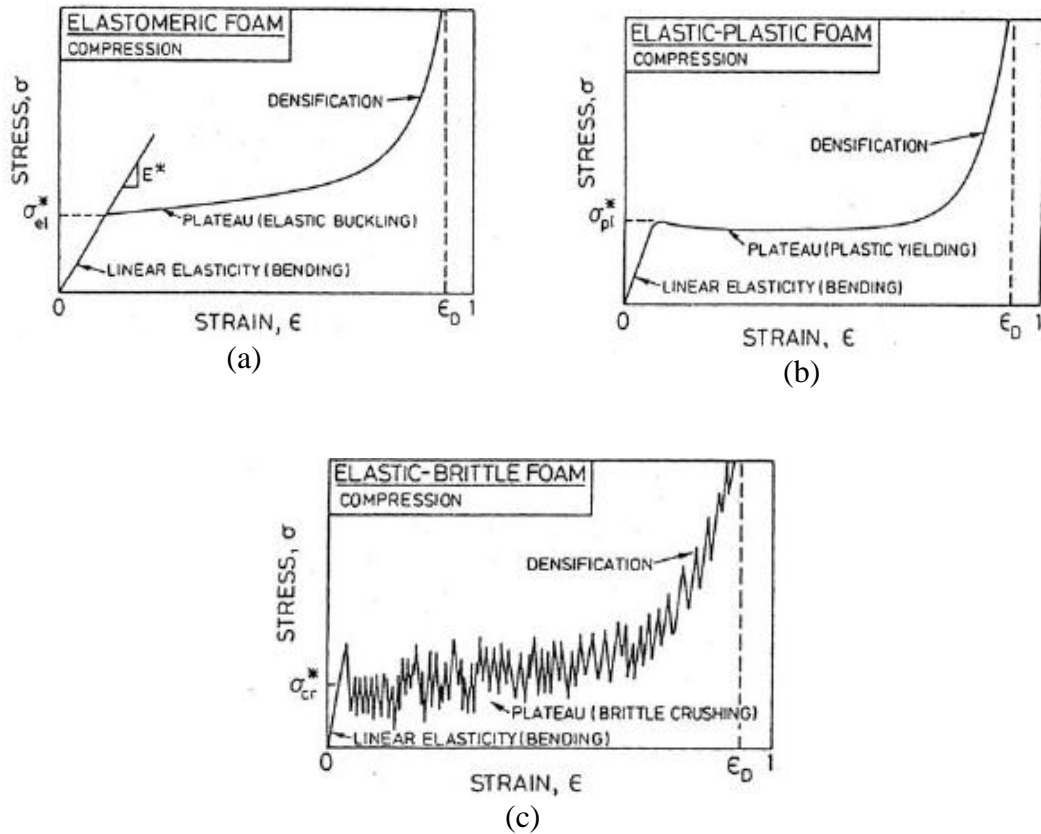
Figure 2.8. Compressive stress-strain curves of foams: (a) Elastomeric foam (b) Elastic-plastic foam (c) Elastic-brittle foam (Source: Gibson and Ashby, 2000).

McCullough et al. (1999) investigated the tensile and compressive characteristics of closed cell ALULIGTH[TM] Al foams by considering their deformation mechanisms. The foams exhibited semi-brittle behavior under tension while they showed ductility under compression due to the different failure modes. Motz and Pippan (2001) made a study about the tensile properties of ALPORAS[TM] Al foams with different densities. The stress-strain curves of foams under tension displayed dissimilarities compared to the compression. The linear elastic regime was followed by a plastic regime with the formation of fracture process zone and the crack progression led to the failure of Al foam. The strain at fracture was rather small under tensile loading and the foams with higher density showed relatively higher failure strains. Deqing et al. (2005) reported the compressive properties of Al foams by considering their cell structures. In their study, both plastic collapse strength and energy absorption capacities of the closed cell aluminum foams were significantly improved by decreasing the cell size of the foams having the same density. Koza and his colleagues (2003) concentrated on the

compression behaviors of Al foams having various densities and dimensions. According to that paper, larger samples showed lower mean strength and narrower scattering of the strength values than the smaller ones. This behaviour was described in terms of a greater probability of the presence of lower density parts in the former foam samples. Bastawros et al. (2000) focused on the plastic deformation progression of Al foams under compressive loading by using digital image correlation procedure. The strain maps were monitored and the deformation patterns of the foams were obtained with this technique.

2.3. Integration Techniques of Layered Structures

The integration of different constituents in the same system is very important and critical in terms of the service performance. For decades many researchers are focused on the appropriate integration technique for the fabrication of hybrid systems and a number of joining methods were developed. Traditional joining methods include mechanical fastening and thermosetting adhesives, however, welding and fusion bonding are the main integration techniques for thermoplastics and thermoplastic based layered structures. Depending on the heat generation, different fusion bonding methods are available such as infrared, hot plate, ultrasonic, resistance and induction. These methods are generally employed to join thermoplastics to themselves and other thermoplastic materials (Guruşcu, 2009).

Polypropylene (PP) is preferred in the industrial applications because of its unique properties like recaycibility. However, PP generally behaves as hydrophobic material and shows low-surface free energy which leads to very poor bondability to other materials. The usage of PP has limitations due to this undesired property. Therefore, some surface modification techniques have been developed in order to overcome this major difficulty and some available pretreatment methods are given in Table 2.1. The main idea behind the pre-treatment is eliminating the potential weak boundary layers, WBLs. This can be achieved by changing the substrate topography, modifying the chemistry of the substrate surface or a combination of these mechanisms. Particularly, the treatments can be separated into two groups: physical and chemical methods. Grit blasting and solvent degreasing are the most commonly used pyhsical techniques. By means of these techniques, cohesively weak layers are removed from the

substrate and they may also modify topography. Flame treatment of plastics and anodising process for metals are the major type of chemical treatmets. Various materials with different chemical and structural properties have their own specific pretreatments. However, some of them can be classified and same pretreatment methods show considerable effect on their chemical structure (Chen, 2007; Green, 2002).

Silane coupling agent application significantly affects and increases the performance of joints involving inorganic glasses (Adams, 2005). The metal surface treatment has also critical importance specifically for the aluminum (Al) due to its common use in many applications. According to the previous studies, chromic acid etching (CAE) and phosphoric acid anodizing (PAA) onto the Al surface increase the performance compared to physical methods and found to be effective even in wet conditions (Guruşcu, 2009). The integration types expressed above have some disadvantages like high toxicity and complex processing. Silane surface modification is safer and simpler pretreatment technique compared to the previous techniques. There are some studies available in the literature about the silane treatment of metals that aimed to increase the effect of silane (Adams, 2005).

The modification routes related to adhesion are focused on creating polar groups on surface of polymers which leads to the increase of surface free energy values and enhancing the adhesive properties of the polymeric materials (Chen, 2007). By considering PP based layered structures, the interphase control can be performed with a silane coupling agent and a binding agent or an additive agent such as maleic anhydride into matrix PP (Hamada, 2000).

Table 2. 1. The surface modification/pretreatment techniques for metallic and non-metallic substrate (Source: Guruşcu, 2009).

Substrate	Modification/Treatment Technique	Effect of Modification/Treatment
Metals	Degreasing	Cleaning of the surface
Metals	Grit blast	Weak boundary layer elimination and increase in contact surface area
Metals	Acid etching	Surface oxidation
Plastics	Corona treatment	Weak boundary layer elimination and surface oxidation
Plastics	Flame treatment	Weak boundary layer elimination and surface oxidation
Plastics	Chemical etching	Weak boundary layer elimination and surface oxidation

2.3.1. Chemical Treatment with Silane Coupling Agent

Coupling agents or adhesion promoters are a special class of bifunctional components that can react chemically with the substrate. Adhesion promoters can be directly applied to the substrate, or they can be mixed with the adhesive itself. The coupling agent is able to migrate to the interface and react with the substrate surface when mixed with the adhesive. The adhesion promoters which directly apply to the substrate form a very thin coating that is approximately only one molecular layer thick. As seen in Figure 2.9, the coupling agents add a new, generally organic layer at the interface. The resultant layer is bifunctional and integrates the substrate (such as metal) and the adhesive (such as polymeric material). This thin layer provides good interfacial bonding between the components (Petrie, 2000).
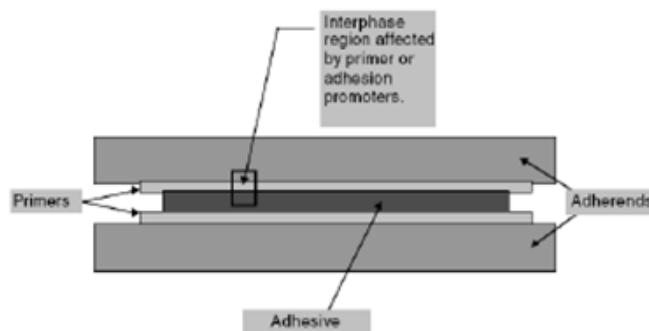
Figure 2.9. Coupling agents provide a stronger interphase region having improved adhesion and permenance (Source: Baker, 2002).

Silanes are the popular type of commercial adhesion promoters and they are extensively used in order to increase the adhesion between polymeric and inorganic materials. The application of coupling agents can be performed by introducing them into the substrate Silane coupling agents are usually react chemically with both substrate and adhesive. Therefore, the formed covalent bonds across the interface have sufficient strength and durability. They generally include molecules with short organic chains having different chemical composition on either end of the chain. Silane coupling agents are broadly used including laminated structures between resin matrix and reinforcing fibers in composites. The resultant interface provides benefits such as a chemical bridge between the surface and organic polymer, a barrier for eliminating moisture penetration onto the interface, stress transfer from the resin to substrate or inorganic filler constituent and effective dispersion of fillers and decrease in the apparent viscosity of the system (Petrie, 2000). The silanes are generally applied to adherents from dilute solution in water or ethanol water (1-2% by volume) and left to drying. In addition, they can also be mixed with the adhesives. Silane coupling agents react with water in aqueous solutions to form hydrolyzed silanes, which react with the surface of the inorganic substrate. Numerous silane adhesion promoters available in the literature and their reactivity degree differs them from each other. Silanes may be produced with amine, epoxy, mercaptan and other functionalities (Adams, 2005).

The R groups in the 3-aminopropyltriethoxysilane (APES) and N-2-aminoethyl-aminopropyltrimethoxysilane (AAMS) includes amines, which would make them reactive with epoxide adhesives or liquid resins. As 3-glycidoxypropyltrimethoxysilane (GPMS) contains epoxide groups, it would react with amine groups in adhesives or resins. The carbon carbon double bonds in 3-methacrylpropyltrimethoxysilane (MPMS)

would copolymerise with styrene and unsaturated polyester in liquid resins, by a free radical mechanism (Guruşcu, 2009). In 1999, Demjen et al. deeply investigated the interaction mechanisms between silane coupling agents and the PP matrix. They evaluated the results of model experiments and developed an explanation in order to express the reactive coupling in an apparently inert system. They used three types of silane coupling agents and showed that aminofunctional silanes strongly integrate the surface of the filler that adhere strongly to the surface of $CaCO_3$ and form a polysiloxane layer. The N-4-vinylbenzyl-N9-3-trimethoxysilylpropyl-ethylenediamine hydrochloride (CVBS), aminosilane coupling agent reacts with the carboxyl groups of PP and forming tertiary amide groups. Reactions are also fast in this case, they are completed during the homogenization of the composite, leading to the reactive coupling effect observed. Lee and Jang (1997) focused on the behavior of APES silane coupling agent. They analysed the mechanical and impact properties of short glass fiber mat reinforced PP composites. The modification of fiber surfaces with this silane coupling agent led to the increase of flexural strength and the flexural modulus of the composites. Demjen and Pukanszky et al. (1998) concentrated on the coupling effect of two aminofunctional silanes, APES and CVBS in PP/$CaCO_3$ composites. They concluded that the tensile strength increased but the deformability decreased compared to the non-treated system. The application of APES silane solution for the Al alloy was analyzed by Chen et al. (2007). According to the experimental results, the pretreatment application to the aluminum surfaces by APES silane resulted in the increase of lap shear strength as seen in Figure 2.10.

Briskham and Smith (2000) manufactured PP based composite to Al fusion bonded joints by performing a number of different aluminum pretreatments. According to the experimental results, aminosilane pretreatment showed pretty good performance. Improvements in shear strength of the silane-treated specimens were observed. Lawcock et al. (1997) studied on the effect of adhesion between the aluminum and fiber/epoxy prepreg in terms of mechanical properties. Based on the interfacial fracture toughness test results, the GPMS silane exhibited an increase up to seven times for the specimens with stronger bonding.

The influence of epoxy (GPMS) and amino (APES) based silane surface modifications on the surface characteristics of flame-treated PP was investigated by Aboudzadeh et al. (2007). The application silane treatment resulted in the increase of adhesion strength of the flame treated PP surfaces. This significant improvement was

attributed to the changes in surface free energy, morphology and generation of functional groups on the PP surface. In addition, the results for the flame treated PP surfaces showed that the effect of epoxy silane of was higher than the aminosilane in terms of adhesion strength.

(a)

(b)
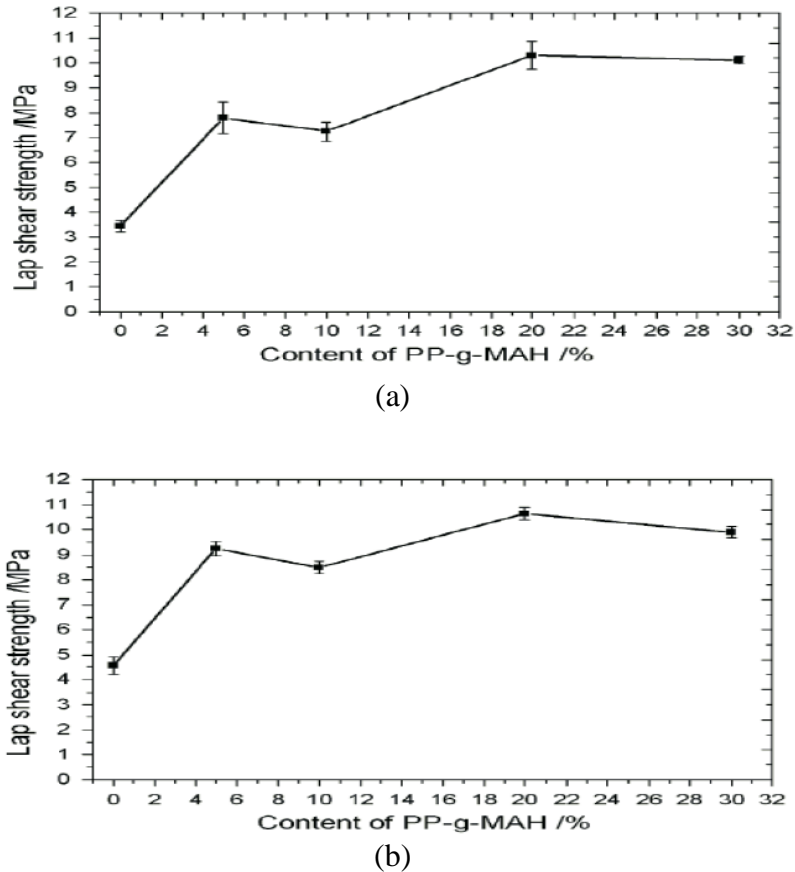
Figure 2.10. Effect of the PP-g-MA content on lap shear strength of PP/CaCO3 composite: (a) Lap shear strength of PP-g-MAh without APES silane pretreatment (b) Lap shear strength of PP-g-MAh with APES silane pretreatment (Source: Chen, 2007).

2.3.2. Chemical Treatment with MAH Grafted Polypropylene

Recently, the usage of maleic-anhydride (MAH) modified type polyolefins are increasingly growing up due to its advantages such as functionalization process, good processibility and cost effectivity. The combination of maleic-anhydride and PP is one of the most popular types of material system and many researchers investigate the

properties and effectiveness of this system. Maleic-anhydride-modified PP (PP-g-MA) are currently employed in many areas like GFPP, metal-plastic laminates for structural applications, anticorrosive coatings for metal pipes and containers, multilayer sheets of paper for chemical and food packaging, and polymer blends. Glass fibers, fillers and functional polymers (such as polyamides) have compatibility with the anhydride group which is a very reactive and efficient coupling agent. Maleic anhydride-functionalized polypropylene has major importance for application as a copolymer precursor in polymer blends, or adhesion promoter with glass and carbon fibers. Maleic-anhydrid-grafted isotactic PP has been broadly employed as a compatibilizing agent in the PP composites and other fillers (Guruşcu, 2009). It is tought that the chemical bonds would be constituted between the introduced polar monomers and surfactants of the pretreated sheet. In this case, the adhesive strength increased significantly.

(a)

(b)
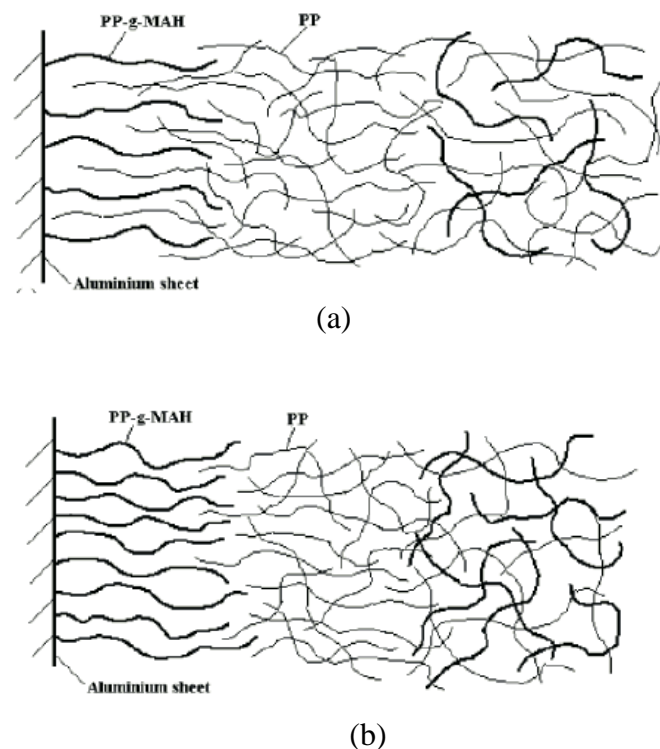
Figure 2.11. Schematic representation of molecules for PP with introduction of PP-g-MA (Source: Chen, 2007).

The schematic illustration of the distribution of PP molecules and PP-g-MA on the Al surface is shown in Figure 2.11 (Chen, 2007). Chen et al. (2007) modified PP by introducing a small amount of functional monomer grafted PP, having very similar

26

molecular structure with PP. Thus, it is easier to produce fiber-reinforced polymer composites and macro-composite components combined of metals and polymer by different fabrication techniques (plastic injection moulding and compression moulding) with this approach. They investigated the effect of the amount of PP-g-MA added into PP and adhesive-bonded aluminum sheets by considering their lap shear strengths. Modification of PP by addition of 5–30 wt. % amount of PP-g-MA led to a significant increase in terms of lap shear strength. It is attributed to the chemical interactions between −OH, Al^{3+} or amino group −NH_2 at the surface of the aluminum sheets and the polar functional anhydride groups and carboxylic groups -COOH on PP-g-MA at the interface. For the 20 wt. % PP-g-MA introduction, the maximum the lap shear strength values are obtained at. In 2000, Reyes and Cantwell et al. carried out amorphous chromate treatment to the Al surface and introduced PP-g-MA at the interface between Al and unidirectional GFPP. According to the single cantilever beam tests, the produced Al/GFPP FMLs exhibited pretty good adhesion due to the introduction of a PP-g-MA layer at the component interface. Compston et al. (2001) performed a similar study and obtained similar results. Bikiaris et al. (2000) used two types of organofunctional silanes and a copolymer for enhancing the interfacial adhesion in GFPP composites. It was observed that the adhesion of copolymer PP-g-MA was more successful than 3-aminopropyltrimethoxysilane and 3- aminopropyltriethoxy silane. The combination of PP-g-MA with the silanes led to further property improvements due to the capability of the MA groups to react with the amino groups of the silanes.

2.4. Mechanical Characterization of Sandwich Structures

Sandwich panels with minimal weights, desired stiffness and strength can be designed for numerous applications. This can be achieved by optimizing different parameters, such as material types of core and face sheets or design geometry of panel with the knowledge of operating failure mechanism at the design loads. The composite sandwiches consist of face-sheet (skin) and core materials have been investigated by many research groups. The fiber reinforced polymer (FRP) composites or metallic layers are generally used as skin materials (Sezgin, 2008). Russo and Zuccarello et al. (2007) investigated the mechanical behavior of fiber-glass laminate skins with two types of core: PVC foam or polyester mat cores. According to the experimental results,

the shorter specimens failed due to the core shear failure with delamination while the relatively longer sandwiches failed after the lower face-sheet tensile failure. Lim et al. (2004) studied about the flexural behaviour of sandwiches composed of E-glass fiber/epoxy face-sheet and PVC foam core. The failure types of the sandwich beams under transverse loading were predicted with the elastic beam theory. According to the test results, the experimental failure modes were in good agreement with the theoretical results under three point bending. Corigliano et al. (2000) concentrated on the mechanical performance and numerical models of the syntactic foam/glass fiber composite sandwich structures. The syntactic foam that filled the core of the sandwich, resulted in the higher strength and stiffness properties. Daniel and Abot (2000) investigated the flexural characteristics of sandwiches composed of unidirectional carbon/epoxy face-sheets and Al honeycomb cores. The sandwich beams were tested under three and four point bending. According to the test results, the skins showed a softening non-linear behaviour on the compression side and a stiffening effect on the tension side. Steeves and Fleck (2004) analysed the bending behaviour of sandwich beams consisted of woven glass fiber/epoxy prepreg and PVC foam core. The geometry and component properties significantly affected the failure types of beams. Core shear, skin micro-buckling and indentation beneath the middle loading roller were the main failure mechanisms observed in the experiments. Sandwich structures with foam core and aluminum face sheets were studied extensively by various researchers in terms of optimum design. Aluminum-Foam-Sandwiches (AFS) are flat structures composed of a foamed aluminum core and aluminum cover sheets. As shown in Fig. 2.12, AFS consist of two external aluminum sheets and an internal layer of aluminum foam. Since the layers are bound to each other metallically, the sandwich is free of any adhesive and suitable for welding. While AFS have the advantages of classical sandwiches such as high stiffness and low weight, they can be reshaped by technologies well known from metal sheet materials (Vogel, 2011). Aluminum foam-based sandwich structures with aluminum skins tested under three-point bending (3PB) have been found to fail by some mechanisms such as indentation, core yielding, face yielding, and face wrinkle (Daniel, 2000 and Steeves, 2004). Chen and co-workers (2001) investigated the plastic collapse of sandwich systems which included aluminum foam core and found that the shear strength of the core increases as core thickness is reduced. In addition to that, closed cell aluminum foam was used in a composite integral armor for ballistic applications.
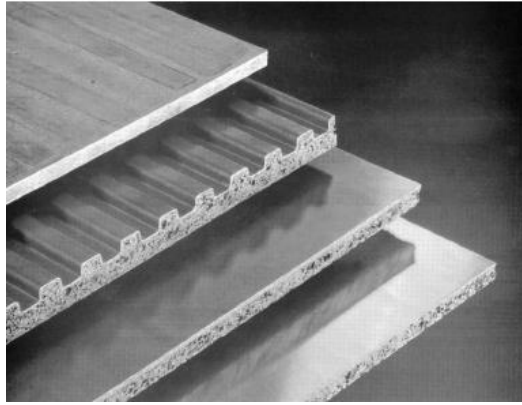
Figure 2.12. Aluminum foamed sandwiches (AFS)
(Source: Simancik, 2001).

Harte et al. (2000) developed and tested fatigue failure maps for Alporas foam with aluminum skins loaded in 4-point bending, observing the common modes of face sheet yield, core shearing and indentation. They found the core shear regime was particularly dominant in fatigue loading. A similar study was conducted by Bart-Smith et al. (2000) using 3-point bending to develop failure maps. Numerical simulations were also conducted and compared with experimental results, showing similar failure mechanisms. Styles and co-workers (2007) focused on the failure modes of thermoplastic composite skin/Al foam core sandwiches under flexural loading. Three different core thicknesses were investigated and their behaviors were evaluated. In that study, the thinner specimens showed skin wrinkling and fracture with core cracking while the core thickness increase led to the core indentation. Langdon and Cantwell (2007) reported the applications of aluminum foam sandwiches with fiber-metal laminates (FML). Several dynamic tests were carried out in order to evaluate the performance of these sandwiches under low and high velocity impact. The combination of thermoplastic based composite face-sheets with aluminum plate and aluminum foam led to the increase of energy absorption capability. It was also found that the use of fiber-metal laminate systems provides significant improvement in terms of ballistic protection and damage resistance. The combination Al/GFPP fiber/metal laminate system with Al foam improves the impact properties and energy absorption capabilities of sandwiches (Carillo, 2009 and Reyes, 2000).

Reyes studied the flexural and low velocity impact behavior of the FML reinforced sandwich panels with aluminum foam core. It was found that the failure mechanisms of the sandwich components contributed to the energy absorption

capability of the system and the proposed energy balance model was in good agreement with the experimental results (Reyes, 2000).

CHAPTER 3

BLAST CHARACTERISTICS OF STRUCTURES

3.1. Explosions and Blast Phenomenon

The explosion term is described as a large-scale, fast and abrupt energy release phenomenon. In the literature, explosions are classified based on their formation characteristics as physical, nuclear or chemical. Numerous examples of physical explosions are present during the life such as collapse of a compressed gas or volcanic eruption. In a nuclear explosion, the change of the protons and neutrons in the nuclei results in the energy release and new rearrangement. The explosive substances can be categorized based on their physical nature (solids, liquids or gases). Primary and secondary explosives are the solid explosive types existent in the literature and the tri-nitro-toluene (TNT) and ANFO are the most commonly used secondary class of explosives (Ngo, 2007).

In the recent days, there is a growing interest for the resistant behaviour of engineering structures under blast loading. Both government authorities and academicians investigate in depth the ways of performance improvement of structures against terrorist attacks. Drastic damages take place where the explosions create high pressure and loading rate, e.g. structural failure, gradual collapse and extensive plastic deformation with/without ballistic penetration (Zhu, 2008). Blast is a special kind of dynamic load and categorized into two groups as internal and external blast. The external type of blast develops due to the high explosives or atomic explosions; however, internal blast forms because of the detonation of high explosives or accumulation of flammable gas/air mixtures (Sriram, 2006). Many studies are available in the literature related with the theory of blast.

In the case of blast loading, with the detonation of a high explosive, the reaction products (hot gases) under pressure up to 300 kilo bar and a temperature of approximately 3000-4000C° are created. The hot gases expand and compress the surrounding air with an outward movement. Eventually, a compressed air layer (called as blast wave) takes place in front of this gas volume including most of the energy

released by the explosion. The blast wave exhibits a sudden pressure increase above the atmospheric pressure which is called as the side-on overpressure. The departure of expanded shock wave from the explosion center leads to the decrease of overpressure value. As shown in Figure 3.1, after a period of time, the pressure may fall down below the ambient pressure and in the negative stage, a partial vacuum is produced and air is taken up (Ngo, 2007).
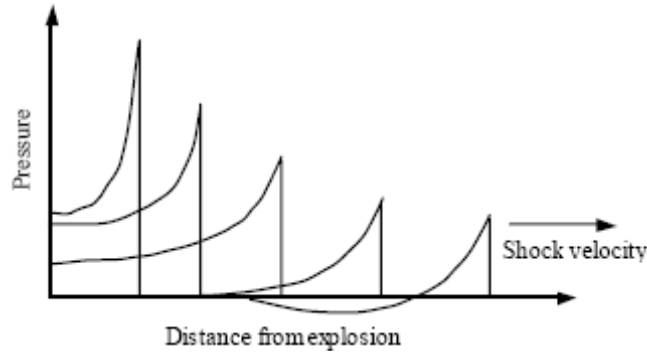
Figure 3.1. Schematic representation of blast wave propagation
(Source: Ngo, 2007)

A characteristic pressure-time history of a blast wave is shown in Figure 3.2. The t_a is the time for the arrival of the blast wave where P_s and P_a represent the peak pressure of the blast wave and ambient air pressure, respectively. The pressure variation from P_a to P_s takes place at t_a time because of the discontinuous at the shock front. However, at $t_a + t_d$ time an exponential pressure decrease is observed. The free-field pressure versus time behaviour is generally expressed by a modified Friedlander formulation as given in equation 3.1. In this formulation, t_d is the positive phase duration and θ represents the time decay of the curve (Zhu, 2008).

$$p(t) = (p_s - p_a)\left[1 - \frac{t - t_a}{t_d}\right]e^{-(t-ta)/\theta} \tag{3.1}$$

Another important blast wave parameter is the specific impulse of the wave during the positive phase I_s, given in equation 3.2. where $p(t)$ is overpressure as a function of time.
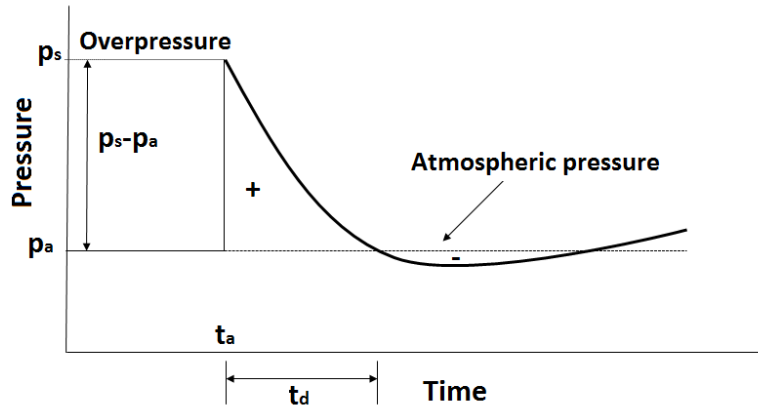
Figure 3.2. Pressure-time curve of idealized blast wave.
(Source: Ngo, 2007)

$$I_s = \int\limits_{t_a}^{t_a+t_d} p(t)dt \qquad (3.2)$$

In the literature, air blast loading is described depending on the explosive weight and stand-off distance. In order to compare the effects of various explosives, the explosive weight is modified to an equivalent value of TNT weight (TNT equivalency) by considering a conversion factor. Thus, the blast characteristic of any given mass of TNT can be adopted with respect to a known reference mass of TNT by means of scaling laws. These scaling laws are sometimes utilized to estimate the features of blast waves arise from large-scale explosions based on much smaller scale tests. The best known blast scaling equation was adopted by Hopkinson-Cranz and called as cube-root scaling law. This law expresses that similar blast waves are produced at identical scaled distances when two explosive charges of similar geometry and of the same explosive, but of different sizes, are detonated in the same atmosphere (Baker, 1983).

$$Z = \frac{R}{W^{1/3}} \qquad (3.3)$$

It is very common to use a scaled distance Z as seen in the formulation expressed above. In equation 3.3, the "R" represents the distance from the centre of the explosive source in meters and "W" is the total weight of a standard TNT explosive in kilograms.

3.2. Failure Modes of Structures under Blast Loading

The deformation and fracture modes observed after tests are reviewed in this section, for monolithic materials, FML systems and sandwich structures. There are many similar studies related with the characterization of metal beams and plates under blast loading. The researchers in the literature examined the metallic structures under different boundary conditions (clamped and built-in), various geometries (quadrangular, circular, stiffened) and loading conditions (uniform blast or localized blast). A number of failure modes of monolithic materials have been observed in blast experiments, and these studies can be found in the literature (Nurick, 1989 and Jones, 1989). Depending on the blast load distribution (uniform or localised) onto the plates, the deformation mechanisms exhibit some variations. Menkes et al. (1973) concentrated on the blast response of Al alloy beams and defined three failure modes as; (mode 1) large inelastic deformation of the whole beam, (mode 2) tearing (tensile failure) of the beam at/over the support and (mode 3) transverse shear failure of the beam at the supports. Similar failure mechanisms were also observed by Nurick et al. (1996) for the uniformly loaded steel plates (Langdon, 2005). The response of same type of plate subjected to localised blast loading showed more localised deformation at the plate centre. The impulse increase led to the tearing and/or shearing of a central ring of material and resulted in cap formation. The transition of failure modes from mode 1 to mode 3 are shown in Figure 3.3 by considering impulsive velocity increase. The residual deflection quantity (Δ) indicated the extent of damage for mode 1; however, the tearing of the structure occurred due to the high impulse values and accepted as threshold for Mode 2. The blast load increase resulted in the overlapping of modes 2 and 3.

The blast response of glass fibre reinforced polymer composites (GFRP) have been investigated by the researchers and reported in the literature. Mouritz et al. (2002) concentrated on the failure, fatigue and flexural properties GFRP panels. Those panels were subjected to underwater blast loading at low overpressure and exhibited failure

modes such as matrix cracking, fibre fracture and delamination with respect to the load increase (Dolce, 2010).

Franz et al. (2002) conducted a set of blast loading experiments on GFRP panels composed of E-glass-chopped strand mat fibre and polyester resin. The prepared composite structures with five different areal densities (300, 600, 750, 900 and 1200 g/m^2) were exposed to localised blast loads via plastic explosive PE4.
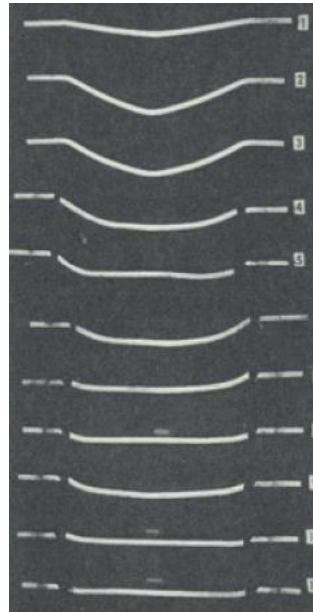
Figure 3.3. Failure mods of a beam transiting from a mode 1 to mode 3 with increasing impulsive velocity (Source: Zhu, 2008).

Fifty-five tests with 163 plates were performed by using ballistic pendulum set up and the schematic representation of the test plate is seen in Figure 3.4. The increase of explosive charges led to the increase of blast impulse and caused to various deformation modes such as matrix cracking, delamination/debonding and penetration.
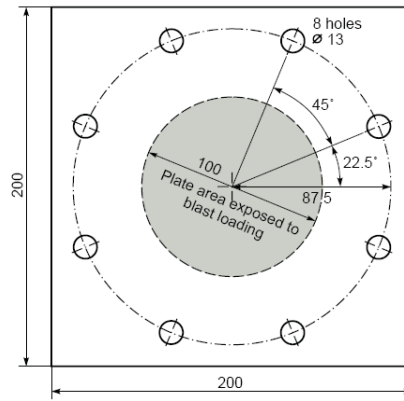
Figure 3.4. Test plate model.
(Source: Franz, 2002)

The areal density and/or laminate thickness increase resulted in the higher resistance and decrease of delamination/debonding failures and Figure 3.5 shows these mechanisms. For the highest blast impulses, tearing with penetration was observed through the fibre-matrix interfaces with a random distribution. Both energy absorption capability and mechanical interaction among the plies of the composite laminates significantly affected the damage distribution along the thickness direction. Maximum damage took place in the front part of the panel for lower impulses while the higher impulses caused damage in the back face of the panel. Based on the whole dynamic test results, Franz et al. (2002) concluded that the damage resistance of the laminated composite panels might be developed by using a gradient of the mechanical properties in the thickness directions.
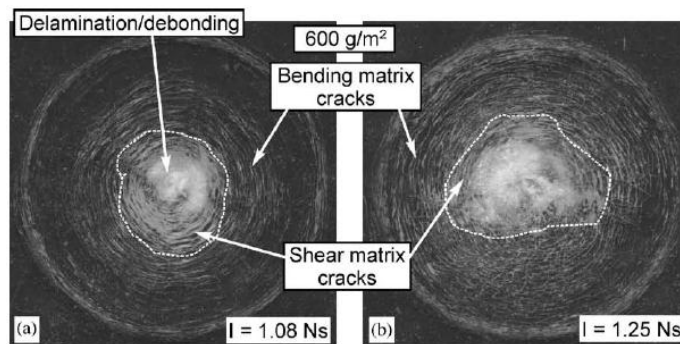
Figure 3.5. Composite panels with various failure modes.
(Source: Franz, 2002)

Tekalur et al. (2008) investigated the responses of composite panels subjected to both quasi-static and blast loading. In their study, E-glass and carbon fibres were integrated with vinyl-ester (VE) resin and fabricated by VARTM technique. The tension, compression and shear tests under quasi-static conditions were conducted to the composites while the blast experiments were performed by utilizing shock tube equipment. Based on the dynamical test results, Tekalur and co-workers concluded that carbon fiber/VE composite samples showed instantaneous destructive damage after the threshold shock pressure (0.6 MPa). It is the pressure that the structure failed beyond this value. The fiber breakage and delamination were the dominant failure mechanisms in the strike face. In contrast, E-glass fiber/VE composite panels exhibited continuous damage progression and different failure types were observed such as plastic deformation, fiber breakage and delamination. The panel images subjected to shock loading is given in Figure 3.6.

<div align="center">(a)   (b)</div>
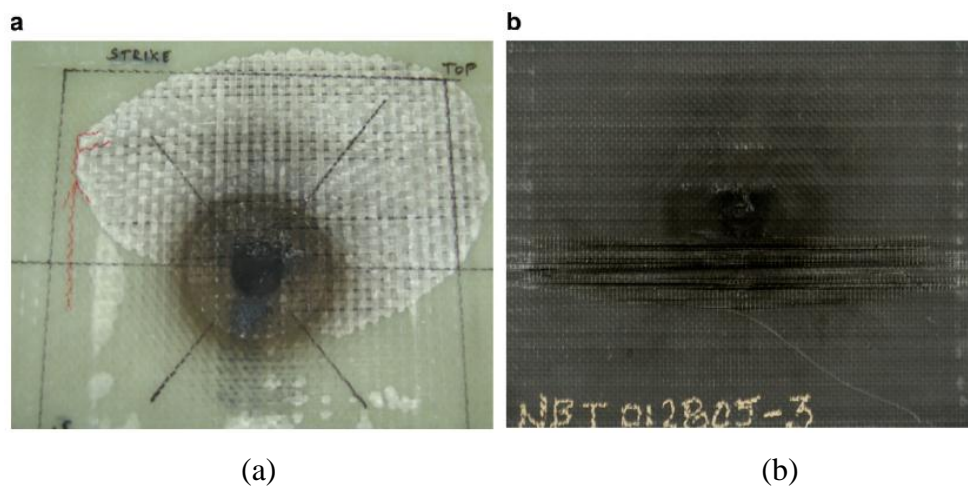
Figure 3.6. (a) Damage in strike face of the E-glass fibre fibre/VE composite under blast loading with delamination among layers. (b) Damage in strike face of the carbon fibre fibre/VE composite under blast loading (Source: Tekalur, 2008).

The high and low velocity impact/blast behaviour of fibre/metal laminates (FMLs) have been deeply investigated by the researchers. Thermoset or thermoplastic type of resin is used as the matrix component of the composite system and aluminium (Al) is generally employed as the metal constituent. The GLARE (glass fibre-epoxy composite with Al), ARALL (aramid composite with Al) and CALL (carbon fibre-epoxy composite with Al) have been widely used in the aerospace and defence

applications due to their excellent fatigue properties, high fracture resistance and relatively lower weights. Some workers have concentrated on the impact responses of the FML systems. Vlot and his co-workers investigated the low and high velocity impact characteristics of GLARE to monolithic Al and carbon fibre reinforced PEEK composite. Based on the test results, the FML samples showed higher damage threshold energy values as compared to the other traditional materials. Under dynamic test conditions (at higher strain rates) the impact durability of the GLARE showed fairly good results because of the positive rate sensitivity of the glass fibres within the composite plies (Vlot, 2000). Fatt et al. (2003) analysed the ballistic performance of GLARE and they reported that for the same areal density, the GLARE FMLs exhibited 15% increase in ballistic limit as compared to the monolithic Al. Lawcock et al. (1997) conducted impact tests by changing the fibre-matrix adhesion properties of carbon fibre reinforced FML system to understand the effect of adhesives/surface treatments. The decrease of surface treatment effect led to high amount of fibre/matrix splitting. The main disadvantages of thermoset resins are the relatively long processing times and lower level of bonding between the composite/metal interface. In order to solve these kinds of problems, thermoplastic resins like polypropylene (PP) has been suggested due to decreasing the manufacturing costs and providing reusability. Also, almost perfect energy absorption capacity and high resistance against impact/blast loading are the other advantageous of PP. At Liverpool University, Langdon and his colleagues examined the behaviour of FMLs based on glass fibre reinforced polypropylene (GFPP) with Al alloy and investigated the responses of the GFPP/Al system under uniform or localized blast loading. They also tested different GFPP/Al configurations by varying plate composition (changing the thickness and distribution of the Al and GFPP layers in the plate), plate area and loading diameter.

Langdon et al. (2005) reported the results of Al/GFPP under localised blast loading. Unidirectional and woven types of composites were fabricated with the same fibre volume fraction. The square FML samples were subjected to blast tests with a ballistic pendulum set up. The loading conditions and photo of the ballistic pendulum is given in Figure 3.7. Plastic explosive (PE4) was used and a polystyrene foam pad was utilized to absorb the blast energy. By varying the stand-off distance (foam pad thickness) and mass of the explosive (height of the explosive disk), the behaviours of the FML system were characterized.
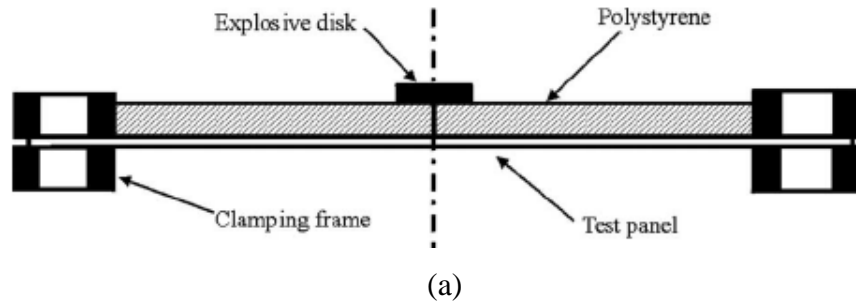
Figure 3.7. The representations of blast loading condition and ballistic pendulum set-up: (a) Schematic configuration of loading conditions (b) Photo of ballistic pendulum (Source: Langdon, 2005).

According to the experimental results, the FMLs absorbed energy from the blast by various deformation mechanisms such as delamination, debonding between the metal-composite interface, perforation of the panels and petalling/spalling of the rear surface of the Al. In addition, the stretching and bending of the fibres absorb energy from the blast. At higher deformation rates, the tensile strength increase of fibres affected the blast resistance in the positive manner. The woven composites showed centrally damaged regions with symmetrical response while the unidirectional composite/Al system exhibited asymmetric character. As expected, the stand-off distance increase led to decrease of damage severity for both unidirectional and woven composite FMLs. The failure mechanisms of Al/GFPP samples are shown in Figure 3.8.

(a)

(b)
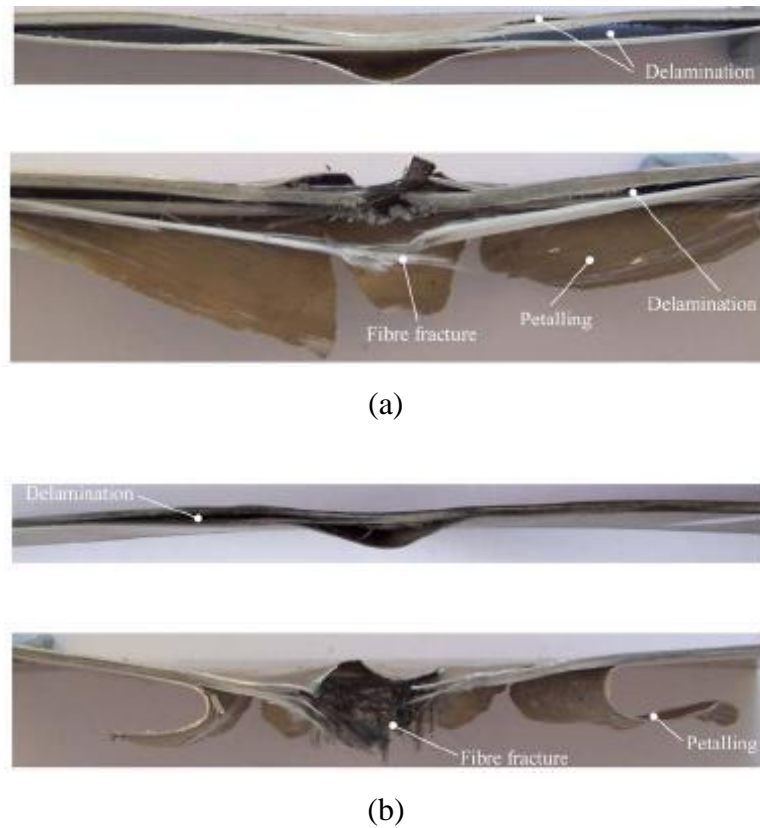
Figure 3.8. Microscopic images of unidirectional and woven composite FMLs after blast test: (a) Polished cross-sections of unidirectional FML system (b) Polished cross-sections of woven FML system (Source: Langdon, 2005).

Langdon et al. (2007) conducted blast tests on Al/GFPP hybrid systems by changing some parameters such as diameter, height and mass of the PE4 explosive. Also different panel configurations with various component layers were tested and the results were evaluated. Based on the experimental results, the thickness or the number of layers significantly affected the front face damage mode together with the shape of debonded zone. The impulse increase resulted in the increase of the back face damage. Also, the FML panels less than 17 layers showed diamond shape debonding while the layers between 19-22 exhibited a transition from diamond shape to cross-shape formation. When the panel had 28 layers the deformation became completely cross-shaped geometry. Global displacement, pitting and ring buckling of the front face were observed as failure modes after the blast tests. The deformation modes and damaged regions of FML panels are given from Figure 3.9 to 3.11.
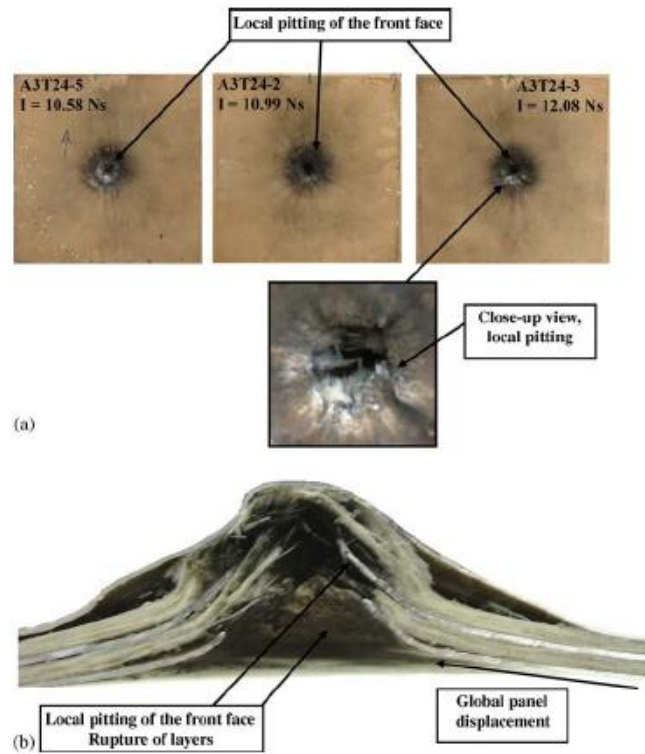
Figure 3.9. Images of FML panels with 11 layers under localized blast loading (a) front face and (b) cross-sectional view (Source: Langdon, 2007).
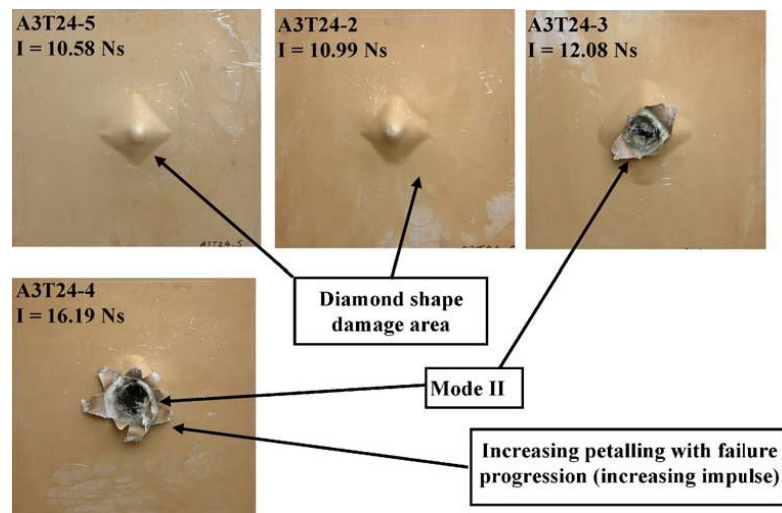
Figure 3.10. Back face images of FML panels with 11 layers under localized blast loading (Source: Langdon, 2007).
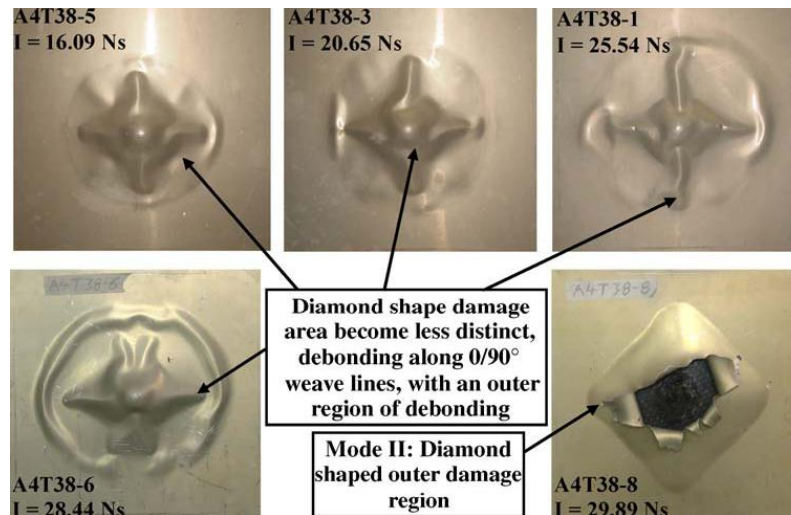
Figure 3.11. Back face images of FML panels with 28 layers under localized blast loading (Source: Langdon, 2007).

Lemanski et al. (2006) conducted localized blast tests to the Al/woven glass fiber reinforced PP composite and revealed the energy absorption characteristics. Based on the experimental test results, the interlaminar debonding was not as important as fibre failure and localized deflection mechanisms. According to Lemanski and his co-workers, the deformation that occurred through the thickness of the thin plates was present because the layers towards the back face plate showed weak structural support to the layers in front. Due to the poor bending stiffness of the plate, the energy for bending the whole plate was lower than for bending the back face of the panel. However, for the thick plates the back face deformation was considerably larger than front face. This was attributed to the significant structural support of the layers behind the front face. The bending stiffness of the entire plate was high and this led to more energy requirement for deforming the whole panel than debonding the back layers. So, for a specific impulse, the thicker panels showed smaller deflections and higher tearing thresholds compared to the thinner panels.

Langdon et al. (2008) examined the response of clamped Al/GFPP system under uniform blast loading. The failure modes obtained from the localized blast tests were not seen under uniform loading condition. For instance, ring-buckling of the front face and cross-shaped or diamond shape debonding type of back face were not observed. Instead of those mechanisms, multiple debonding, plastic deformation, metal tearing and internal buckling were present. Figure 3.12 shows the back face regions of FML panels with different component configurations.
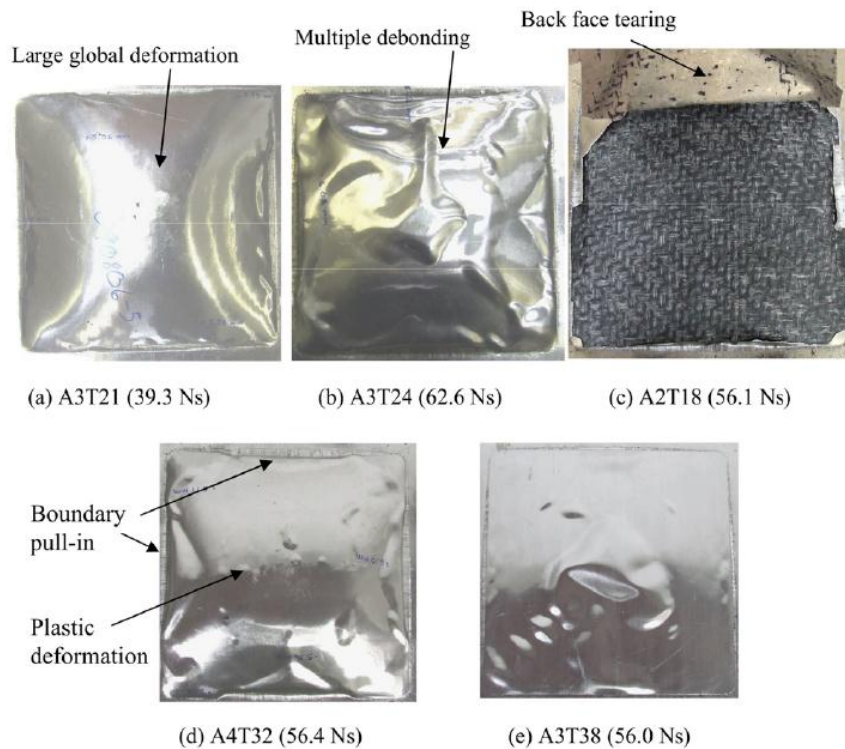
Figure 3.12. Back face images of the FML panels under uniform blast loading.
(Source: Langdon, 2008)

The sandwich panels composed of cellular cores such as honeycomb or metallic foam have significant capacities of considerable energy dissipation by large permanent deformation under quasi-static or dynamic loading conditions. Due to their cellular microstructures, the foams can be subjected to large plastic deformation and absorb high amount of kinetic energy before collapsing. The behaviors of foams and foam based sandwiches under blast loading are still very limited. Specific research groups develop experimental and modeling techniques and their investigations are accepted as the reference studies in the literature.

Nurick et al. (2009) investigated the response of honeycomb core/mild steel skin sandwich structures under uniform and localized air blast loading. In their study, uniform loading was produced by detonating with a disc shaped explosive and the blast was canalized to the target. However, the localized blast loading was generated with the same explosive near to the test panel. The air core sandwich samples were also manufactured to compare the failure modes with honeycomb core sandwiches under the same loading conditions. The characteristic deformation modes of panels are given in Figure 3.13 and 3.14. According to Figure 3.13, at impulses above 20 Ns, the air core sandwiches showed larger back plate deformation compared to the honeycomb core

sandwich specimens. This was attributed to the better absorption mechanisms of honeycomb materials such as crushing and bending. On the contrary, below 20 Ns, the air core sandwich panels exhibited lesser deformation because of the load transfer through the honeycomb. Based on the experimental results, the panels under uniform loading showed better performance compared to the specimens under localized blast loading
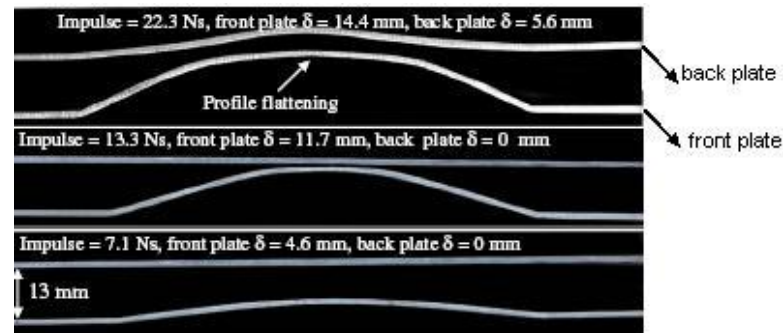
(a)
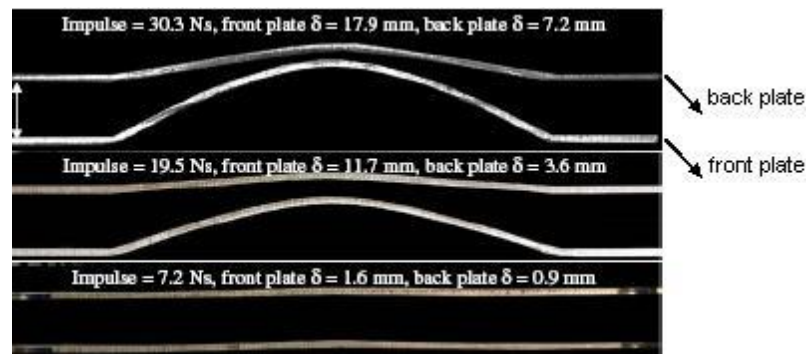
(b)

Figure 3.13. The deformation modes of sandwich plates under uniform loading: (a) Images of sandwich plates with an air core under uniform loading (b) Images of sandwich plates with a honeycomb core under uniform loading (Source: Nurick, 2009).

Hanssen and his co-workers conducted blast tests to rectangular aluminium foam layers with and without metallic cover panels via ballistic pendulum set-up. Based on the experimental results, they observed that (a) when a cover plate was attached the non-covered low density panels, fragmentation occurred but kept their structural integrity, (b) charge mass increase led to the increase of panel fragmentation, (c) the high density panels without cover plates were not significantly fragmented and (d) both

front cover and front surface of the high density panels deformed with inwardly curved shape (Hanssen, 2002).
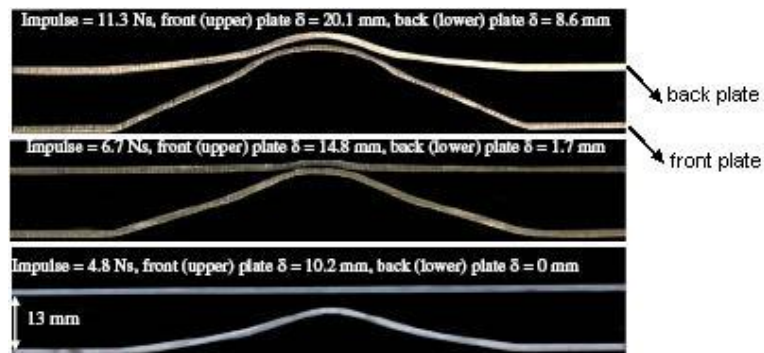
(a)
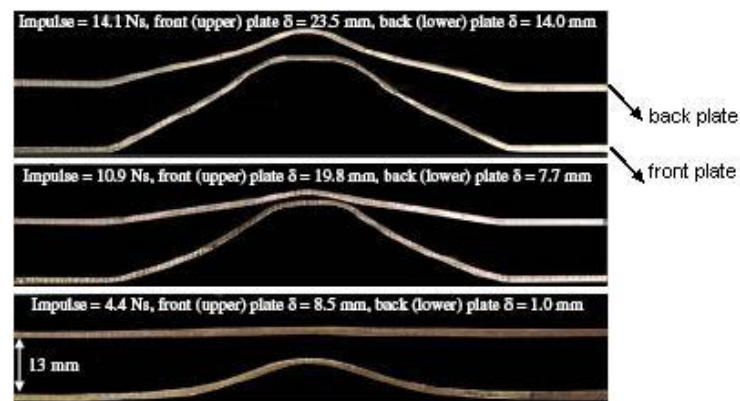
(b)

Figure 3.14. The deformation modes of sandwich plates under localized loading: (a) Images of sandwich plates with an air core under localized loading (b) Images of sandwich plates with a honeycomb core under localized loading (Source: Nurick, 2009).

Radford et al. (2006) concentrated on the behaviour of clamped sandwich plates with metallic foam core under blast loading. They compared the blast response of monolithic stainless steel and sandwich panel with the same areal density. Alporas™ Al foam was used as core material where AISI type stainless steel acted as face-sheet of the sandwich. They presented a novel experimental technique which conducts high intensity pressure pulses to the structures by using metal foam projectiles. The working principle of that technique was based on the imitation of shock loading in air and water by using applied pressure versus time pulse. Figure 3.15 shows the schematic representation of sandwich plate geometry. In that study, the test specimens were subjected to blast loading at mid-span by metal foam projectiles. The permanent deflections and core

compression of the sandwich samples were measured as a function of the projectile momentum. Based on the experimental results, it was found that the sandwich plates showed higher projectile momentum values compared to monolithic steel for the same areal density. Providing that the areal density was fixed, the foam thickness increase resulted in the higher shock resistance magnitudes. The profiles of the plates given in Figure 3.16 were continuously curved due to the travelling plastic hinges, and an apparent amount of core crushing was observed in the central area.
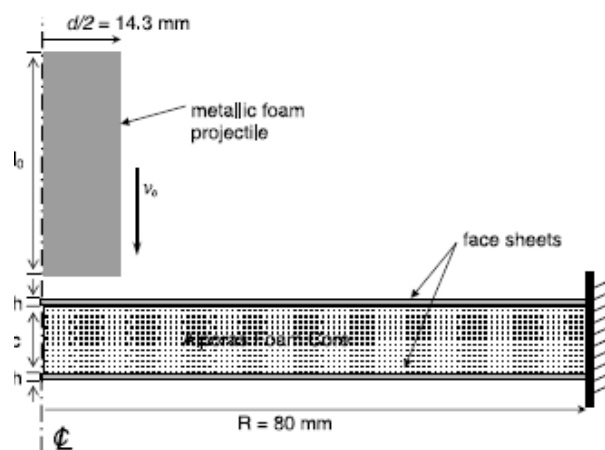
Figure 3.15. Configuration of sandwich plate geometry.
(Source: Radford, 2006)
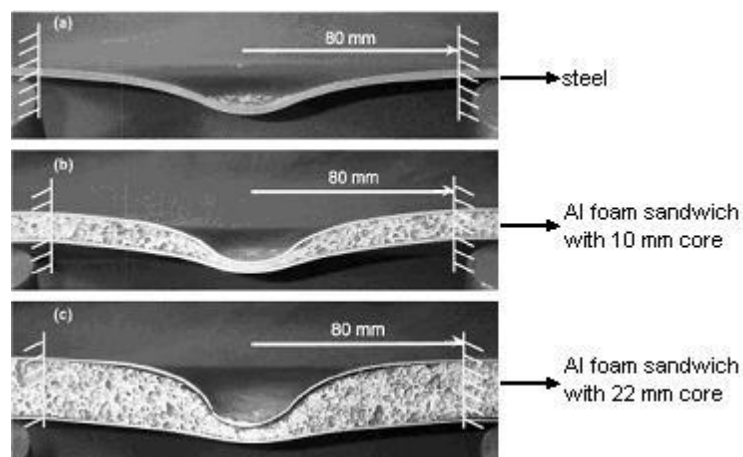
Figure 3.16. The deformation profiles of monolithic steel and Al foam sandwiches with different thicknesses under blast loading (Source: Radford, 2006).

Zhu et al. (2008) investigated the blast response of Al foam and honeycomb core sandwich structures with metallic skins. Different panel configurations were experienced by varying skin thickness, cell size and foil thickness of the honeycomb to

reveal their performance under blast loading tests. The mass of the charge and the impulse level variations were also examined. The test samples composed of Al skin and Al foam or Al honeycomb core were produced by bonding the components with a proper adhesive and the schematic representations of the sandwiches are seen in Figure 3.17. The ballistic pendulum was used to simulate blast loading. The square shaped panels peripherally clamped between steel frames of pendulum and the charge was fixed in front of the specimens with a constant stand-off distance, 200 mm.
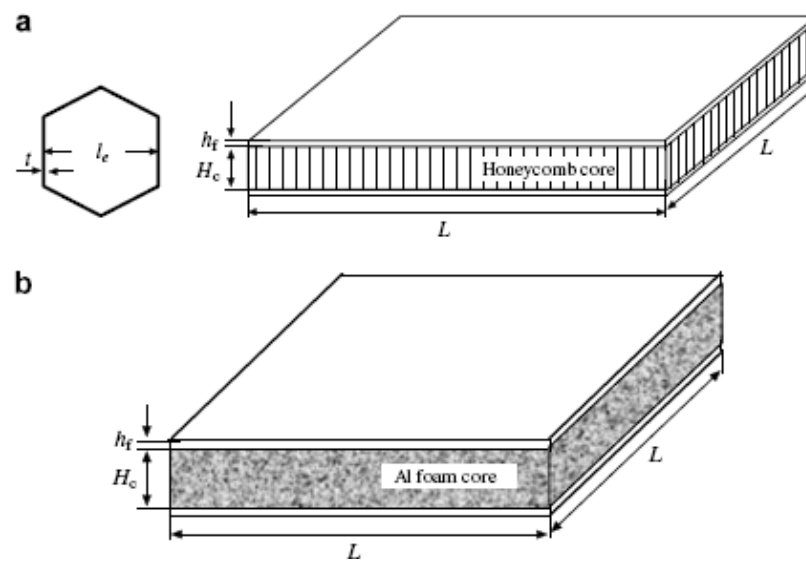
Figure 3.17. Blast test specimen configurations (a) Honeycomb core sandwich panel,(b) Al foam core sandwich panel (Source: Zhu, 2008).

Based on the experimental results of honeycomb core sandwich panels, face-sheet thickness, core density and charge mass increase resulted in localized deformation on the front face. However, the global panel deformation was observed when these parameters decreased. Pitting and indenting were also seen at the central parts of the specimens while the back faces of the all panels' exhibited dome-shaped deformation. According to the quantitative analysis of Zhu's study, thicker face-sheets and high density cores can reduce the back face deformation while higher impulse values led to more deformation. The deformation patterns and failure modes of honeycomb core sandwich panels are shown in Figure 3.18.

The blast responses of Al foam based sandwiches were also examined and their deformation patterns and failure modes were monitored. The Al foams had two relative densities: high density (10%) and low density (6%). From the experimental results, it

was concluded that, the panels with thinner skins showed larger deformation. All the samples' front faces exhibited localized failure on the centre part (tearing and indenting) and global deformation in the peripheral region. The failure modes of the specimens are given in Figure 3.19. The back faces of the panels showed similar deformation type. They showed a uniform dome shaped profile, moving out from the centre varying a more quadrangular shape towards the clamped edges.

Zone 1
Zone 2
Zone 3

Zone 1: Indenting failure
Zone 2: Flower-shaped deformation
Zone 3: Global deformation

(a)

Zone 1
Zone 2
Zone 3

Zone 1: Pitting failure
Zone 2: Flower-shaped deformation
Zone 3: Global deformation

(b)

dome-shaped deformation

(c)
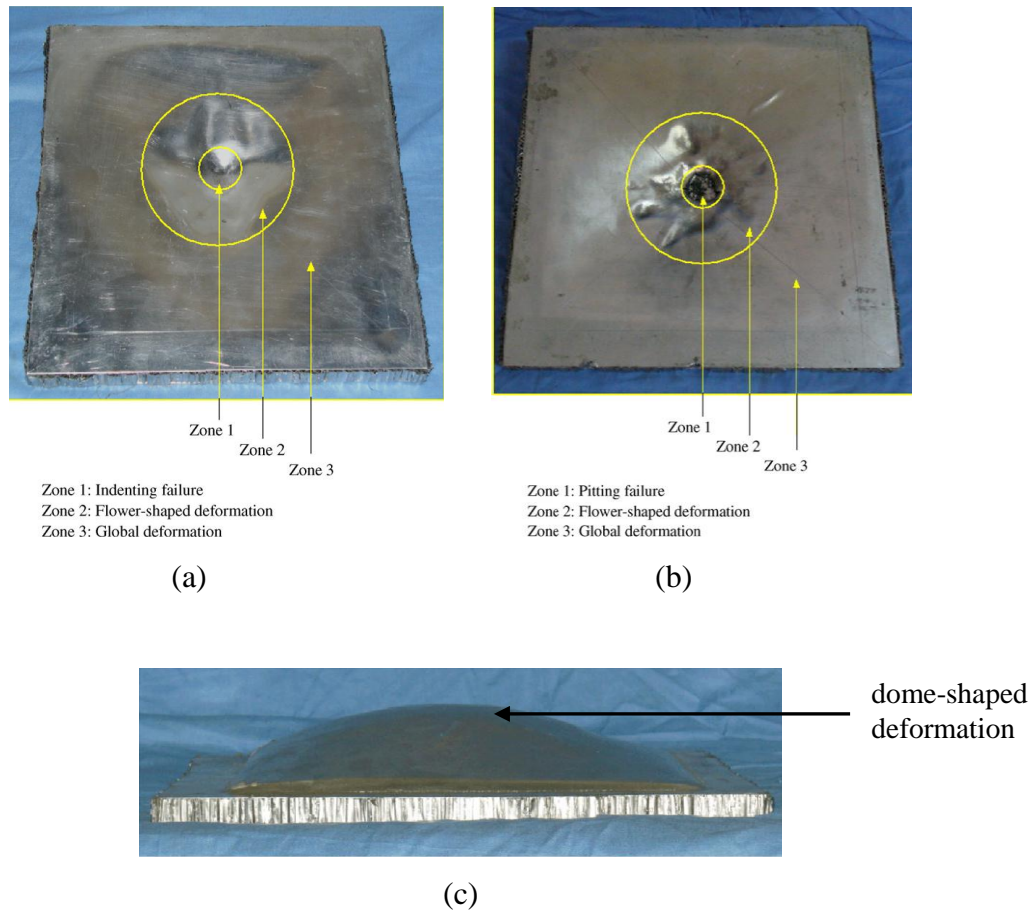
Figure 3.18. Deformation patterns of back and front faces of honeycomb cores after blast test: (a) Indenting failure of front face (b) Pitting failure of front face (c) Dome-shaped deformation occurred at the front face (Source: Zhu, 2008).
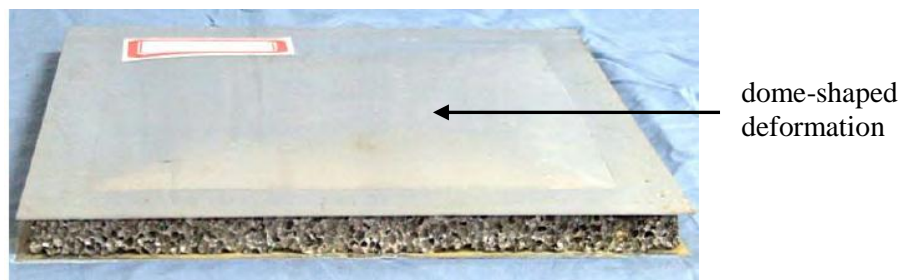
Figure 3.19. Deformation patterns of back and front faces of the Al foam based sandwich panels after blast test: (a) Indenting failure of front face (b) Tearing failure of front face (c) Deformation/failure pattern of the back face (d) Typical cross-section of the blast test specimen (Source: Zhu, 2008).

Based on the test results, the structural integrity of the Al foam based sandwiches were substantially kept after the blast tests and fragmentation was not observed. As seen in Figure 3.19 (d), core crushing accompanied by a cavity between the front skin and foam core. The panels with dense cores and composed of thick skin and/or core showed smaller deflection.

3.3. Blast Analysis for Sandwich Panels

In the recent decade, the application of composite sandwiches as anti-blast systems has been increasingly growing. The performance of such material systems has great importance in order to sustain the safety and survivability. There are a number of studies dealing with the response of composite structures under dynamic loading. Both experimental and numerical characterization of these systems are investigated by many researchers in the literature. Ballistic pendulum is generally used to generate micro-scale blast loading in order to determine the performance of materials. In addition, drop tower tests are commonly employed for the evaluation of energy absorption characteristics of structures. However, the presence of these equipments is not as common as quasi-static loading test machines. Andrews et al. (2009) focused on the situation of air blast loading of lightweight foam core sandwich panels. The compressive quasi-static loading was carried out and dynamic effect was included in the analysis by considering the panel as a single degree of freedom mass-spring system. Variable design parameters such as sandwich thickness, skin/core thickness or core density can be altered and this analysis can help designers to evaluate these differences with a relatively easy way. This approach was based on the theory described in W. Baker's book (Baker, 1983). As it is known, the explosive detonations create blast waves which lead to high pressure loads. Because these loads are generally suddenly applied, and maintain their effects in a millisecond to at most seconds, the response of damage to loaded structures is almost always dynamic. Thus, the structural response or damage usually depend on both static and dynamic properties of the applied system such as the magnitude of the amplitude (peak overpressure) of the blast loading, the loaded area, mass or inertia of the structure and the duration of the transient pressure loading (the applied specific impulse). These concepts can be adopted into simple dynamic mechanical systems as shown in Figure 3.20. Equations of motion under the applied (simplified) force pulse can be easily written and solved. The dimensionless form of the maximum response can be plotted versus another dimensionless ratio which relates loading time T to structural natural period as seen in Figure 3.21 (Andrews, 2009; Baker, 1983).
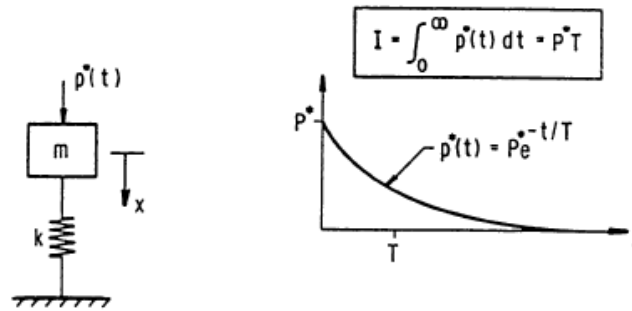
Figure 3.20. Linear oscillator loaded by a blast wave.
(Source: Baker, 1983)
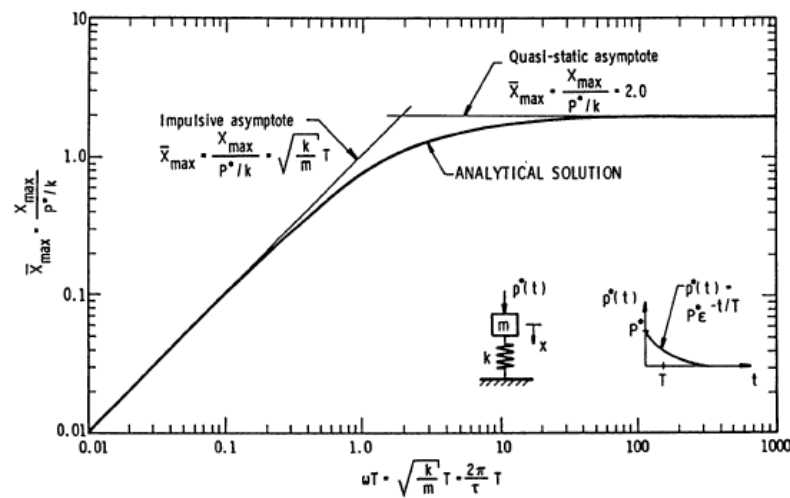
Figure 3.21. Shock response for blast loaded elastic oscillator
(Source: Baker, 1983)

The used symbols in the figures related with blast loading are P^*, t, T and m which represent the peak applied force, time, effective blast wave duration and mass, respectively. In addition, x, k, ω and τ represent the displacement, spring constant, circular vibration frequency and vibration period, respectively. In Figure 3.21, the scaled maximum response shows an asymptotic behavior for both small and large time values. Based on Figure 3.21, same solution is adapted into another form as presented in Figure 3.22. It should be noted that the maximum scaled response curve transforms into a rectangular hyperbola and first asymptote depends only on the level of applied peak force. The other asymptote depends only on the level of applied total impulse. During the intermediate loading zone (the "knee" of the hyperbola), both peak force and total impulse should be known in order to determine the response of the structure. As

51

shown in Figure 3.22, the *P*-I* curve can also be adapted for a simple rigid-plastic mechanical system. A pure coulomb friction element represents the spring in the system with resisting force *f*, which is independent of displacement once the mass starts to move (Baker, 1983).
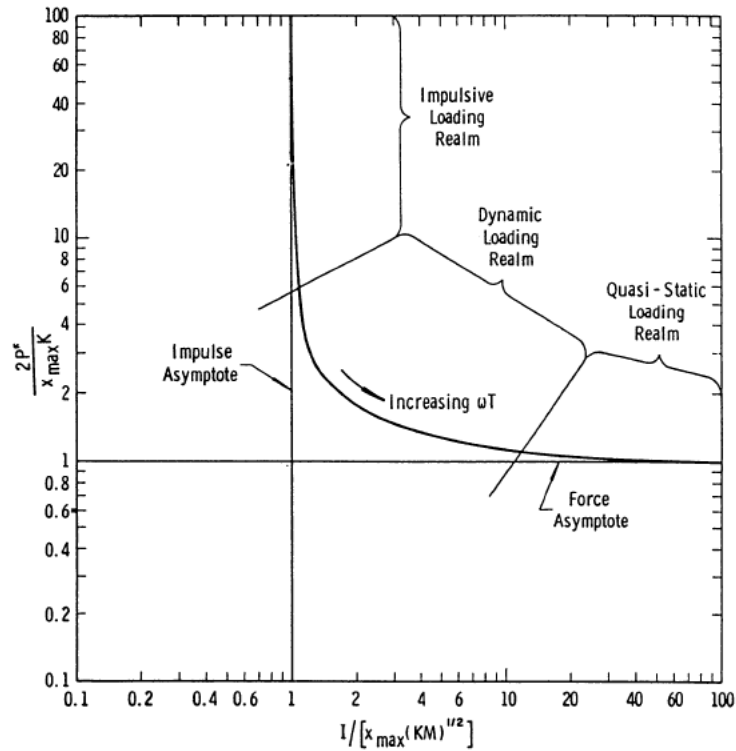
Figure 3.22. P*-I diagram for blast loaded elastic oscillator
(Source: Baker, 1983)

Even though the curves plotted in Figures from 3.20 to 3.22 were improved for transient loads identified by total applied forces and impulses, they can be developed by emphasizing an applied pressure transient loading with its accompanying specific impulse and loaded area. Thus, the concept can be modified to simple structures under blast loading conditions. The initial response of structures eventuate to peak overpressure if their vibration periods are much shorter than the blast duration. Otherwise, if their vibration periods are much longer than the blast duration, they respond firstly to specific impulse. As a third situation, if blast duration and vibration periods become approximately equal, both blast loading parameters are becoming critical (Baker, 1983).

CHAPTER 4

EXPERIMENTAL

4.1. Materials

In this study, non-crimp commingled glass fiber/PP fabrics ($0/90^0$ biaxial glass) were used to manufacture thermoplastic based composite structures. Polypropylene (PP) and glass fibers were used as a matrix and reinforcement components, respectively. The non-crimp fabrics used in this study were developed in collaboration with TELATEKS™ A.Ş and the properties of the non-crimp glass f/PP fabric are shown in Table 4.1. Aluminum (Al) sheet and aluminum foam with various thicknesses were used to produce sandwich structures in this study. The physical and geometrical properties of the materials used in the experiments are tabulated in Table 4.2. The closed-cell aluminum foam material (supplied by Shinko Wire Company™ Ltd., Austria) with the trade name ALULIGHT-AFS® was employed as core material, as shown in Figure 4.1. The Al foam specimens were cut from the large panels of various foam thicknesses of 8, 20 and 30 mm (Figure 4.2). The foam panels were covered on both surfaces with about 0.6 mm thick and strongly bonded skin, produced during manufacture of the foam. Dupont™ Fusabond® P613, a maleic anhydride modified polypropylene (PP-g-MA) was obtained in granular form. The Fusabond® P613 has a density of 0.902 g/cm^3, and a melting point (T_m) of 162°C. The polypropylene (MH418) which is an injection grade of homopolymer with a density 0.855 g/cm^3 and melting point of 160°C was provided by PETKİM Petrochemicals, Turkey.

Table 4.1. Properties of glass fiber/PP non-crimp commingled hybrid fabrics

Fibers	Tex (g/10000m)	Composition by Weight (%)	Nominal Weight (g/m^2)	Weaving Angle
Glass	300	60	767	$0/90^0$
PP	200	40.0		

Table 4.2. Physical and geometrical properties of materials used in mechanical
test (mean value ± standard deviation).

	Thickness (mm) (+/- standart deviation)	Density (gr/cm^3) (+/- standart deviation)
Al Foam	8 (0.2)	0.409 (0.006)
	20 (1.05)	0.395 (0.003)
	30 (0.1)	0.456 (0.007)
GFPP	0.65 (0.2)	1.254 (0.04)
Al Sheet	2.01 (0.2)	2.7 (0.01)

Figure 4.1. Fabricated ALULIGHT™-AFS foams
(Source: Alulight, 2011)

Figure 4.2. As-received ALULIGHT™-AFS Al foam panels with 8, 20 and 30 mm thickness.

4.2. Production of Layered Structures

This section considers the fabrication of glass fiber reinforced polypropylene composites (GFPP) and sandwich structures with aluminum (Al) foams of various thicknesses in conjunction with skins composed of fiber/metal laminates (FMLs). The FMLs with Al sheet and GFPP composite were integrated with Al foam for composing the sandwich panels. In the subsequent sections, the manufacturing techniques of the layered structures used in this study are described. Various bonding methods and/or surface modification techniques were utilized during this thesis. The Al sheet/Al foam sandwiches were also prepared by bonding the components with an epoxy adhesive for comparing the effect of GFPP on the mechanical performance of the sandwich structures. The adhesives, sandwich configurations and their processing techniques are listed in Table 4.3.

Table 4.3. Adhesive types and surface modification techniques used for the integration of sandwich components.

Sandwich Configuration	Adhesive Type	Surface Modification	Processing Technique
Al foam/Al sheet	Epoxy adhesive	-	Cold pressing at room temperature
Al foam/GFPP composite/Al sheet	-	Silane coupling agent	Hot pressing at 200°C and 1.5 MPa
Al foam/GFPP composite/Al sheet	PP adhesive film	-	Hot pressing at 200°C and 1.5 MPa
Al foam/GFPP composite/Al sheet	PP adhesive film	Silane coupling agent	Hot pressing at 200°C and 1.5 MPa

4.2.1. Production of Glass Fiber Reinforced Polypropylene (GFPP) Composites

Continuous glass fiber reinforced thermoplastic based composite materials were manufactured by compression moulding of hybrid glass fiber/PP non-crimp fabrics. The first step for the composite fabrication was the cutting of fabrics based on the dimensions of the mould as seen in Figure 4.3-a. The mould was transferred to hot press (Figure 4.3-b) and the pressure was applied to the fabrics up to the lamination temperature. In case of heating without application of pressure of the fabrics, it was observed that glass fiber orientations are affected negatively because of the melting and shrinkage of the polypropylene matrix. Considering the melting temperature of PP fibers, the process temperature and the lamination pressure was determined as 200^0C and 1.5 MPa, respectively. After holding at 200°C for 15 minutes, the samples were cooled down to room temperature by water cooling. The manufactured GFPP composites were obtained after removal from the mold (Figure 4.3-c).

4.2.2. Production of Al Foam Sandwiches with Epoxy Adhesive

A commercial epoxy adhesive (Bison®) was applied between the Al face-sheet and Al foam in order to obtain Al sheet/Al foam sandwiches. The surfaces of the face-sheets and core were sanded and then cleaned with acetone before adhesive application. The Al foam and Al sheet were integrated with epoxy and subjected to cold pressing at room temperature. The sandwiches with different thicknesses and their components are shown in Figure 4.4-a and 4.4-b, respectively.

(a)

(b)

(c)
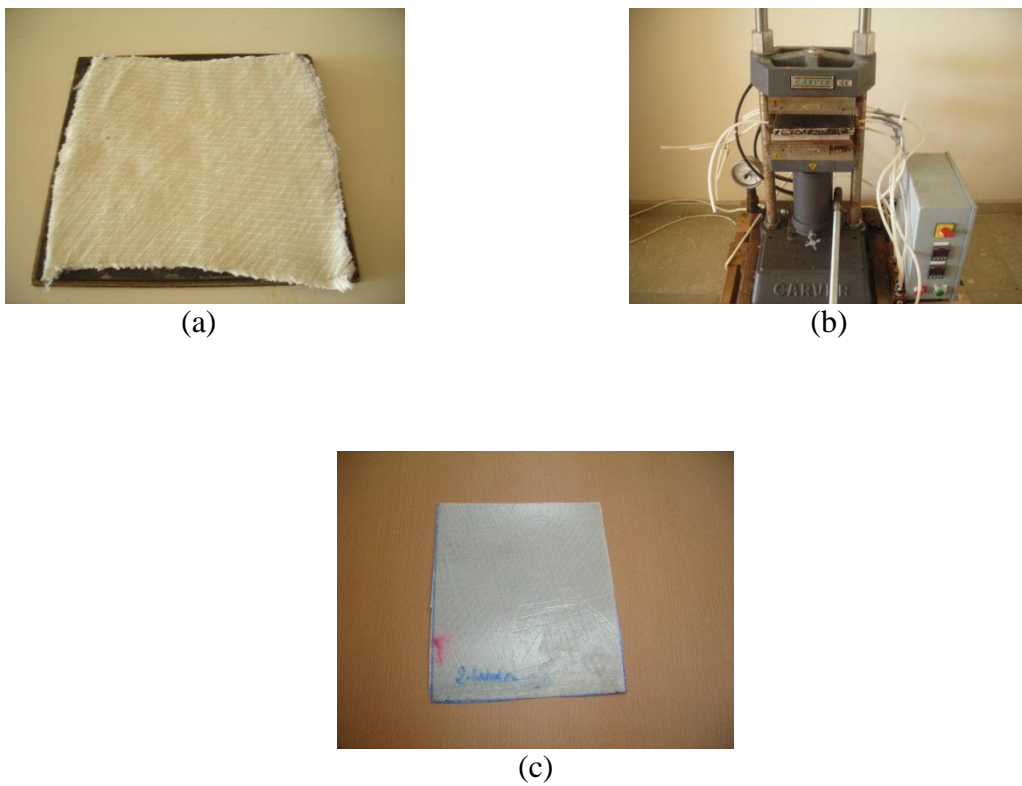
Figure 4.3. Processing steps of GFPP composite: (a) GFPP hybrid non-crimp fabric before compression moulding (b) Hot press and cooling unit used during the GFPP production (c) GFPP composite after compression moulding.
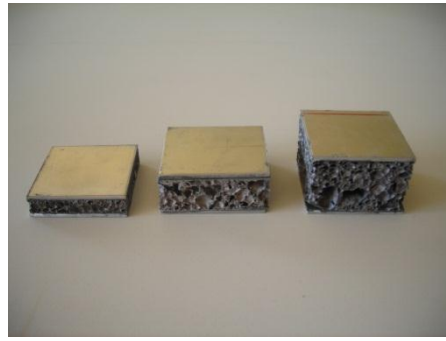
(a)
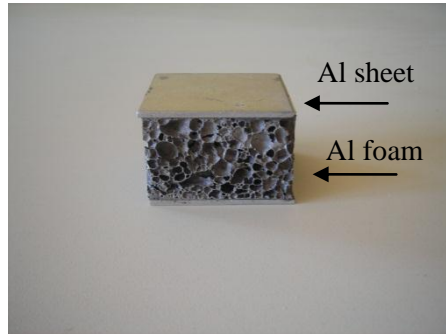
(b)

Figure 4.4. Fabricated Al foam sandwich and its constituents: (a) Al foam sandwiches bonded with an epoxy adhesive with three different foam thicknesses (b) components of Al foam sandwich bonded with epoxy.

4.2.3. Production of Al Foam Sandwiches with Silane Treatment

The non-crimp fabrics consisting of co-mingled glass and polypropylene fibers (GFPP) with a glass fiber volume fraction of 34.5 % were stuck between Al sheet and Al foam as an intermediate layer for producing hybrid Al sheet/GFPP/Al foam sandwich structures. The non-crimp fabrics were developed by Telateks Inc, Turkey and Dr. Tanoğlu's group within another project. Dow-Corning® Z-6032 silane was used for providing robust bonding between GFPP-Al sheet and GFPP-Al foam interfaces. For the surface modification with silane coupling agent, Al sheet and Al foam surfaces were firstly degreased, and then modified with Dow Corning Z-6032 silanes based on the procedure reported by the manufacturer. The silane "surface treatment procedure is schematically shown in Figure 4.5.
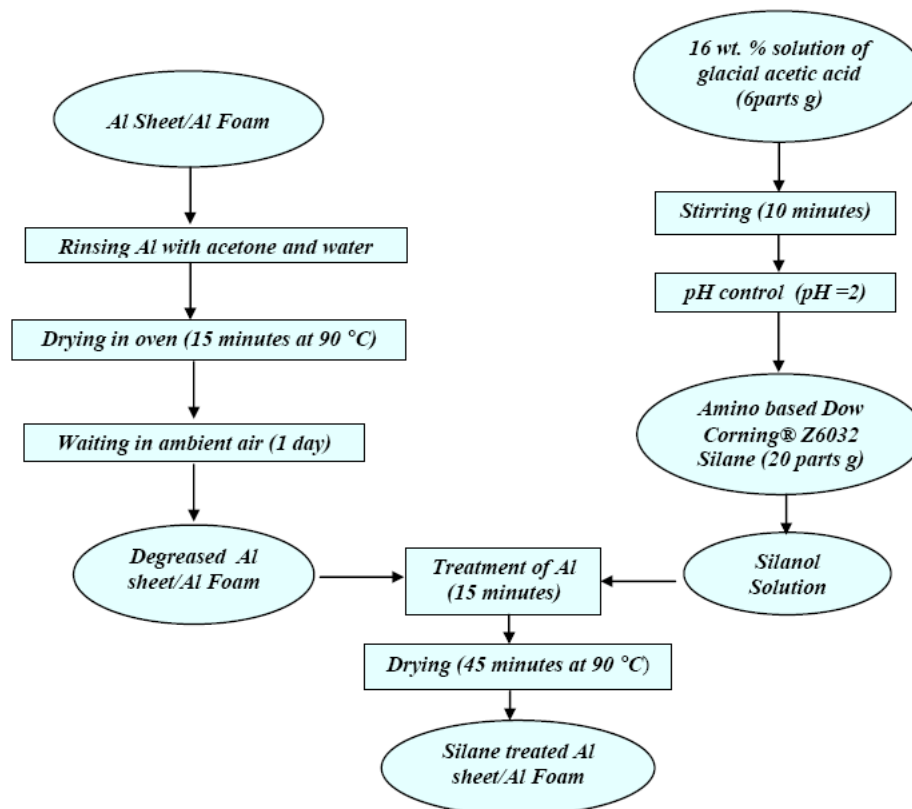
Figure 4.5. Silane surface treatment procedure

As seen in Figure 4.5, the Al surfaces were treated with acetone at room temperature for fully degreasing and rinsed with water for providing a neutral bonding surface. The Al sheets were dried and subsequently held in an air-circulating oven at 100°C for 15 minutes. After waiting for 1 day in ambient air, they became ready to be modified with silane. The 16 wt. % solution of glacial acetic acid was mixed with a ratio of 1 parts glacial acetic acid to 5 parts distilled water under continuous stirring for 10 minutes for the preparation of Z-6032 silane solution. The pH of the solution was set to 2 by the introduction of 20 parts Z-6032 silane coupling agent into to the 16 wt. % solution of glacial acetic acid. The mixture was blended using a mechanical stirrer for 30 minutes. The degreased Al sheets were dipped into the prepared Z-6032 silane solution and they were left in the solution for 15 minutes. After removal of the samples from the solution, the samples were then dried at 90°C for 45 minutes, which is an effective drying cycle for this silane coupling agent. The sandwiches integrated with silane surface treatment and their components are shown in Figure 4.6-a and 4.6-b.

(a)
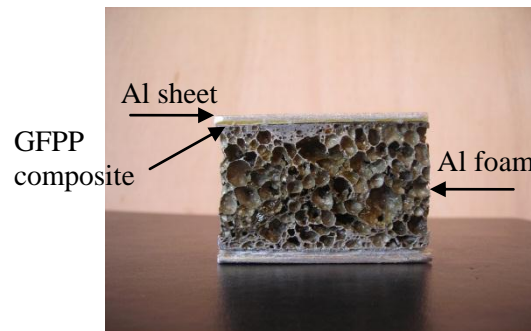
(b)

Figure 4.6. Fabricated Al foam based sandwich bonded with GFPP after silane treatment and its constituents.

4.2.4. Production of Al Foam Sandwiches with PP Based Film

Sandwich structures with modified polypropylene (PP) adhesive layers were also developed in this study. For this purpose, 20 wt. % maleic anhydride modified polypropylene (PP-g-MA) and PP blends were prepared using twin screw extruder (EUROLAB®) as seen in Figure 4.7-a. The produced blend was formed as fine granules and shown in Figure 4.7-b. The cooled blend was pressed at 185°C under the fixed pressure of 1 MPa by hot pressing (Figure 4.7-c) to obtain PP-g-MA based adhesive films with 0.5 mm thickness as shown in Figure 4.7-d. PP-g-MA layer was incorporated at the Al-GFPP interface during the preparation of samples.
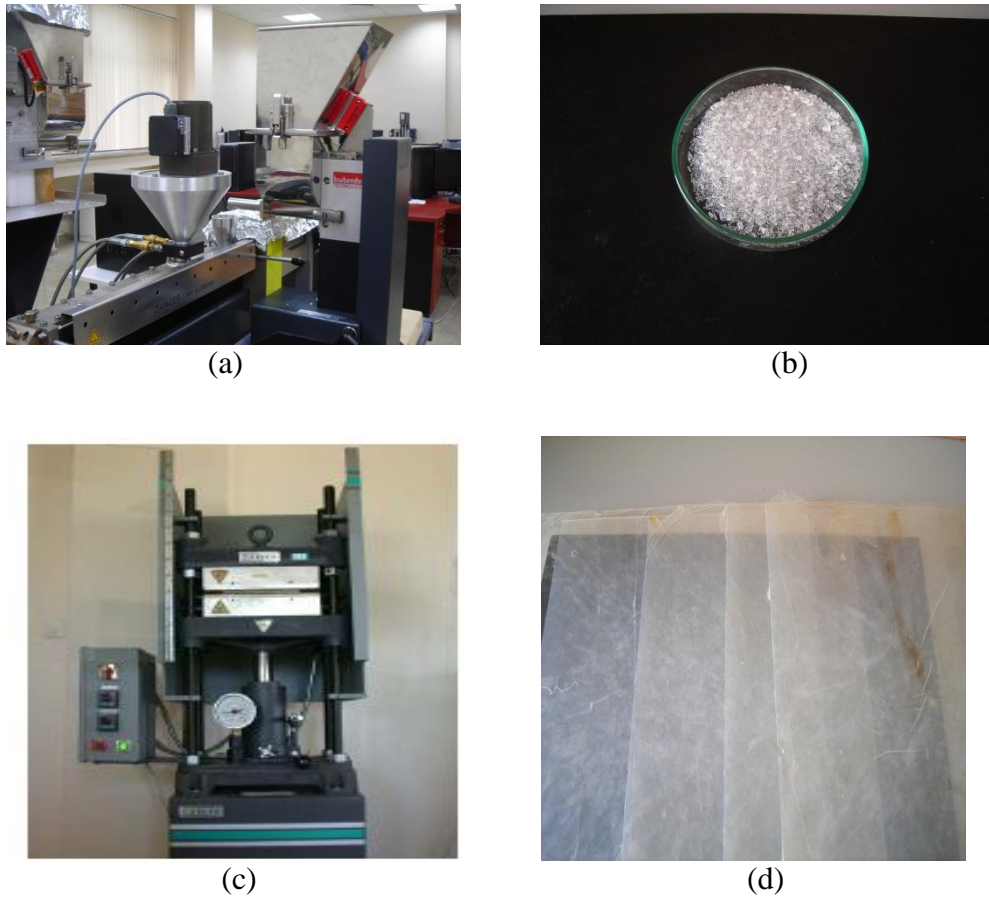
Figure 4.7. Processing steps of PP based adhesive film: (a) Photo of twin extruder (b) Fine granules of PP-g-MA/PP film (c) Photo of hot press (d) Produced PP-g-MA/PP film.

4.2.5. Production of Al Foam Sandwiches Bonded with Silane Treatment and PP Based Film

The combined effect of silane surface modification and PP based adhesive film application on the same sandwich samples was also investigated in this study. The production steps of these sandwiches were the same with the silane treated Al sheet/GFPP/Al foam sandwiches, except the introduction of PP based films. The Al sheet and Al foam surfaces were first treated with silane and then prepared PP-g-MA/PP based films were introduced at the interface of the components during sandwich fabrication. The sandwiches with different core thicknesses were pressed under 200°C and 1.5 MPa. The schematic representation for the processing steps of Al foam based sandwiches is given in Figure 4.8.
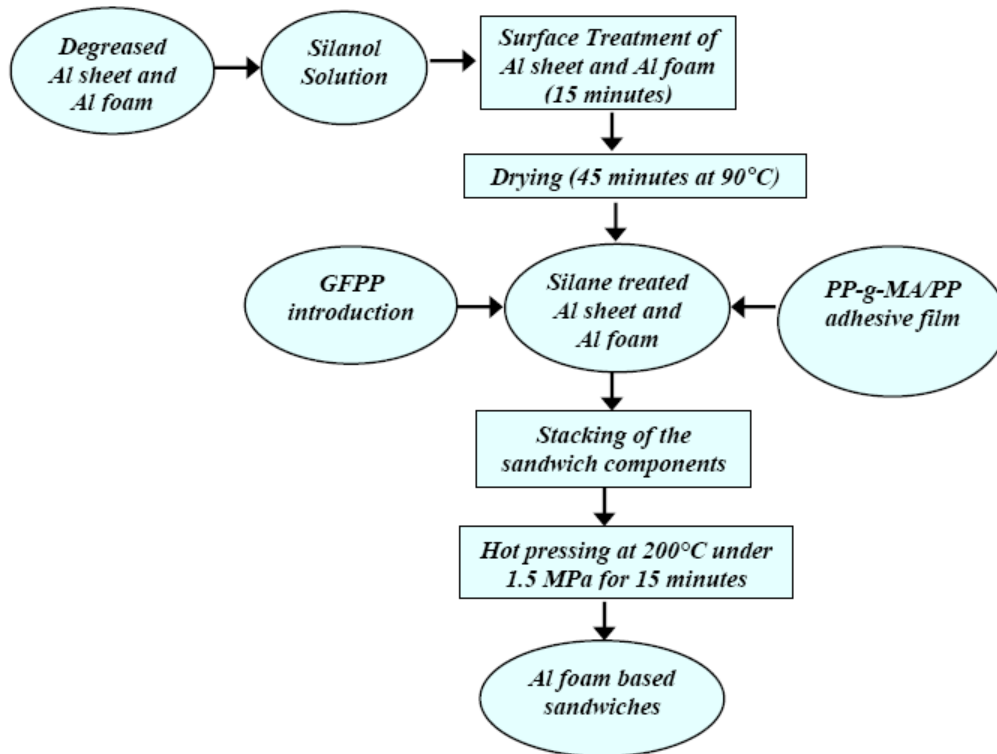
Figure 4.8. Production steps of Al foam sandwiches bonded with silane treatment and PP based film.

4.3. Mechanical Characterization of Aluminum Foams

The mechanical properties of Al foams have great importance for the characterization of Al foam based sandwich structures. The microstructural properties as well as densification behavior significantly affect the mechanical performance of Al foams under various loading conditions. Specifically, the flexural response of test samples strongly influenced by the components of sandwiches in terms of failure strengths and failure modes. In this study, the compression, tension and shear properties of the Al foams were tested and the testing procedures were described in this section.

4.3.1. Compression Testing of Aluminum Foams

The flatwise compression tests were applied to the samples in order to characterize the compression behavior of as-received Al foams and Al foam sandwiches. The compression test samples were prepared with about 50 mm x 50 mm

by sectioning from larger panels. At least three specimens were tested and forces versus stroke values were recorded. All tests were conducted at room temperature with 250 kN loading cell using the Schimadzu™ universal test machine at a crosshead speed of 2 mm/min. In order to reveal the cross-sectional views of Al foams, the samples were also sectioned and their cross-sections were polished. The macroscopic images of the foam based structures were taken using an optical microscope. The 30 mm thick Al foam before loading and at 50% deformation is shown in Figure 4.9-a and 4.9-b, respectively. The formulation of flatwise compressive strength (σ) and strain (ε) are given in equation 4.1 and 4.2, respectively. The *(P)* and *(A)* represent the applied load and cross-sectional area, respectively where *(δ)* is displacement and *(l)* is the specimen thickness. The stress-strain curve of foams show three distinct regions and the elastic module *(E)* of the foams were calculated from the slope of the elastic part of the stress-strain curves.

$$\sigma = \frac{P}{A} \qquad\qquad (4.1)$$

$$\varepsilon = \frac{\delta}{l} \qquad\qquad (4.2)$$

$$E = \frac{\sigma}{\varepsilon} \qquad\qquad (4.3)$$

Figure 4.9. Compression characteristics of 30 mm Al foam: (a) before loading, (b) at 50% deformation

4.3.2. Tension Testing of Aluminum Foams

Tensile tests were performed according to the ASTM C 365-03 standard, in order to determine the flatwise tensile properties that are in a direction parallel to the skin. Three coupons were prepared for each thickness of foams in the form of a prism. The samples had a constant square cross section face area of the specimen was 2500 mm^2. The specimens were adhesively bonded to a specially prepared T-shape steel sections using Bison$^®$ bond epoxy adhesive as shown in Figure 4.10. The purpose of the steel sections is to facilitate gripping during the tension test. The tests were performed using a Schimadzu$^{™}$ universal test machine. The speed of the test was determined as 0.5 mm/min. The longitudinal strain was measured using the extensometer. The strain data as well as the load and stroke of machine were recorded using a data acquisition system. The tensile strength parameters were formulated as in the compression test section and the elastic modules of the foams were calculated from the linear part of the stress-strain curves.

Figure 4.10. Aluminum foam tension test coupons

4.3.3. Shear Testing of Aluminum Foams

Three coupons for each thickness were tested to determine the shear properties of the Al foam cores. The coupons had a constant rectangular cross-section and the length-to-thickness ratio was 12 as recommended by ASTM C273-61. The specimens were adhesively bonded to specially prepared Al/Cr alloy plates by Bison® high bond epoxy matrix, as shown in Figure 4.11. The plates were machined to Schimadzu™ universal test machine and test was carried out by applying tension on the two edges. The longitudinal strain was measured using the extensometer. The shear stress (τ_s) and shear strain (γ) of the foam is calculated according to the formulas given below where (P) is the applied load, (L) and (b) represent the length and width of the specimen, respectively. The shear strain is determined by using the measured relative displacements (r) parallel to the metallic plates divided by the thickness (t) of the specimen.

Figure 4.11. Aluminum foam shear test coupons

$$\tau_s = \frac{P}{Lb} \tag{4.4}$$

$$\gamma = \frac{r}{t} \tag{4.5}$$

4.4. Mechanical Properties of FML Systems and Their Components

The bonding strength of hybrid material systems are considerably critical and affect the service performance significantly. Some test methods are available in the literature for the evaluation of strength properties of hybrid systems. In this part of the study, the interfacial bonding of FMLs were determined by means of lap shear and peel tests. These tests were only applied to the FMLs which were integrated with both silane surface treatment and PP based film addition together. The tests referred above were carried out before by the colleague, Aslı Guruşçu (MSc Thesis, 2009), for each surface modification and adhesive film introduction. In addition, the tensile properties of FMLs and Al sheet were also determined in order to compare the performance of monolithic and hybrid material systems.

4.4.1. Tensile Testing of Aluminum

At least five test coupons with the shape of dog bone type were tested according to the ASTM E 8M-04 standard. The test coupon dimensions were taken as 228 mm long and 12 mm wide. The coupon thickness was that of the skin and Figure 4.12 shows the samples used in tests. Tension test was performed using Schimadzu™ universal test machine with wedge-type mechanical grips. The speed of the test was set to provide a constant strain rate in the gage length of 2 mm/min as recommended by the standards. The longitudinal strain values were measured using extensometer and the data were collected by means of a data acquisition system. Mechanical parameters such as elastic modulus and strength were calculated with the similar formulations given for the Al foam compression/tension testing. The only difference in the tension testing of dog bone type specimens, the strain is calculated by dividing the displacement to the specimen length.
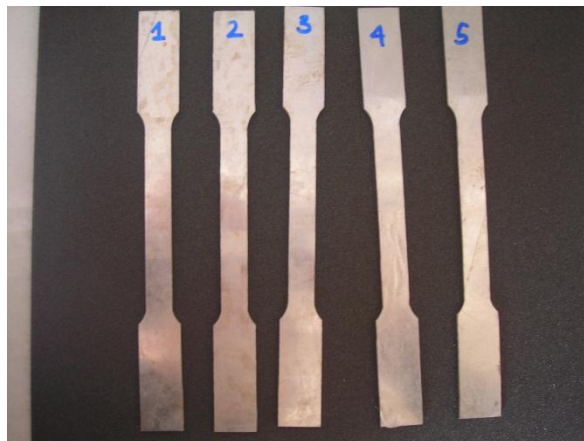
Figure 4.12. Aluminum tensile test coupons

4.4.2. Tensile Testing of GFPP Composite

Tensile test technique, ASTM D 3039M-93 were used to determine tensile strength and modulus of the GFPP composites. Test specimens were prepared using a diamond saw according to ASTM standard. As the composite exhibits similar behavior for 0^0 and 90^0 directions only one direction was tested. At least 5 samples were tested at room temperature using mechanical test machine (Shimadzu™ universal) at a cross

head speed of 2 mm/min (Figure 4.13). Tensile strength, strain and elastic module values were calculated using the equations from 4.1 to 4.3.

Figure 4.13. GFPP tensile test coupons

4.4.3. Tensile Testing of FML Systems

In the literature, the fiber/metal laminates can be used as skin materials for the Al foam sandwiches. In this study, except from the sandwiches integrated with epoxy, the Al and GFPP combination was used as skin material. The tensile test was performed to determine the mechanical properties of this hybrid Al/GFPP system and both Al and GFPP composite were sectioned in the shape of dog bone. The Al sheet was subjected to silane treatment and GFPP layer was bonded to it under 200°C and 1.5 MPa pressure. The Al/GFPP test coupons are shown in Figure 4.14. The mechanical parameters such as strength and elastic module were calculated by utilizing the formulations available for the Al dog bone samples.

Figure 4.14. Al/GFPP tensile test coupons

4.4.4. Lap Shear Testing of FML Systems Bonded with Silane Treatment and PP Based Film

The lap shear test was performed to evaluate the interfacial properties of FMLs bonded with PP based film addition after silane treatment. The specimen geometries of the tensile single lap shear tests were selected based on the ASTM D 3164-03 standard and prepared from 2 mm thick Al sheet and 2 plies of GFPP layers. The lap shear strength values of fiber/metal laminates with different bonding techniques (silane treatment, PP based film addition) were investigated by the colleague, Aslı Guruşçu (MSc Thesis, 2009). In order to increase the effect of bonding between the components of the FMLs, the combination of silane treatment and PP based film addition was investigated in this study. After the application of silane surface modification, Al sheets were integrated with GFPP composite with the addition of PP-g-MA/PP based film. The preparation steps of the test samples are shown in Figure 4.15-a. Lap-shear specimens (20 mm in width) were sectioned from the test panel by a metal saw after hot-pressing of the laminates and displayed in Figure 4.15-b. At least five specimens were tested and shear force-displacement data were collected. The shear strength was calculated based on the maximum load divided by the area of bonded overlap.

(a)

(b)

Figure 4.15. (a) Lap shear test sample preparation steps, (b) produced samples after lamination.

4.4.5. Peel Test of FML Systems Bonded with Silane Treatment and PP Based Film

Peel testing was performed to determine the strength of adhesives in cleavage peel by tension loading. In order to characterize the adhesion between the Al sheet and GFPP composite, the specimens were prepared according to ASTM D3807 standard. The peel strength values of fiber/metal laminates with different bonding techniques (silane treatment, PP based film addition) were investigated by the colleague, Aslı Guruşçu (MSc Thesis, 2009). In this study, the combined effect of silane treatment and PP based film addition into the FML system was tested in cleavage peel under tensile force. Before lamination, Al sheets were cut 26 mm in width and 180 mm in height as shown in Figure 4.16-a and 4.16-b. Laminated test panels consist of two 4 mm thick aluminums and two plies GFPP were bonded according to the procedure described in

lap shear test sample preparation section. A crack approximately 77 mm in length was induced by the placement of a Kapton[TM] film between GFPP and Al sheet before bonding with PP based film. The peel test specimens were sectioned from Al/GFPP composite laminates with 26 mm in width and 180 mm in length. At least five specimens of Al/GFPP composite laminates were tested using the Schimadzu[TM] universal test machine with a crosshead speed of 12.7 mm/min. The load-displacement data were recorded and average peel strength values were calculated by dividing the maximum force value to the corresponding displacement.

(a)

(b)

Figure 4.16. (a) Peel test sample preparation steps, (b) produced samples after lamination.

4.5. Mechanical Characterization of Aluminum Foam Sandwiches

4.5.1. Compression Properties of Aluminum Foam Sandwiches

The compressive characteristics of Al foam based sandwich structures were also investigated in this study. The sandwich structures were integrated by means of four bonding methods: epoxy adhesive, silane surface modification, PP based film introduction and silane surface treatment with PP based film addition. The detailed information was tabulated in Table 4.3 and given in the previous parts of the experimental chapter. The GFPP composite was used as the component of FML skin except the samples bonded with epoxy. Both dimensional properties and test conditions were same with the Al foams and the mechanical parameters were calculated based on the formulations given in the compression testing of Al foam section. The sandwich system before loading and at 50% deformation is shown in Figure 4.17-a and 4.17-b, respectively.

(a)	(b)

Figure 4.17. The Al sheet/GFPP/Al foam sandwich with 30 mm Al foam thickness (a) before loading (b) at 50% deformation.

4.5.2. Flexural Properties of Aluminum Foam Sandwiches

The three point bending test (3PB) according to the ASTM C 393-62 standard was applied to the prepared sandwiches in order to measure the flexural properties such as core shear strength, face-sheet strength and collapse loads. At least three specimens for each type of bonding were tested and force versus stroke values was recorded using

a 100 kN capacity Devotrans® universal test machine at a crosshead displacement rate of 2 mm/min. The total sandwich thickness was calculated by summing the face-sheet and core thickness values as shown in equation 4.6. The core shear *(S)* and face-sheet stress *(F)* values are expressed in equations 4.7 and 4.8. In these equations P is the maximum load, h is sandwich thickness, c represents the core thickness, b is the sandwich width, a_1 represents the span length and f is the face-sheet thickness.

The three point bending test configuration and a fabricated sandwich sample during flexural test are seen in Figure 4.18-a and 4.18-b, respectively. In order to determine the effect of core thickness, the span length and sample length values were fixed as 150 and 200 mm, respectively. Three samples per each thickness were tested and their flexural behaviors were evaluated.

$$h = c + 2f \tag{4.6}$$

$$S = \frac{P}{(h+c)b} \tag{4.7}$$

$$F = \frac{Pa_1}{2f(h+c)b} \tag{4.8}$$

4.6. Energy Absorption Characteristics of Aluminum Foams and Aluminum Foam Sandwiches

The energy absorption capabilities of Al foams and Al foam based sandwiches were also investigated in this thesis. This feature has great importance in terms of the blast application and determination of specific absorbed energies (SAE) of the sandwich structures. The absorbed energies were calculated from the area under the force-displacement curves of the samples and each sample's specific energy was obtained by dividing the energy value to its mass.

The typical load-displacement graph of compression test is shown in Figure 4.19 and $P,$ δ and m parameters used in equations 4.9 and 4.10 represent the load, displacement and mass of the sandwich, respectively. The elastic modulus (E) is

determined from the slope of the elastic part in the stress-strain curve and the collapse stress is defined as the stress at the beginning of the plastic region.

(a)

(b)
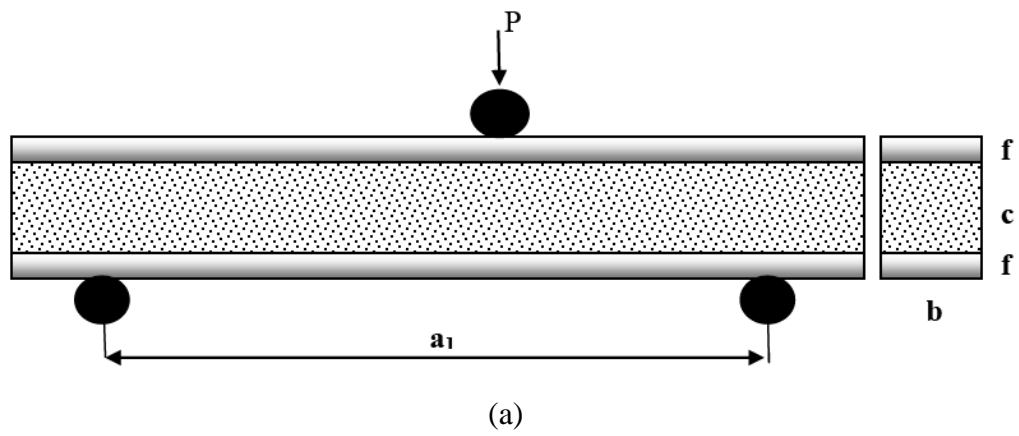
Figure 4.18. Schematic representation and of flexural test samples: (a) three point bending test configuration according to the ASTM C 393-62, (b) flexural test specimen under load.
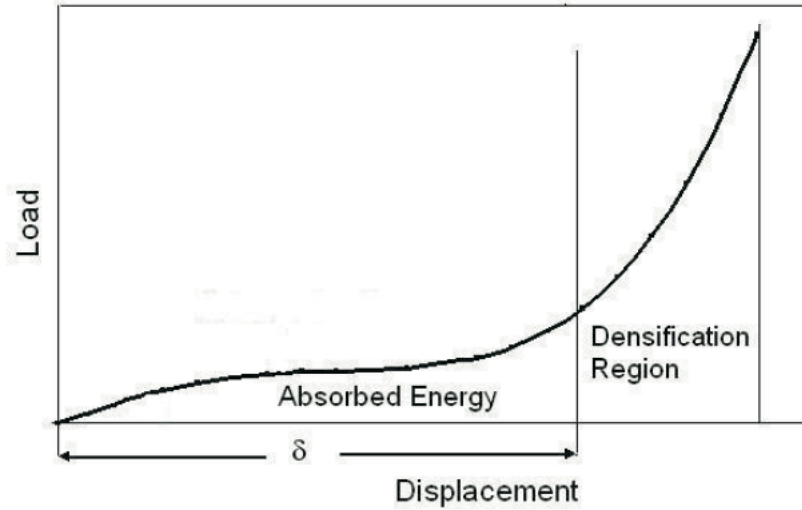
Figure 4.19. Compression load-displacement curve of ideal foam

$$AE = \int_0^\delta P d\delta \qquad (4.9)$$

$$SAE = \int_0^\delta \frac{P d\delta}{m} \qquad (4.10)$$

4.7. Development and Testing of Hybrid Material Systems Against Blast Loading

The hybrid material systems such as fiber-metal laminates (FMLs) and foam based sandwich structures have been studied by many researchers in the literature. The application of these systems provide some advantages in terms of weight reduction and various deformation mechanisms which leads to higher blast and/or impact performance. In this study, both monolithic materials and layered structures were produced and tested by the financial support of TUBITAK-107A014 project and collaboration with partner BARIŞ ELEKTRİK company and Prof. Mehmet Türker's research group at Gazi University, Ankara. The non-crimp glass fiber/PP fabrics (GFPP) used in this study was developed by TEKNOMA Technological Materials Inc. and TELATEKS Inc. of Turkey. The Al/GFPP panels were manufactured in Composite Research Laboratory at IZTECH and subjected to air blast testing. In order to compare

the performance of these systems, some reference commercial products were also tested under blast loading.

4.7.1. Material Systems for Blast Loading

The materials used in this study can be classified into five groups:

- Monolithic materials (aluminum and armor steel)
- Thermoplastic based composites (glass fiber/polypropylene composite, PP based Miliken Tegris)
- Thermoset based composites (glass fiber/vinylester composite, glass fiber/polyester composite, glass fiber/epoxy composite, aramid, PE based Dyneema)
- Fiber/metal laminates (aluminum/glass fiber reinforced polypropylene composite, Al/PE based Dyneema)
- Metal foam based sandwich structures (Al foam/aramid)

The thermoset based polymer composites such as glass fiber/vinylester (GFVE), glass fiber/polyester (GFPE) and glass fiber/epoxy (GFE) were manufactured with vacuum infusion technique with the exception of aramid. The thermoplastic based composites and Al/GFPP fiber-metal laminates were produced via hot pressing technique while the Al foam based sandwich components were bonded by using a proper adhesive. The test samples were produced as 500 mmx500 mm and their images are shown in the Figures from 4.20 to 4.24.
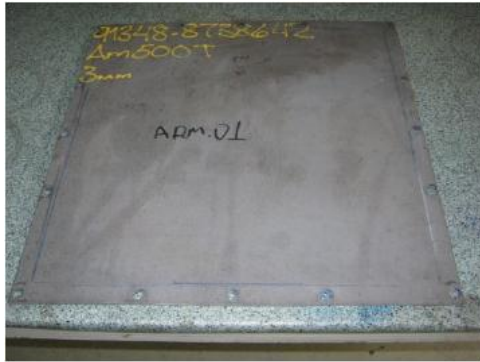
(a) (b)

Figure 4.20. The images of monolithic reference materials before blast testing: (a) Armour steel (b) Aluminum
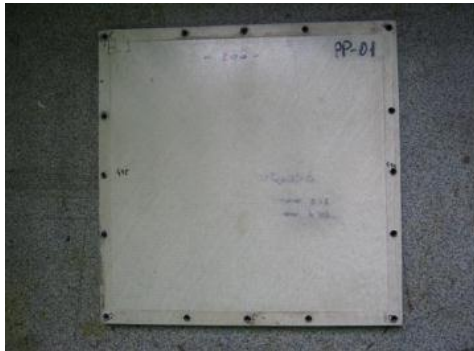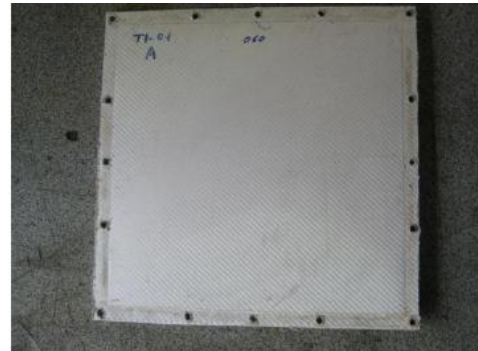
(a) (b)

(c)

Figure 4.21. The images of thermoplastic based composites before blast testing: (a) GFPP composite (b) PP based Miliken Tegris (c) Polyethylene based Dyneema composite.

Figure 4.22. The images of thermoset based composites before blast testing: (a) GFVE composite (b) GFPE composite (c) GFE composite (d) Aramid composite.

Figure 4.23. The images of FML systems before blast testing: (a) Al/GFPP system (b) Al/Dyneema system

Figure 4.24. The image of Aramid/Al foam sandwich before blast testing

4.7.2. Design of Blast Test Apparatus

The design of test apparatus and shape of the explosive have critical importance in terms of the blast test results of the specimens. The sandwich panels were subjected to air-blast loading in order to detect the pressure effect of the explosive on the samples. The C4 was used as plastic explosive during the tests and spherical type of geometry was selected. The mold of explosive and its carriage support used during the tests are given in Figure 4.25 (a) and (b), respectively. In order to fix the test samples, the 50x50x5 mm and 50x50x3 mm square type of module profiles were designed and prepared as seen in Figure 4.26. The lower modules were welded with supporters and back fillet frames were manufactured from the metal sheets with respect to the specimen thicknesses. One kg C4 was used and the stand-off distance (the distance between the specimen and explosive) was determined as 55 cm.

(a)
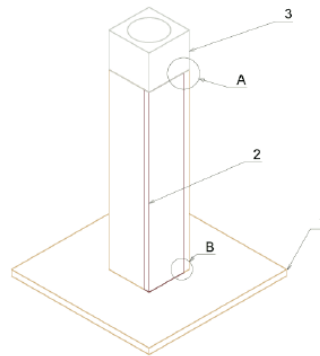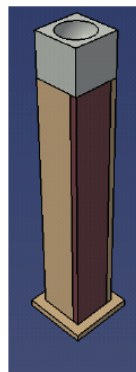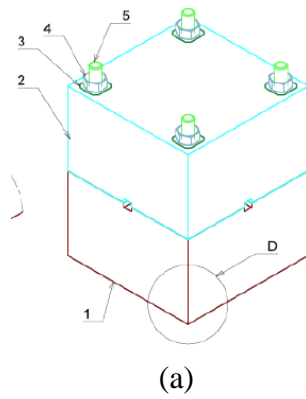
1: base plate	
2: vertical body	
3: foam	
A,B: linkage surface	

(b)

Figure 4.25. The computer models of blast test apparatus: (a) Mold of spherical explosive (b) Explosive carriage support

(a)   (b)
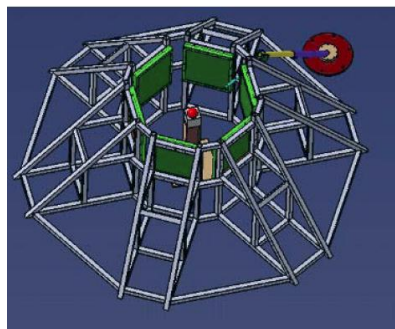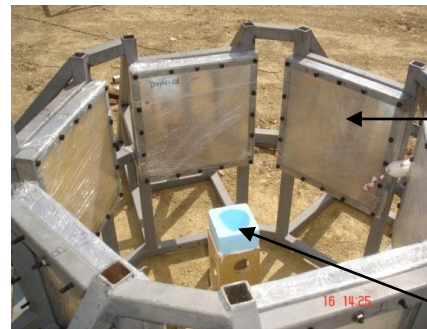
Figure 4.26. The air-blast test apparatus images: (a) Computer model of test apparatus (b) Real test apparatus

Some numerical analyses were performed by using LS Dyna CONWEP module to determine the pressure-time history of the blast loading according to the explosive amount and stand-off distance parameters. In Figure 4.27, the simulation was carried

out for 1 kg C4 (1.37 kg equivalent TNT) and the stand-off distance was varied from 0.2 m to 2.5 m. Similar type of simulation was performed by varying the explosive amount from 0.1 kg TNT to 12 kg TNT as seen in Figure 4.28. Based on these figures, the decrease of stand-off distance or increase of TNT amount significantly promote the effect of blast loading.
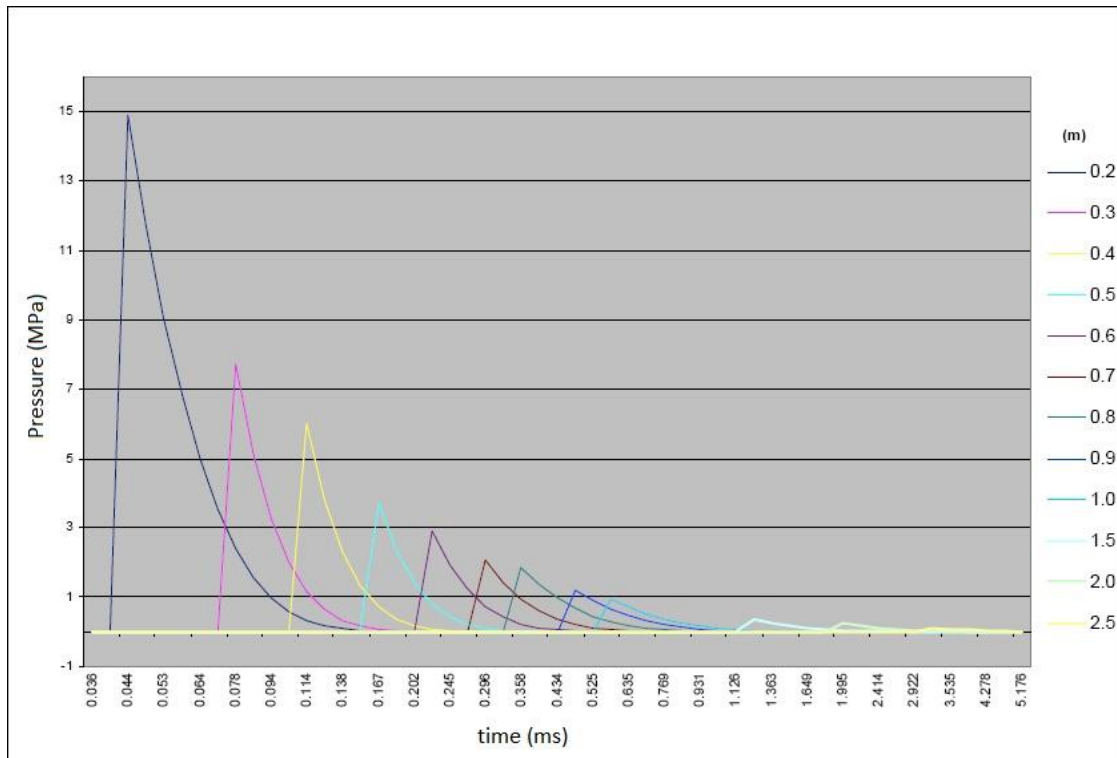
Figure 4.27. The pressure versus time variation according to the stand-off distance. The graphs were obtained using LS-Dyna CONWEP Module for 1.37 kg TNT explosive.
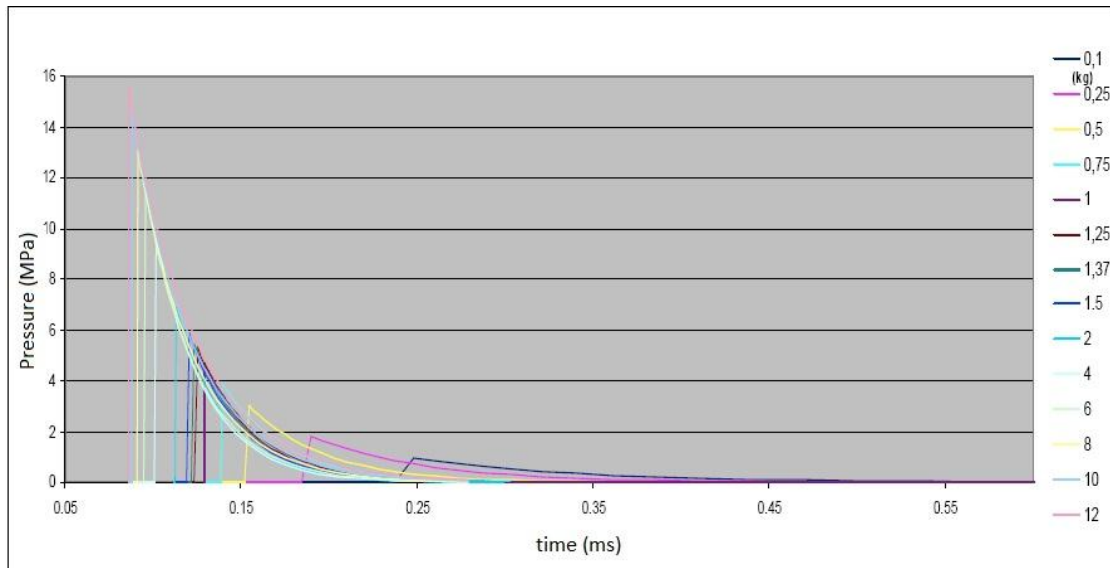
Figure 4.28. The pressure versus time variation according to the TNT explosive amount
The graphs were obtained using LS-Dyna CONWEP Module for 45 cm
stand-off distance.

4.8. Experimental Set Up for Panel Analysis under Simulated Blast Testing

This study considers the situation of air blast loading of sandwich structures with Al foam core and FML skins. In this study, the quasi-static loading was applied to the sandwich panels with three foam thicknesses (8, 20 and 30 mm). The 500 mm x 500 mm Al foam structures were sectioned from larger panels and the Al sheet/GFPP FML system was integrated with PP based film under 200°C and 1.5 MPa pressure. The produced sandwich structure was cut with a jigsaw and divided into four equal parts with the dimension of 250 mm x 250 mm.

The sandwich was considered as a single degree of freedom mass-spring system that allows simulating the effect of blast loading on the panels. The simply supported boundary conditions were assumed in the analysis and the distance between the supports was measured as 226 mm. The system had three main components: upper support frame, a liquid soap filled rubber bladder and a lower frame. The sandwiches were located in the lower frame and the support frame acting as simple support boundary condition to the samples. The supports were made out of split cylindrical rods that were welded on to the frame. Lower frame protected the sandwich and bladder

during testing. The liquid soap filled rubber bladder was placed under the aluminum foam sandwich to provide uniformly distributed load over the surface of the panel. The pressure is controlled by operating the compression test machine; hence the variation of the load that presses the sample against bladder was monitored. The linear variable differential transformer (LVDT) was used in order to detect the central deflection of the panels under compressive loading. An extra apparatus was manufactured to protect the LVDT measurement system and placed upon the upper support frame. A rigid steel plate was also located on to the LVDT protection apparatus for homogeneously distribute the load from the compression test head to the whole system. Technical drawings of the frames and manufactured test rig are seen in Figures 4.29 and 4.30 while the components of the simulated blast test configuration are shown in Figure 4.31. The prepared sandwich panels with various thicknesses are also exhibited in Figure 4.32. The simulated blast tests were conducted at room temperature with 250 kN loading cell using the Schimadzu™ universal test machine at a crosshead speed of 5 mm/min. Maximum applied load was determined as 200 kN for the test panels. The calibration voltage value of the LVDT was 10 V and each deflection data was collected per 20 msec time interval.
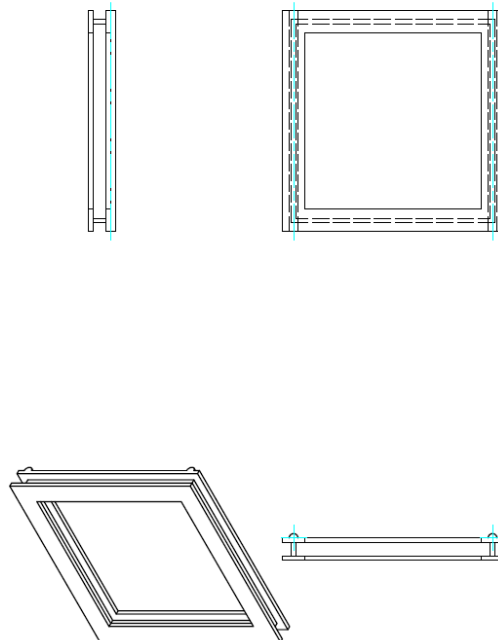
Figure 4.29. Technical drawing of upper support frame
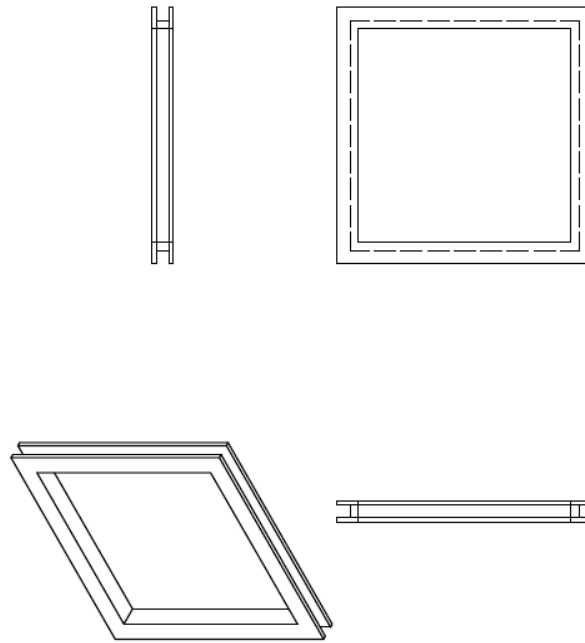
Figure 4.30. Technical drawing of lower frame
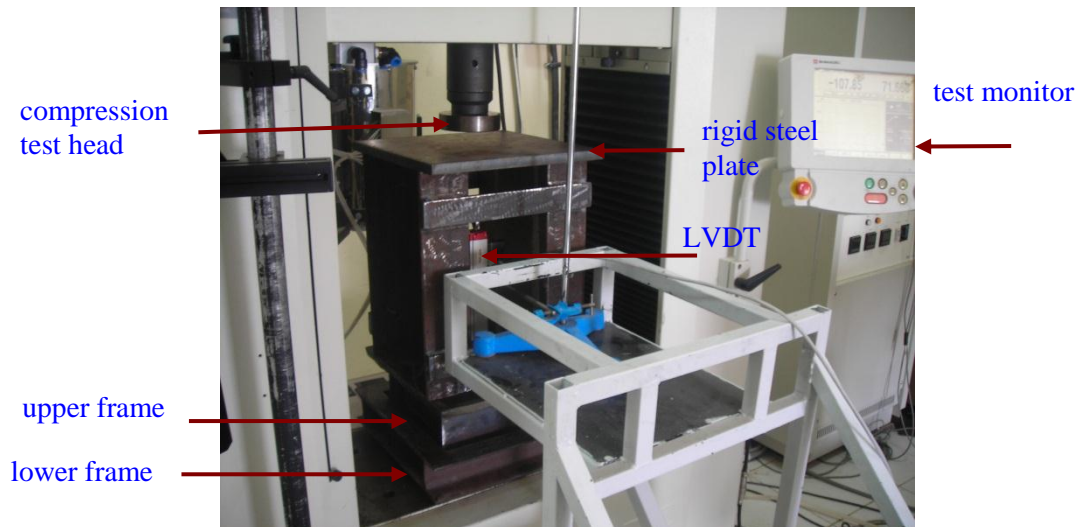
Figure 4.31. Simulated blast test apparatus

(a)

(b)

(c)
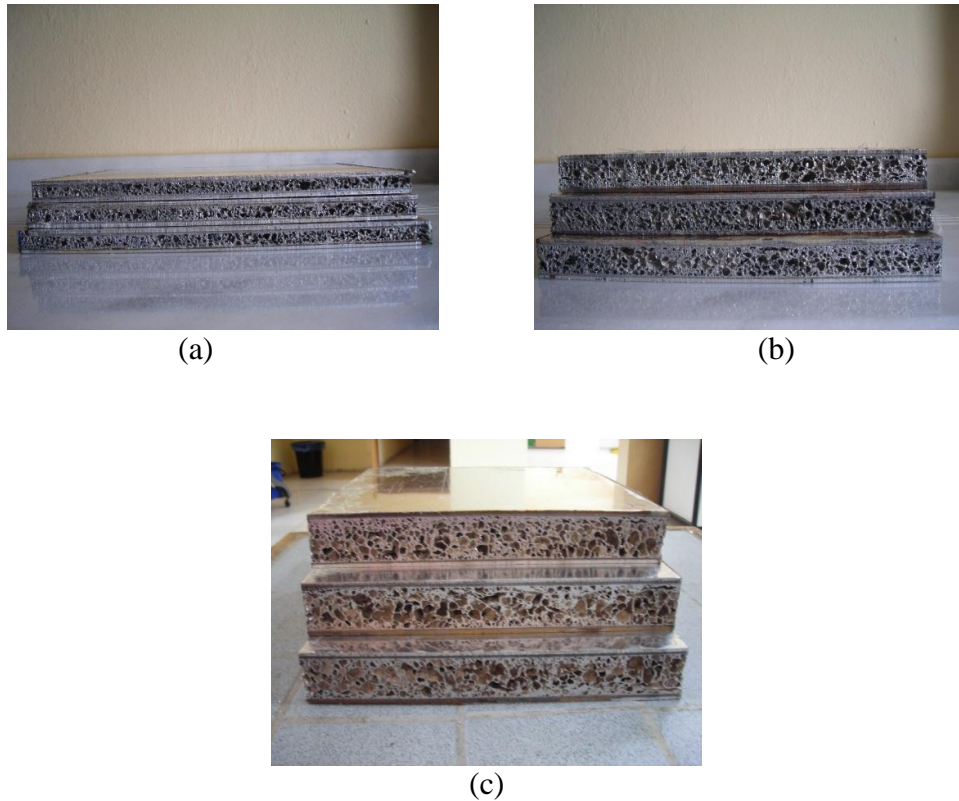
Figure 4.32. The prepared Al foam sandwich panels with various thicknesses: (a) 8 mm Al foam sandwich panel (b) 20 mm Al foam sandwich panel(c) 30 mm Al foam sandwich panel.

4.8.1. The Blast Response Evaluation of Sandwich Panels under Simulated Blast Test

4.8.1.1. Natural Frequency of the Sandwich Panel

In the simulated blast test analysis, natural frequency (ω) for the lowest mode of the panel should be considered. Other parameters like θ and ρ^* can be calculated by using the equations 4.11 and 4.12. The constants L_1 and L_2, E_f, h_f, h_c, d, v_f, G_c, ρ_c and ρ_f represent panel dimensions, face-sheet elastic modulus, face-sheet thickness, core thickness, face-sheet and core thickness summation, face-sheet Poisson ratio, core modulus, core density and face-sheet density, respectively (Andrews, 2009).

$$\omega = \pi^2 \left[\left(\frac{L_2}{L_1} \right)^2 + 1 \right] \sqrt{\frac{\dfrac{E_f h_f d^2}{2\rho^* L_2^4 \left(1 - v_f^2 \right)}}{1 + \pi^2 \theta \left[\left(\dfrac{L_2}{L_1} \right)^2 + 1 \right]}}.$$ (4.11)

$$\theta = \frac{E_f h_f h_c}{2 G_c L_2^2 \left(1 - v_f^2 \right)} \quad , \quad \rho^* = \rho_c h_c + 2\rho_f h_f$$ (4.12)

4.8.1.2. Compliance of the Sandwich Panel

Compliance expressions of the panel has critical importance for the simulated blast analysis. The compliance term is defined as the ratio between the central deflection of the panel and corresponding applied pressure, which is called as p_0. Basically, two deflection components affect the total central deflection (w_t): bending term (w_b) and shear term (w_s). Therefore, the effective compliance of the panel denoted as C_p can be formulated by implementing both bending and shear deflection terms as in equation 4.13. In our analysis, total deflection terms of the panels were determined from the sensitive LVDT measurements and these results were used to determine the final deflections under blast loading conditions (Andrews, 2009).

$$C_p = \frac{\left(w_b + w_s \right)}{p_0} = \frac{w_t}{p_0}$$ (4.13)

4.8.1.3. Blast Wave Representation

In simulated blast test analysis, the blast pressure is represented with its characteristic pressure-time response as shown in Figure 3.2. Based on this figure, when the blast wave hits to the panel it suddenly run up to a peak value with an exponential decrease. The pressure–time history $P(t)$ can be defined as in equation 4.14:

$$P(t) = P_{max} e^{-t/T}$$ (4.14)

where P_{max} is the maximum blast pressure, t is time and T is the characteristic time specifying the decay of the blast pressure. The blast impulse, which is the time integral (from $t=0$ to ∞) of the pressure–time response, is equal to $P_{max}T$ (Andrews, 2009).

4.8.1.4. Single Degree of Freedom (SDOF) Analysis

In the general blast analysis, the imposed load shows dynamic properties, however, the system that has been under this load shows a static characteristic. It is assumed in our analysis that the panel can be idealized as a single degree of freedom (SDOF) mass-spring system in order to predict its response under dynamic pressure loading. The deformation behavior of structures under blast loading can be predicted by this basic assumption which was presented by Baker and usually resulted in realistic results. Based on the analysis of the differential equation controlling this simple system, the peak deflection δ_{peak} of the panel under the dynamic pressure loading is equal to the quasi-static deflection that would be seen under the maximum blast pressure P_{max}, multiplied by $f(T\omega)$ product. The "T" is the blast characteristic time and "ω" is the natural frequency of the panel. The effective panel compliance expression given in Eq. 4.13 is used to calculate the static deflection term (δ_{static}) with the knowledge of maximum blast pressure P_{max}. Thus we may represent the peak deflection as in equation 4.15 (Andrews, 2009).

$$\delta_{peak} = \delta_{static} f(T\omega) \qquad (4.15)$$

Figure 3.21 represents the dimensionless deflection $\delta_{peak}/\delta_{static}$ (function f) with respect to $T\omega$ product. According to this graph, if the blast durations are very long as compared to the natural period of the system ($T\omega$ product high) the peak deflection reaches a constant value which is equal to twice of the static deflection (δ_{static}). Otherwise, for shorter blast durations ($T\omega$ product low), the dimensionless deflection term equals to the $T\omega$ product which is lower than the constant value observed for higher $T\omega$ values. By considering this information if the duration is short, the system can hang on higher pressures. In order to evaluate the panel failure, the predicted peak deflection is compared with the deflection at which failure takes place (Andrews, 2009).

CHAPTER 5

RESULTS AND DISCUSSIONS

5.1. Mechanical Properties Al Foams

The mechanical properties of the components significantly affect the performance of hybrid structures. In order to reveal the characteristics of sandwiches, the compression, tension and shear features of Al foams were tested and the results are evaluated from section 5.1.1 to 5.1.3.

5.1.1. Compression Properties of Al Foams

The stress-strain behavior of as received (monolithic) Al foams with three different thicknesses were obtained based on the compression test. Figure 5.1 shows the stress-strain curve of foams with respect to the deformations up to 60% strain. At least three specimens for each thickness were tested and typical representative data for each thickness set of foams are plotted. The average mechanical properties such as elastic modulus and collapse strength are tabulated in Table 5.1. It is the fact that the densities and the morphological features of the foams showed close relation with the densification behavior of the samples. It is obvious from the figure 5.1 that the stress-strain curve initially increases almost linearly up to a specific value of the compressive stress and then the stress remained almost constant up to a certain value (plateau region). The densification region started as the completion of the plateau region. The collapse of foam cells ends and they start to densify at a specific strain. As the density of the specimen increases, the plateau region begins to shorten and densification starts at lower strains. Based on the Figure 5.1, the stress values of foams at the same displacement vary based on the thickness change. The foams with similar density for each thickness were compared in Figure 5.1 to investigate the mechanical property variation. Although the density difference was smaller than 21 %, the 8 mm Al foams showed significantly higher collapse strength and lower elastic modulus. The foam

thickness increase resulted in the increase of elastic modulus for the as-received Al foams. It was also revealed from the experimental results that some foams with higher densities showed higher elastic modulus and/or collapse strength values while some of them exhibited the opposite characteristics. A direct correlation was not observed between these parameters due to the variations in foam cell shapes, subsistent defects, density and non-homogeneities of the microstructures.

The effect of the foam thickness on the collapse strength of the foam structures was also investigated by considering the test results and it was found that the foam thickness increase generally resulted in collapse strength decrease. As the thickness increases, the structural defect probably increases and the lower strength values of thicker foams are attributed to this. In the literature, similar type of response was observed by Idris et al. They investigated the compression characteristics of ALPORAS[®] and ALULIGHT[®] foams by considering the foam thickness. They noticed that the ALPORAS[®] samples did not show thickness dependency, however, the collapse stresses of ALULIGHT[®] foams decreased with the increase of foam thickness.

Table 5.1. Physical and mechanical properties of as-received Al foam compression test samples. (The average values are given with standard deviations)

Foam Thickness	Average Density (gr/cm^3)	Average Elastic Modulus (MPa)	Average Collapse Strength (MPa)
8	0.329 (0.03)	29.06 (4.79)	2.07 (0.46)
20	0.416 (0.02)	36.21(4.48)	1.11 (0.06)
30	0.381 (0.06)	54.61 (10.85)	1.15 (0.66)
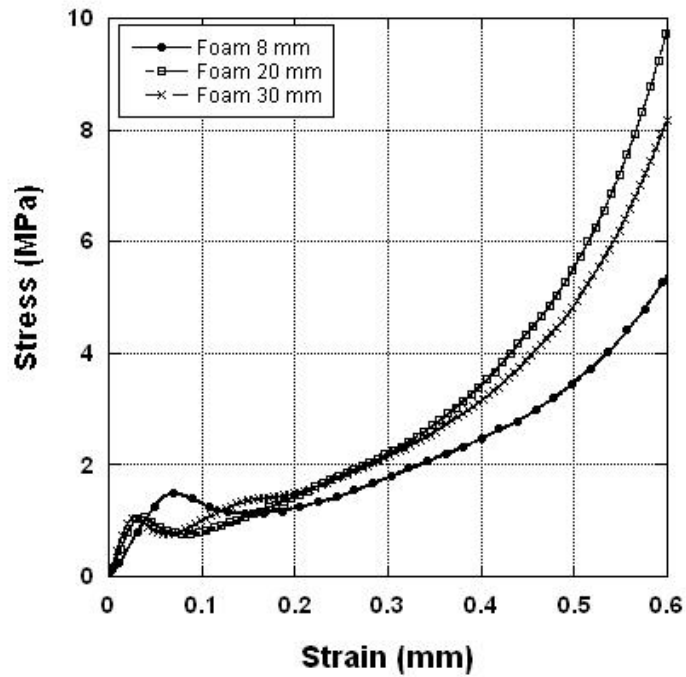
Figure 5.1. Compressive stress versus strain curves of as received Al foams
with three different thickness.

The typical views of Al foams with 8, 20 and 30 mm thicknesses before and after compression test are shown in Figure 5.2. In this figure, the densification of foams at 60% deformation is showed. During compression test, the cell walls are compressed against to each other and touch to close pores with a dramatic porosity decrease. The deformation steps of 30 mm thick Al foam as a function of percent strain are displayed in Figure 5.3. After the initiation of the first collapse, both deformed and undeformed zones are existent in the foam structures. Some cells were found to collapsed while the rest of them were still elastic and two strain states were present at nearly same stress. As it is seen in Figure 5.3, the deformation was localized from the locations of the largest cell size or the lowest density exhibited by the white arrow at 0 % strain.
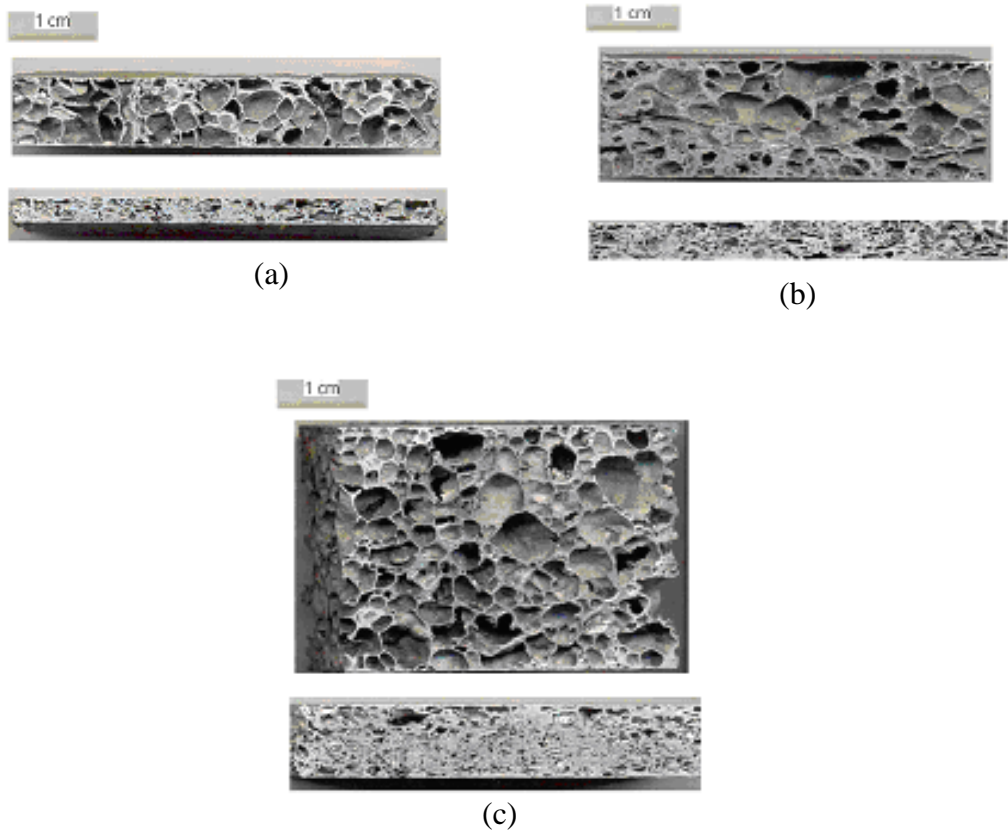
Figure 5.2. Deformation views of as-received Al foams: (a) 8 mm as-received Al foam compressed at 75% strain, (b) 20 mm as-received Al foam compressed at 70% strain, (c) 30 mm as-received Al foam compressed at 70% strain.

0 % strain

6.6 % strain

13.3 % strain

20 % strain

26.6 % strain

33.3 % strain

Figure 5.3. The compressive deformation steps of Al foam sample at various strains.

(Cont. on next page)

40 % strain   46.6 % strain

53.3 % strain   60 % strain

Figure 5.3.(Cont.)

As the strain increased, the deformation localization propagated along the undeformed regions of the foam. As seen in Figure 5.3, cell collapse developed by plastic yielding of the cell walls through the deformation bands and deformation occurred perpendicular to the compressive stress direction as seen at 6.6 % strain. The more increase of strain led to the decrease of distance between the deformed and undeformed regions as can be seen from deformation steps of Figure 5.3. As the compression continued, the deformed structure began to closer and cell crushing occurred.

In the literature, all the foams are characterized in terms of their density, cell morphology and cell wall properties. Characterization of cell morphology included the geometrical features such as the distribution of cell wall thicknesses and cell sizes. In order to reveal the microstructures of the sandwiches, the samples were sectioned and their cross-sections were polished. In this study, the macroscopic images of the foams and foam based structures were taken using Nikon™ optical microscope. The microstructures of as-received Al foams before and after compression test are seen in figures from 5.4 to 5.6. The deformation mechanisms of foams were determined considering the optical microscope results. As it is known that, the foams at low deflection deform almost elastically and cell walls bend. With the increase of compressive stress, the cell edges bend and/or buckle. This results in the stretching and crushing of the cell walls as seen in the figures below. Localized zones have shown that the main deformation type in the foams was cell wall bending independent of thickness.

(a)   (b)
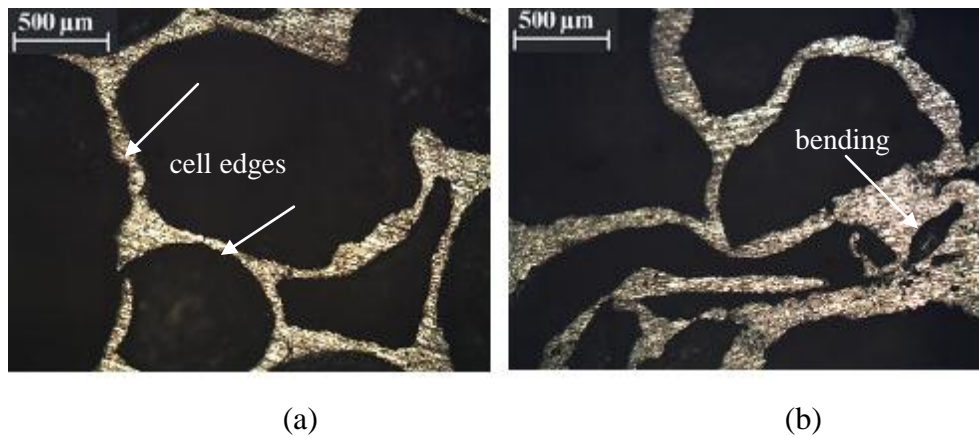
Figure 5.4. Microstructural images of 8 mm Al foam: (a) before compression, (b) after compression.
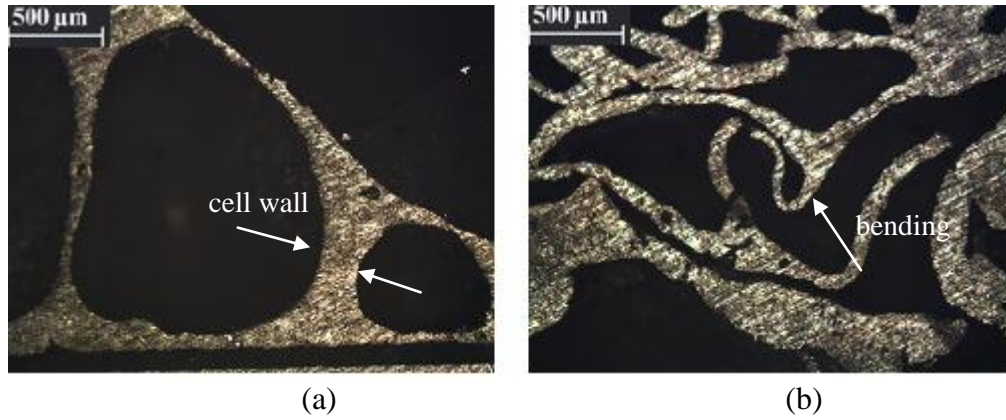
Figure 5.5. Microstructural images of 20 mm Al foam (a) before compression (b) after compression.
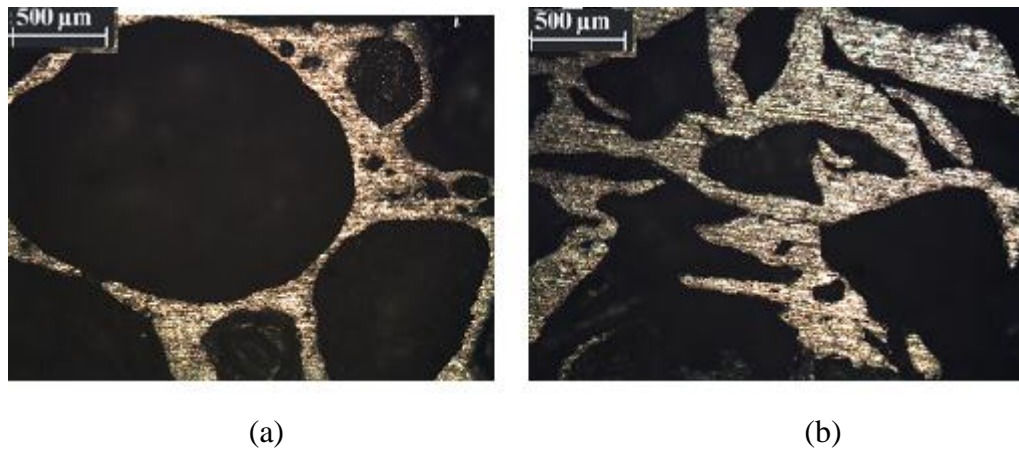
Figure 5.6. Microstructural images of 30 mm Al foam (a) before compression, (b) after compression.
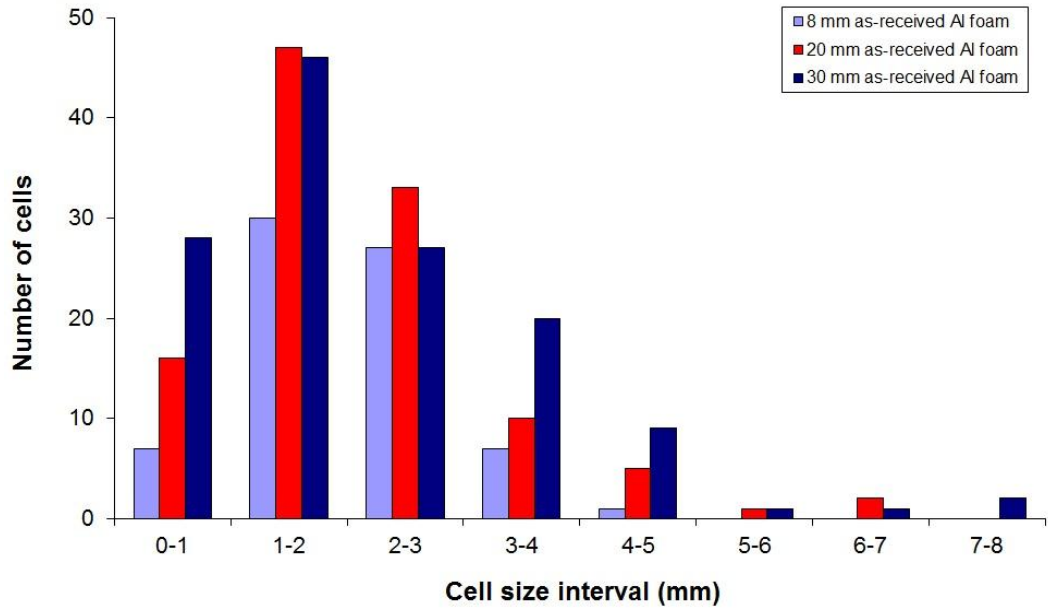
Figure 5.7. Cell size distribution of as-received Al foams with respect to number of cells.
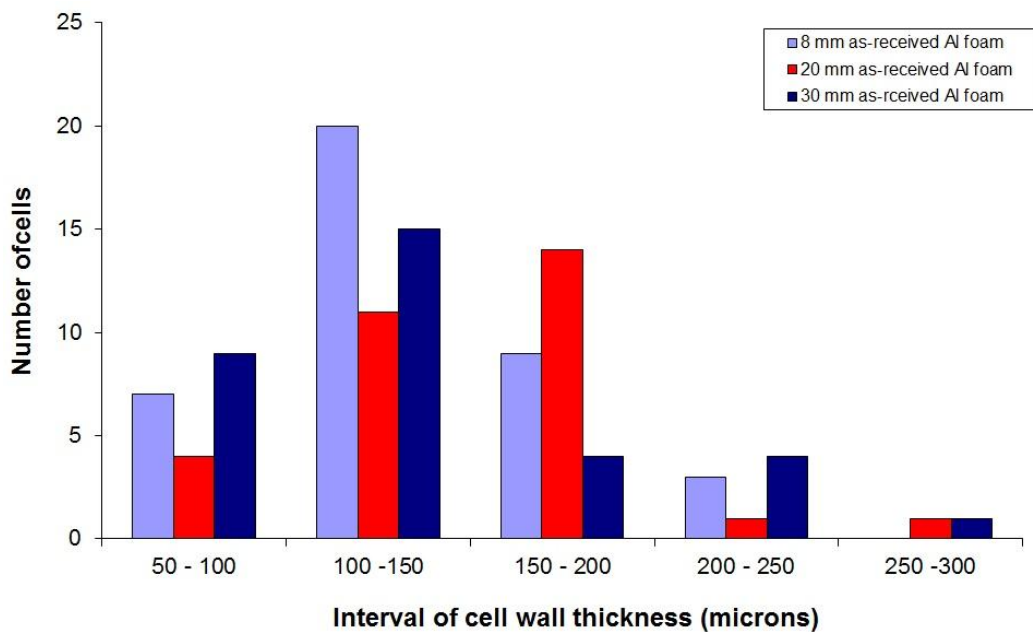
Figure 5.8. Cell wall thickness distribution of as-received Al foams with respect to number of cells.

The cell size distribution of Al foams with different thickness is given in Figure 5.7. It was found that the cell sizes in the range of 1-3 mm are significantly higher

compared to the other sizes for 8 mm thick Al foams. Similar situation is also valid for the 20 and 30 mm thick Al foams. The cell sizes higher than 5 mm were rarely observed in the structures. Another critical term in the foam structures is the cell wall thickness. This value prominently affects the elastic region and compressive modulus of the structure. For 8, 20 and 30 mm foams, the cell wall thickness values are compared in Figure 5.8. The cell wall sizes were found to be in the range of 50-200 microns is significantly observed for 8, 20 and 30 mm thick foams.

5.1.2. Tensile Properties of Al Foams

Based on the force-deflection data, the stress-strain behaviors of Al foams were determined. The average density, elastic modulus and ultimate tensile strength values of test coupons are tabulated in Table 5.2. The samples before and after test are shown in Figure 5.9-a and 5.9-b, respectively. The typical tensile stress-strain responses of the foams per each thickness are exhibited in Figure 5.10. The data of Al foams showed highly scattered behavior under tension loading so that the curve fitting option was carried out. The density values of tensile test coupons showed similarity with the compression test samples. However, a significant difference between the elastic modulus values of compressive and tensile test samples was observed. In the literature, some researchers found the tensile elastic modulus of the Al foams higher than compressive modulus. Motz et. al (2001) reported that the Young's modulus in compression for the same density is about two to four times smaller than the Young's modulus in tension at small strains. This can be attributed to the deformation and collapse mechanism difference under different loading conditions. In the mechanical tests of the foams, the variation of elastic modulus and/or yield strength does not only depend on the density but also imperfections and microstructural nonhomogenities affect these parameters. During the tests, some foams with higher densities showed higher elastic modulus and/or yield strength values while some of them exhibited the opposite response. Particularly, the foams with the highest density for each thickness set generally showed maximum ultimate tensile strength values.

It was found that the foam thickness increase resulted in the decrease of yield strength and increase of elastic modulus. As compared to the compressive strength results, the ultimate tensile strength magnitudes decreased for each thickness set of

foams. According to Figure 5.10, the curves showed linear elastic behavior at a strain rate of roughly 0.01, smaller than in compression followed by plastic yielding. For the closed cell Al foams, bending of cell edges are accompanied by stretching of the cell faces during compression. However, in tension test, the foams show local fracturing and failed at low applied strains due to the highly defective and thin cell faces.

Figure 5.9. Al foam samples subjected to tensile testing: (a) 20 mm Al foam during tension test, (b) Test coupons after test tension test.

Table 5.2. Physical and mechanical properties of tensile test foam samples. (The average values are given with standard deviations)

Foam Thickness	Average Density (gr/cm^3)	Average Elastic Modulus (MPa)	Average Tensile Yield Strength (MPa)
8	0.346 (0.02)	92.58 (47.3)	2.01 (0.3)
20	0.376 (0.04)	170.65 (52.4)	1.21 (0.19)
30	0.332 (0.03)	239.7 (22.61)	0.87 (0.15)
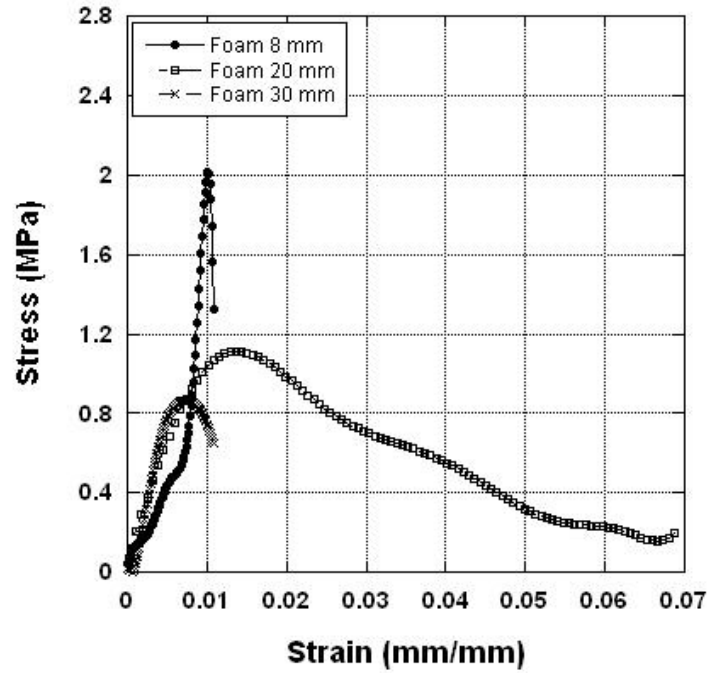
Figure 5.10. Typical tensile stress versus strain graphs of as received Al foams with three different thicknesses.

5.1.3. Shear Properties of Al Foams

In the literature, the shear characteristics of Al foams are limited. As it is well known that the generation of pure shear is rather difficult on the cellular materials. In this study, the shear stress was developed by the application of tensile stress from the loading plates. As the strain increased, the plates moved crossed to each other and the foam began to separate. The samples before and after test are exhibited in Figure 5.11-a and 5.11-b, respectively. Figure 5.12 shows the typical stress-strain relationship of the tested Al foams. Shear strength and shear modulus values were calculated according to the ASTM C273 standard. The shear stress was determined based on the applied load divided by the sample area and the shear strain was calculated by using the measured relative displacements obtained from extensometer divided by the foam thickness. Measured mechanical properties of the foams are rather scattered due to the inhomogeneous nature of the Al foams. Fractures occurred at the interface between foam and loading plate and the failures, which existed in the bond between the loading plates, were not considered.

As shown in Table 5.3, the shear strength and shear modulus values of the 8 mm Al foams are significantly higher as compared to the thicker foams (20 mm and 30 mm). The increase of foam thickness led to the decrease of yield strength between the magnitudes of 30%-60% compared to the tension test. The foams showed an initial linear behavior followed by yielding with a subsequent peak load. After the material reaches its peak load, the load carrying ability drops dramatically. A small group of shear samples exhibited a short stress plateau after reaching the peak load, however, high percentage of foams showed a sharp drop in load after initial failure.

Table 5.3. Physical and mechanical properties of shear test foam samples. (The average values are given with standard deviations)

Foam Thickness	Average Density (gr/cm^3)	Average Shear Modulus (MPa)	Average Shear Strength (MPa)
8	0.337 (0.02)	51.12 (9.68)	1.209 (0.21)
20	0.414 (0.06)	18.57 (6.60)	0.829 (0.02)
30	0.421 (0.04)	20.02 (3.22)	0.386 (0.01)

(a)   (b)

Figure 5.11. Foam samples subjected to shear testing: (a) 20 mm Al foam during shear test (b) Test coupons after shear test.
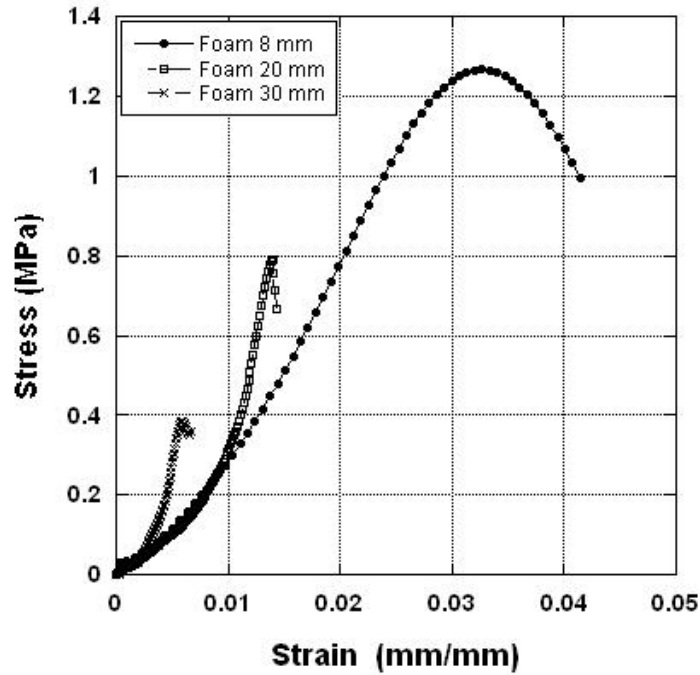
Figure 5.12. Shear stress versus strain graphs of as received Al foams with three different thickness.

5.2. Tensile Properties of Aluminum

Tensile mechanical behavior of Al sheet samples were obtained at loading speed of 2 mm/min. The photos of Al specimens after tension test is shown in Figure 5.13. At least four specimens were tested and average resultant data are plotted in Figure 5.14. The samples showed ductile behavior according to the stress-strain graphs of samples, as expected. The average mechanical properties such as elastic modulus and collapse strength are tabulated in Table 5.4. The average elastic modulus and ultimate tensile strength (UTS) values are 64.03 (±4.76) GPa and 148.03 (±10.41) MPa, respectively. The test results are tabulated in Table 5.4.
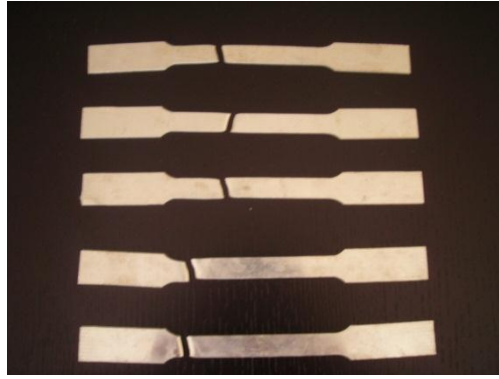
Figure 5.13. Al sheet samples after tension test

Table 5.4. Physical and mechanical properties of Al sheet tension test samples. (The average values are given with standard deviations)

Sample ID	Elastic Modulus (GPa)	Ultimate Tensile Strength (MPa)
Al sheet-1	70.18	155.5
Al sheet-2	64.39	154.91
Al sheet-3	58.69	148.57
Al sheet-4	62.77	133.14
Average Al sheet	64.03 (4.76)	148.03 (10.41)
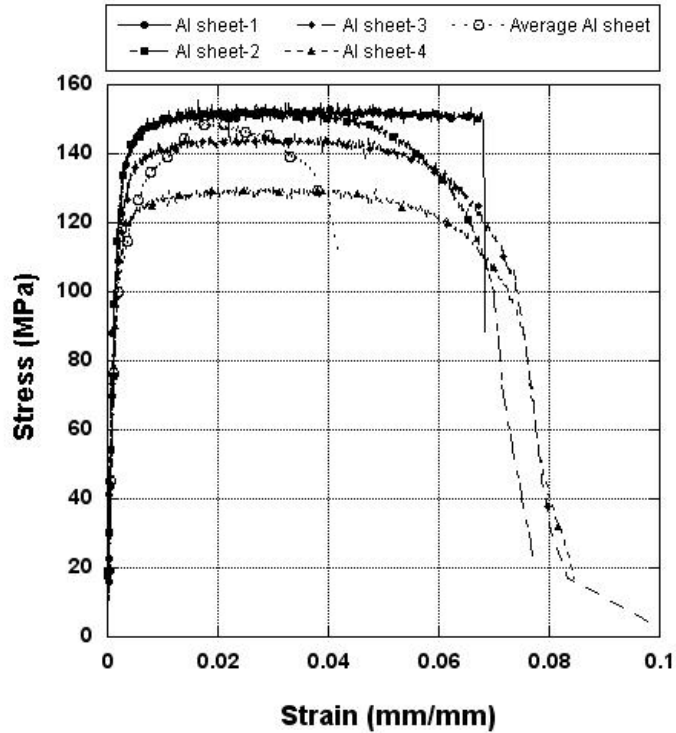
Figure 5.14. Stress versus strain graph of Al sheets under tension

5.3. Tensile Properties of GFPP Composites

Tensile tests were performed in order to investigate the tensile properties of non-crimp PP/glass fiber thermoplastic composites. Figure 5.15 shows GFPP composite samples after tensile testing. At least four specimens were tested and average resultant data are plotted in Figure 5.16. The average mechanical properties such as elastic modulus and collapse strength are tabulated in Table 5.5. The average elastic modulus and ultimate tensile strength (UTS) values are 14.52 (±1.32) GPa and 243.37 (±26.9) MPa, respectively and the fiber volume fraction of the samples were measured as 34.5%. As expected, the GFPP composite exhibited brittle characteristic and showed higher UTS magnitudes as compared to the ductile aluminum material.
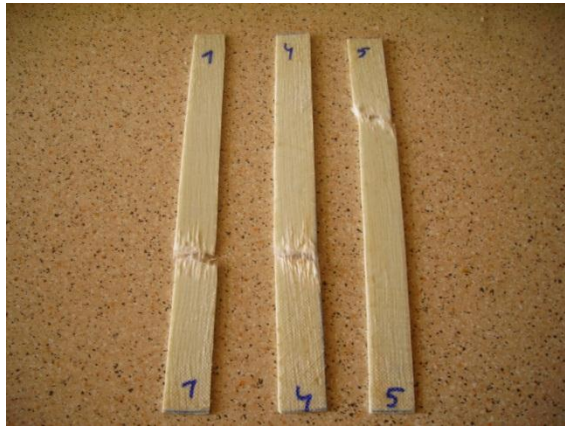
Figure 5.15. GFPP composite samples after tensile testing.

Table 5.5. Physical and mechanical properties of GFPP composite tension test samples (The average values are given with standard deviations)

Sample ID	Elastic Modulus (GPa)	Ultimate Tensile Strength (MPa)
GFPP-1	14.28	290.85
GFPP -2	13.04	223.89
GFPP -3	16.26	236.24
GFPP -4	14.51	230.38
Average GFPP	14.52 (1.32)	243.37 (26.9)
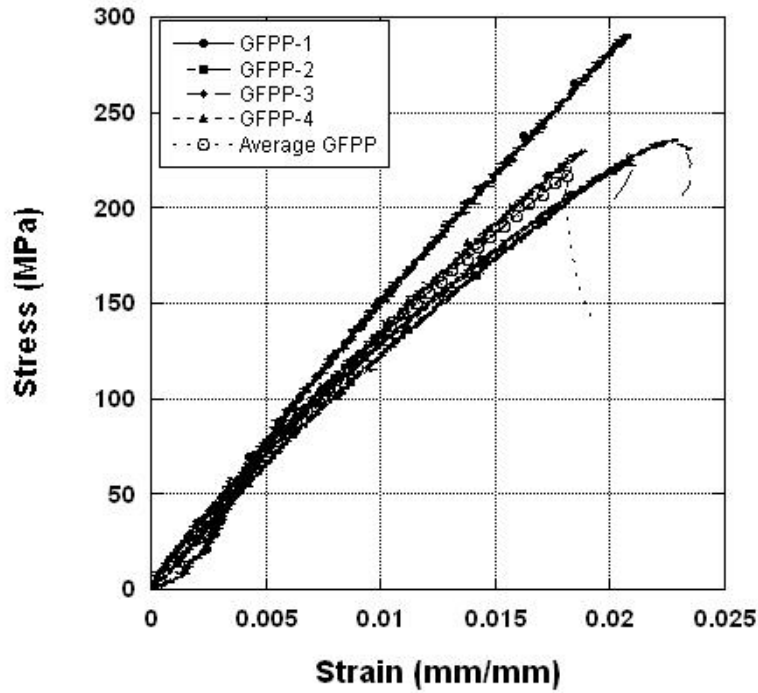
Figure 5.16. Stress versus strain graph of GFPP composite under tension

5.4. Tensile Properties of Al/GFPP FML System

The Al/GFPP samples after the tension test are given in Figure 5.17. The combination of ductile aluminum and glass fiber reinforced polypropylene in FML systems resulted in a complex tensile behavior and stress-strain properties (Figure 5.18). Due to the plasticity of aluminum as metal component of FMLs, it is expected that the Al/GFPP shows elasto-plastic behavior. The average elastic modulus and ultimate tensile strength (UTS) values are 40.06 ($\pm$2.140) GPa and 169.906 ($\pm$2.369) MPa, respectively. The test results are reported in Table 5.6. The higher UTS values can be attributed to the stiffness contribution of GFPP along fiber axis.

(a)   (b)

Figure 5.17. Al/GFPP system tension test samples: (a) Test coupon image during tension test (b) Test coupon after tension test.

Table 5.6. Physical and mechanical properties of Al/GFPP system tension test samples (The average values are given with standard deviations).

Sample ID	Elastic Modulus (GPa)	Ultimate Tensile Strength (MPa)
Al/GFPP-1	37.77	169.40
Al/GFPP -2	42.48	171.58
Al/GFPP -3	41.03	166.76
Al/GFPP -4	38.74	171.88
Average Al/GFPP	40.06 (2.14)	169.9 (2.36)
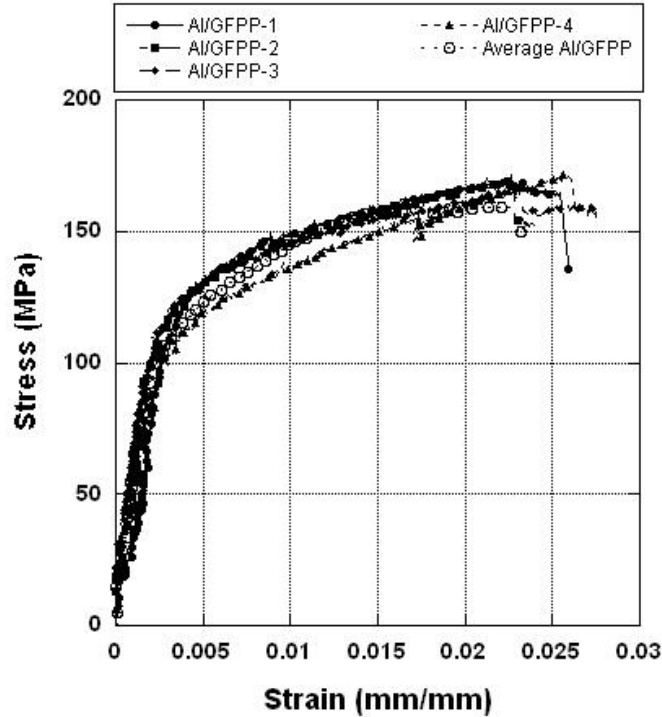
Figure 5.18. Stress-strain graph of Al/GFPP composite under tension

5.5. Interfacial Strength Properties of Al/GFPP FML System Bonded with Silane Treatment and PP Based Film

The interfacial strength between the components of the composite sandwiches has a critical importance. The quality and compatibility of the adhesives considerably influence the mechanical performance of the composite systems. In this study, the interfacial strength of the hybrid materials which were subjected to various surface modifications and/or adhesive addition, was determined with lap shear and peel tests.

5.5.1. Lap Shear Testing of Al/GFPP FML System Bonded with Silane Treatment and PP Based Film

The lap shear samples after the test are shown in Figure 5.19. Interfacial shear stress- displacement graphs of Al sheets modified with silane surface treatment and bonded with GFPP with the addition of PP based film (PP-g-MA) was determined and illustrated in Figure 5.20. As seen in Figure 5.20, with increasing displacements, shear

stress values of Al/GFPP system increased almost linearly until the failure point. Sudden drops were observed at about 4.5 MPa stress level. The maximum shear stress (5.93 ($\pm$0.43) MPa) of the mentioned FML system was found with the addition of PP based film. The lap shear test results are given in Table 5.7 and average shear stress of Al/GFPP system prepared with silane treatment and PP based film addition combination was found as 4.49 ($\pm$1.31) MPa. Although the positive effect of combination of these two bonding techniques was expected, the experimental results showed that this combination does not yield the desired high bending strength. This may be due to the insufficient bonding of silane groups with PP based film.
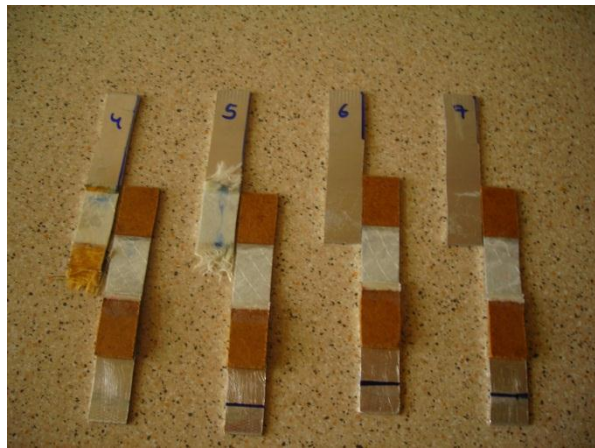
Figure 5.19. Lap shear test samples made of Al/GFPP with silane modification and PP-g-MA based adhesive film addition.

Table 5.7. Lap shear strength of Al/GFPP system lap shear test samples with silane modification and PP-g-MA based film addition. (The average values are given with standard deviations)

Sample ID	Shear Strength (MPa)
LS Sample-1	3.06
LS Sample -2	5.29
LS Sample -3	5.01
LS Sample -4	4.62
Average	4.49 (1.31)
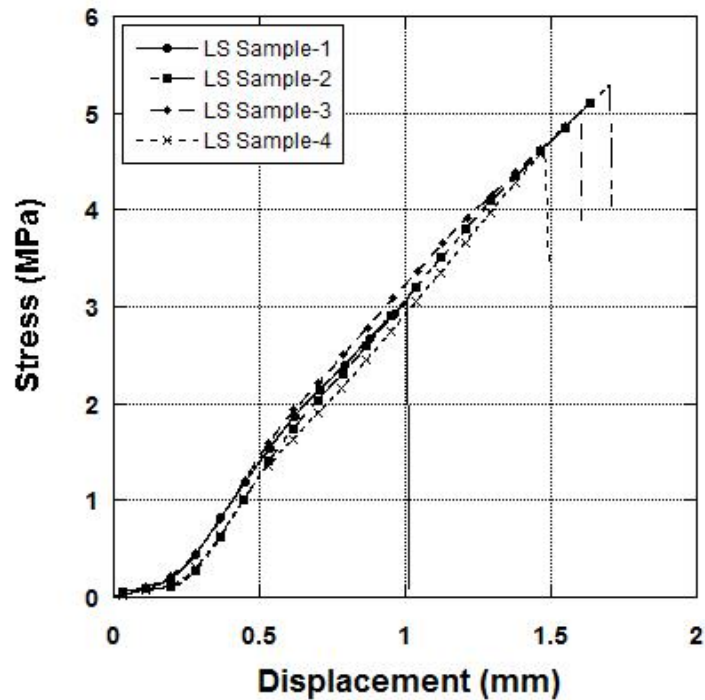
Figure 5.20. Stress-displacement graph of lap shear test samples with silane modification and PP-g-MA based adhesive film addition

5.5.2. Peel Testing of Al/GFPP FML System Bonded with Silane Treatment and PP Based Film

Peel testing was carried out to measure the strength of adhesives in cleavage peel by tension loading. In the study performed by Aslı Guruşçu (Msc, 2009), the Al/GFPP system exhibited the highest peel strength (6.61 N/mm) with the addition of PP-g-MA film. Combination of silane surface modification and PP-g-MA film introduction for the same FML system resulted in the lower peel strength compared to the PP film modified system. The average peel strength of the Al/GFPP laminate produced with the combination of silane treatment and PP-g-MA film addition was calculated as 3.98 (±0.98) N/mm. This situation can be attributed to the weak interaction of Al sheet and GFPP surfaces due to the thin silane layer. The peel test samples after the test and force-displacement curves are shown in Figure 5.21 and Figure 5.22, respectively. The samples exhibited smoother increase of the load and the peel strength values are tabulated in Table 5.8.
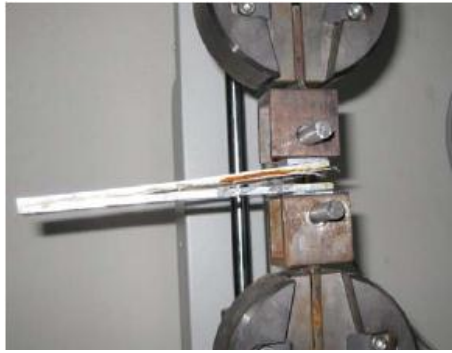
Figure 5.21. Al/GFPP composite peel test samples: (a) Test coupons under loading (b) Test coupons after peel test.

Table 5.8. Peel strength values of Al/GFPP system lap shear test samples with silane modification and PP-g-MA based film addition. (The average values are given with standard deviations).

Sample ID	Peel Strength (N/mm)
Peel Sample-1	5.04
Peel Sample -2	4.41
Peel Sample -3	2.73
Peel Sample -4	3.79
Average	3.98 (1.22)
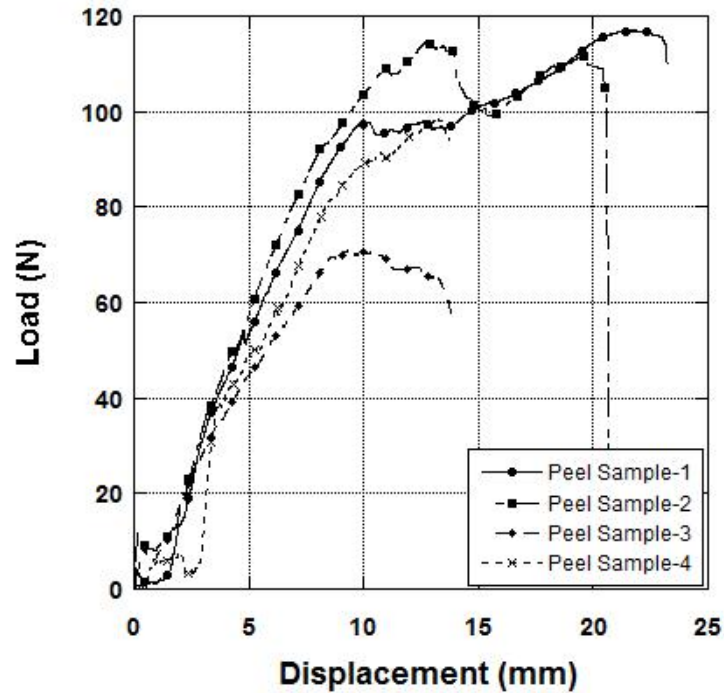
Figure 5.22. Load-displacement graph of peel test samples with silane modification and PP-g MA based film addition.

5.6. Mechanical Properties of Al Foam Based Sandwiches

The mechanical properties of sandwich structures have great importance in terms of their application area. There are some available test methods in the literature for the determination of the sandwich systems' performances. In this thesis, compression and flexural characteristics of composite sandwiches were deeply investigated. Flat-wise compression and three point bending tests were applied to the samples for each integration technique.

5.6.1. Compression Properties of Al Foam Sandwiches

The stress-displacement behaviors of Al foam based sandwiches with three different thicknesses were obtained based on the compression testing and Figures from 5.23 to 5.26 show the stress-displacement graphs of these sandwich structures. At least three specimens per each thickness were tested and typical representative data for each thickness set of foam based sandwiches are plotted. The average mechanical properties

111

such as apparent elastic modulus and collapse strength are tabulated in Table 5.9 and calculated based on ASTM C 365-00 standard. The flat-wise compression characteristics of sandwich samples showed close similarity with the monolithic Al foams. Three distinct zones are present and the typical deformation mechanisms of foams were observed during the test.

The effect of the foam thickness increase on the behavior of the sandwich structures were investigated by considering the test results. The sandwiches with 8 mm foams switched to densification region before the thicker foams and they also showed maximum collapse strength regardless of the integration type. Similar behavior was previously observed for the as-received Al foams with the same thickness. It was found that the foam thickness increase generally resulted in collapse strength decrease. Also, a significant data scattering was observed as seen in Table 5.9. As the thickness increases, the structural defects probably increase and the foam irregularities becomes more effective. The lower strength values of thicker foams are attributed to those effects. It was also revealed from the experimental results that, the foams with higher elastic modulus showed generally higher collapse strength for each thickness set of foam based sandwiches.

Table 5.9. Physical and mechanical properties of Al foam based sandwiches (AFS). (The average values are given with standard deviations).

Sample Type	Sample Density (gr/cm^3)	Apperant Elastic Modulus (MPa)	Collapse Strength (MPa)
AFS-8 mm (epoxy bonded)	1.10 (0.14)	54.45 (11.3)	2.16 (0.84)
AFS-20 mm (epoxy bonded)	0.80 (0.03)	74.98 (16.3)	1.69 (0.43)
AFS-30 mm (epoxy bonded)	0.62 (0.02)	58.81 (10.9)	0.66 (0.54)
AFS-8 mm (silane bonded)	1.13 (0.04)	61.98 (6.4)	2.90 (0.6)
AFS-20 mm (silane bonded)	0.92 (0.02)	63.71 (10)	2.39 (0.6)
AFS-30 mm (silane bonded)	0.73 (0.07)	77.80 (40.4)	2.05 (0.9)
AFS-8 mm (PP based film bonded)	1.14 (0.01)	37.37 (17.9)	1.84 (0.4)
AFS-20 mm (PP based film bonded)	0.82 (0.01)	59.10 (33.1)	1.90 (0.9)
AFS-30 mm (PP film bonded)	0.61 (0.04)	53.82 (12.2)	1.03 (0.5)
AFS-8 mm (silane treated+PP based film bonded)	1.16 (0.07)	71.19 (5.6)	3.78 (1.1)
AFS-20 mm (silane treated+PP based film bonded)	0.82 (0.04)	42.27 (34.2)	1.31 (0.3)
AFS-30 mm (silane treated+PP based film bonded)	0.66 (0.04)	95.25 (35.3)	2.02 (0.5)
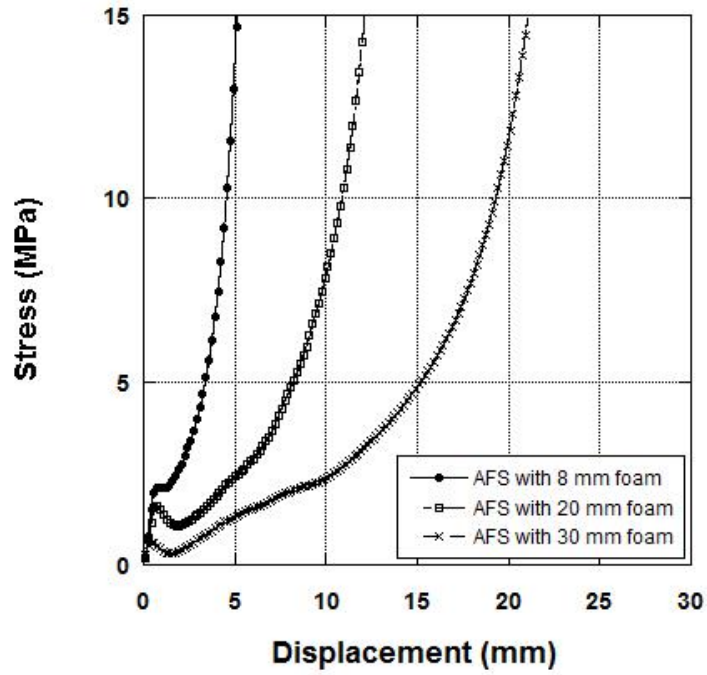
Figure 5. 23. The typical stress-displacement graph of Al sheet/Al foam sandwiches bonded with epoxy.
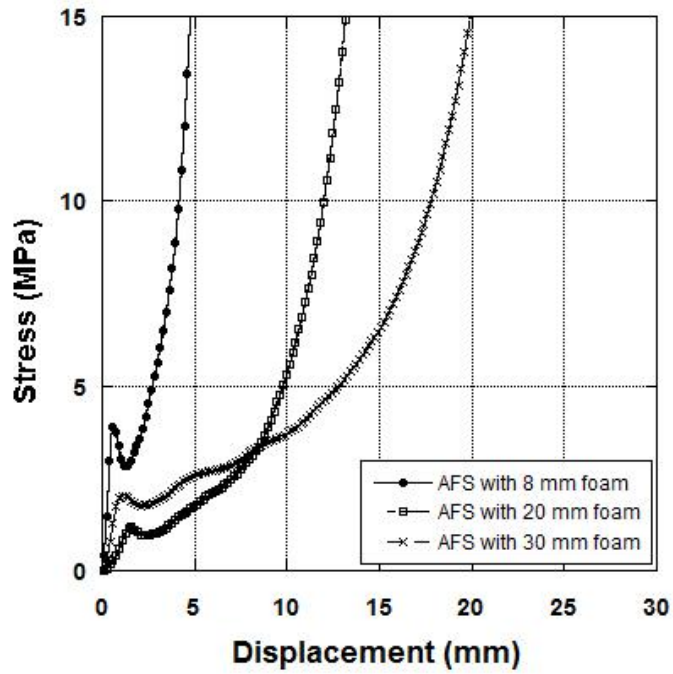
Figure 5.24. The typical stress-displacement graph of Al sheet/Al foam sandwiches bonded with GFPP after silane surface treatment.

114
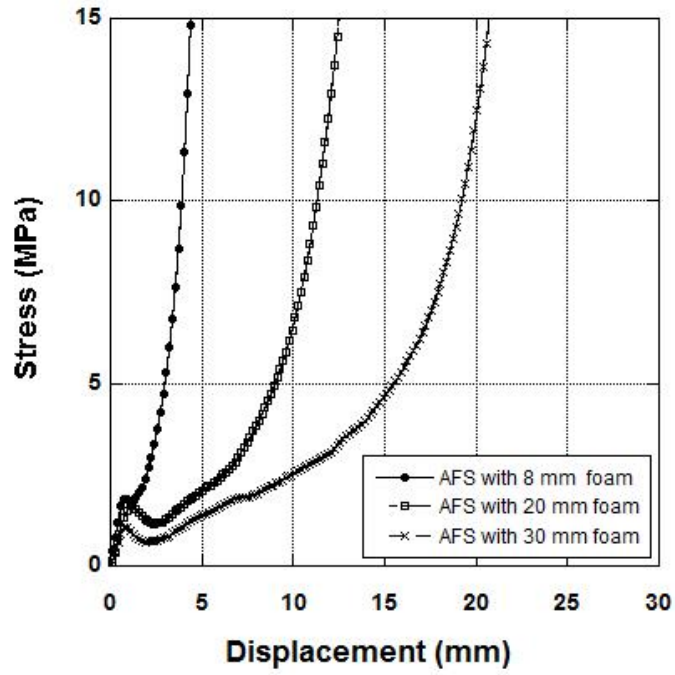
Figure 5.25. The typical stress-displacement graph of Al sheet/GFPP/Al foam sandwiches bonded with PP-g-MA based film.
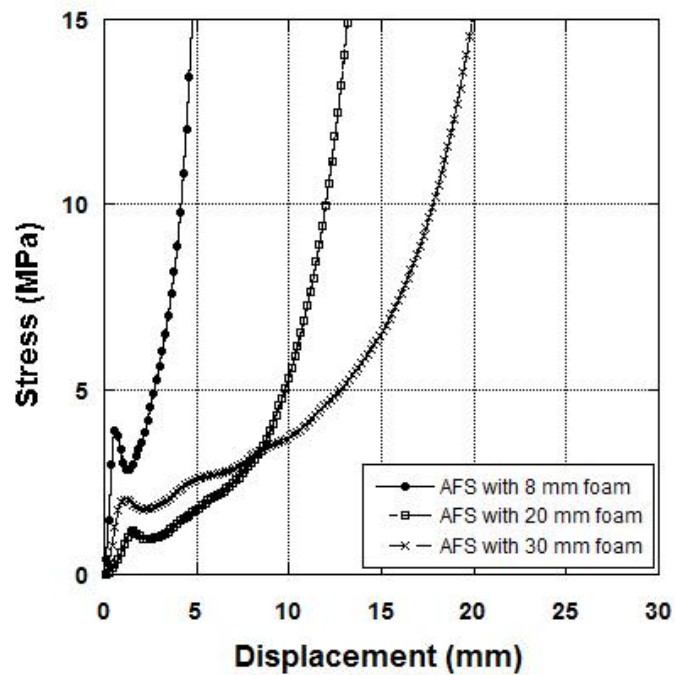
Figure 5.26. The typical stress-displacement graph of Al sheet/GFPP/Al foam sandwiches bonded with PP-g-MA based film after silane treatment.

The typical microstructures of an Al foam based sandwich with and without GFPP are given in the Figures from 5.27-a to c. In Figures 5.27-a and 5.27-b, the samples included 8 mm foams were not exposed to any deformation. The 0/90° oriented co-mingled GFPP was placed between Al foam and Al sheet as an intermediate layer. The horizontal lines and small dotted segments in the mid region are the images of the 0° and 90° oriented fibers, respectively. The foam cells are placed under the GFPP composite layer. A typical cell wall image is also seen on the micrograph. The microstructures of Al foam based sandwich samples after compression had close similarity with the as-received Al foams as shown in Figure 5.27-c. Same deformation mechanisms were observed with the increase of compressive stress. The crushing and stretching of cell walls are present in the optical microscope photos due to the bending and/or buckling of cell edges.

5.6.2. Flexural Properties of Al Foam Sandwiches

The force-deflection data of the sandwiches were recorded during the bending test. The figures from 5.28 to 5.31 show the typical flexural force-deflection curves of sandwiches with various bonding types. The sandwiches exhibited an initial linear elastic region with a subsequent non-linear part resulted in the decrease of slope near to the maximum force. The foam thickness increase led to the increase of both equivalent flexural rigidity and the slope of linear elastic region. The force level after maximum force values showed some differences among the samples. Regardless of the bonding type and the core thickness, some sandwich structures showed a smooth force drop while some of them exhibited a sudden drop followed by a plateau region in which the foams fail by buckling of the cell walls and edges. Based on the test results, the plateau parts in the graphs, in general, showed fluctuation rather than flat characteristics over larger displacements.
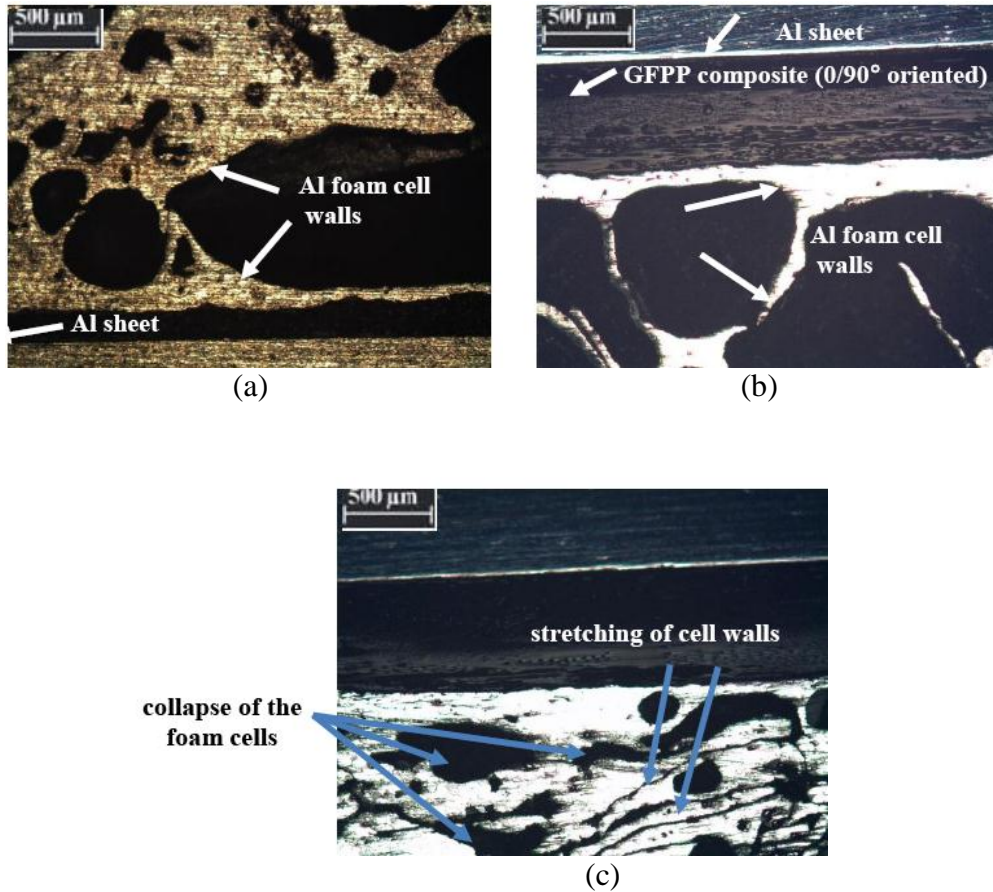
Figure 5.27. Microstructure of Al foam based sandwiches before and after compression test: (a) Al sheet/Al foam sandwich bonded with epoxy before compression, (b) Al sheet/GFPP/Al foam sandwich bonded with silane treatment before compression, (c) Al sheet/GFPP/Al foam sandwich bonded with silane treatment after compression.

The average collapse load (maximum load) values of sandwiches consolidated together with different bonding types are summarized in Figure 5.32 with respect to foam thickness. The core thickness increase generally led to the increase of maximum load for all of the samples regardless of the type of bonding. The core thickness increase from 8 to 20 mm resulted with an average increase of 14.75 % of the collapse load while this value reached to 32.8 % increase for the foam thickness changes from 20 to 30 mm. When the collapse load values of Al sheet/Al foam sandwiches and Al sheet/GFPP/Al foam sandwiches are compared, it is clearly seen that the former samples exhibited lower values. The combination of GFPP composite and Al metal layer resulted in the decrease of the elastic modulus of the hybrid system, however, the same system exhibited higher tensile/compressive strength values. As it is known, in sandwich structures, the skin materials bear the in plane compressive and tensile

stresses. The higher loads exposed to the Al sheet/GFPP/Al foam system was attributed to this fact. In addition, a weaker bonding of epoxy adhesive may result with the lower collapse load values of Al sheet/Al foam sandwich samples.
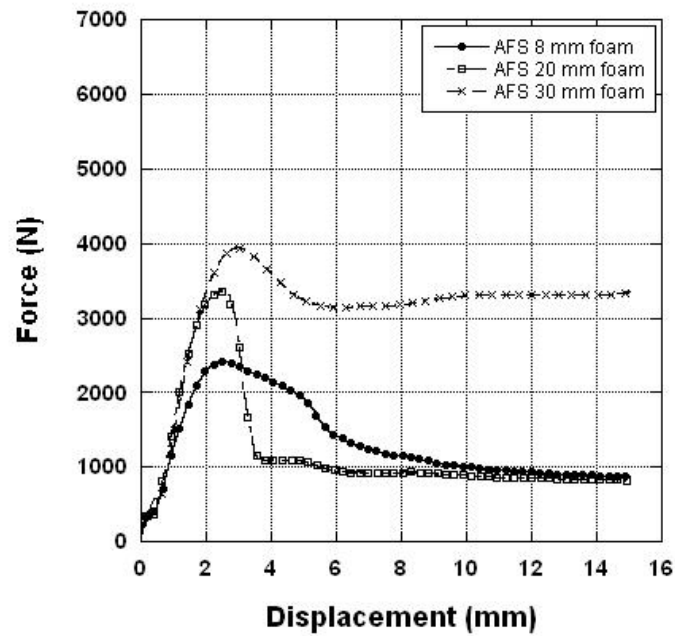
Figure 5.28. Force-displacement graphs of Al sheet/Al foam sandwiches bonded with epoxy.
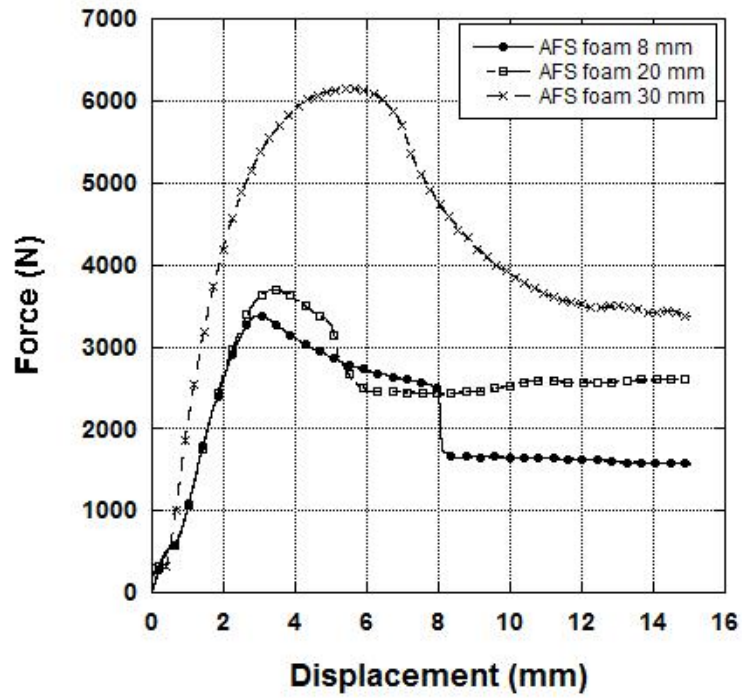
Figure 5.29. Force-displacement graphs of Al sheet/Al foam sandwiches bonded with GFPP layer after silane surface treatment of Al surfaces.
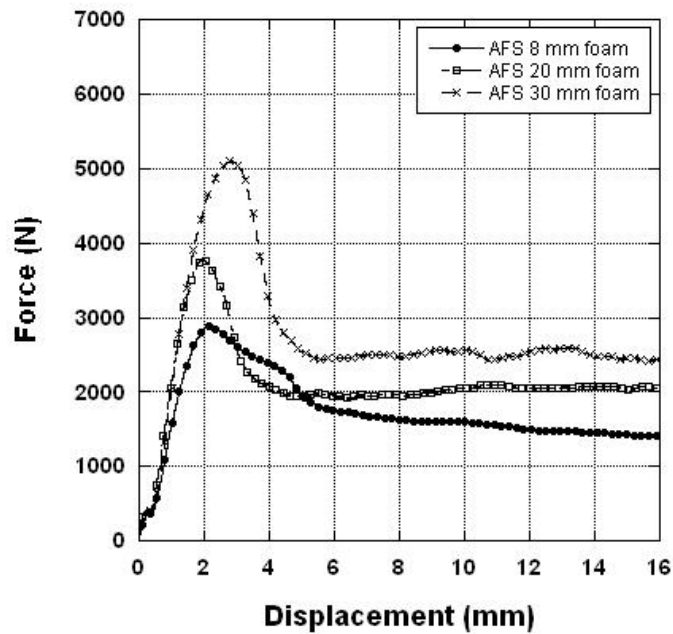
Figure 5.30. Force-displacement graphs of Al sheet/Al foam sandwiches bonded with PP-g-MA based adhesive film.
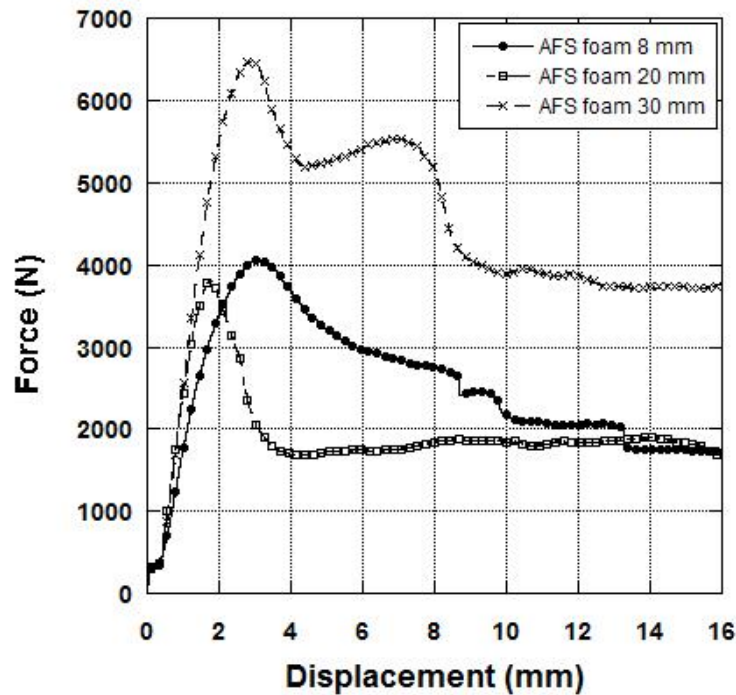
Figure 5.31. Force-displacement graphs of Al sheet/Al foam sandwiches bonded with PP-g-MA based adhesive film after silane surface treatment of Al surfaces.

The aim of silane surface modification and PP-g-MA based film addition into the sandwiches was to provide robust integration between the components. Compared to the average collapse loads of sandwiches bonded with silane surface modification and PP-g-MA based film, the former bonding type is more effective. The silane treated samples showed higher collapse loads regardless of the foam thickness. The sandwiches modified with silane coupling agent and incorporating PP-g-MA based film layer, in general, showed better performance among all the bonding types. The variations of core shear and face-sheet strength of sandwiches with respect to core thickness are shown in Figures 5.33 and 5.34. Based on these figures, the samples with 8 mm core showed the highest core shear and face-sheet strength. The increase of foam thickness led to the decrease of face-sheet and core shear strength values for the Al sheet/Al foam sandwiches integrated with epoxy. The sandwiches bonded with GFPP after silane surface treatment showed higher core shear strength values for the 20 and 30 mm core thicknesses. The effect of PP-g-MA based film addition with the silane coupling agent application, in general, inceased the collapse loads.
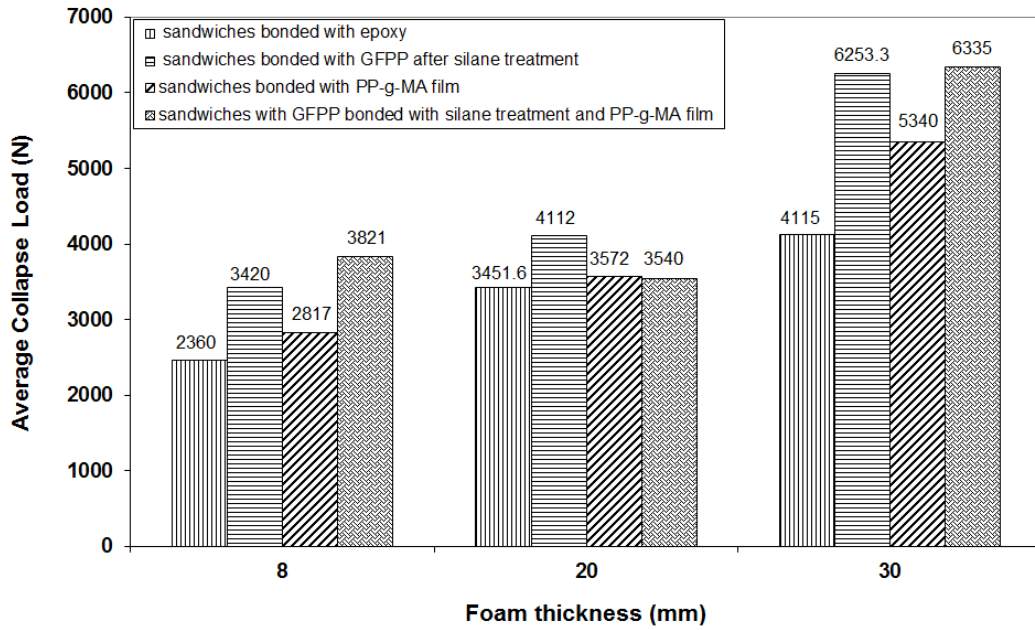
Figure 5.32. The collapse load versus foam thickness variation of sandwich sample consolidated with various adhesives.
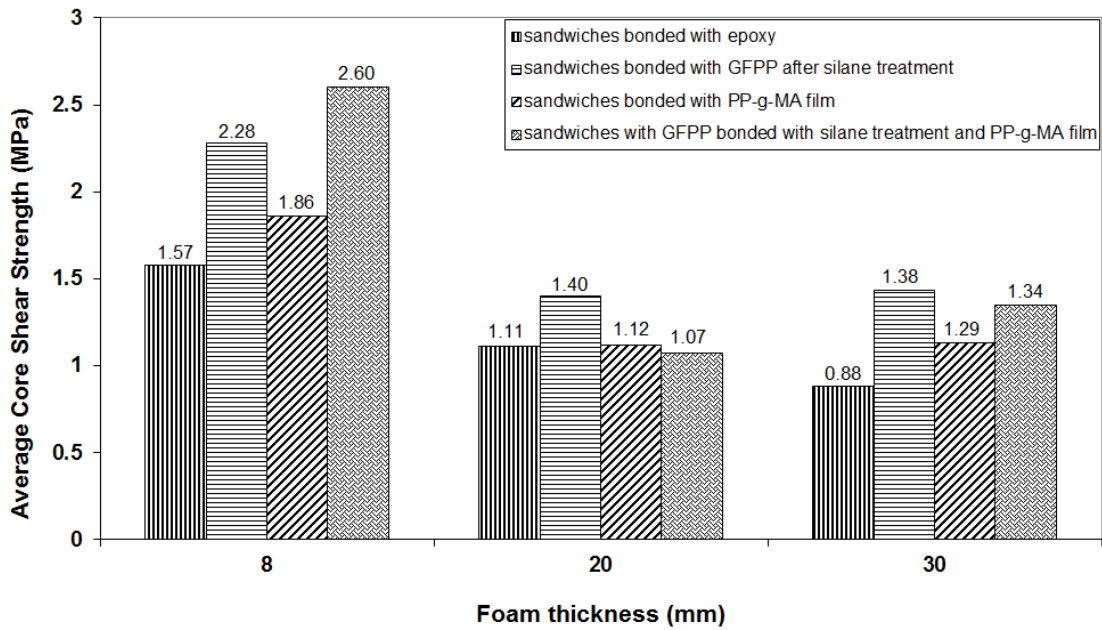
Figure 5.33. Average core shear strength versus foam thickness variation of sandwiches with various adhesives.
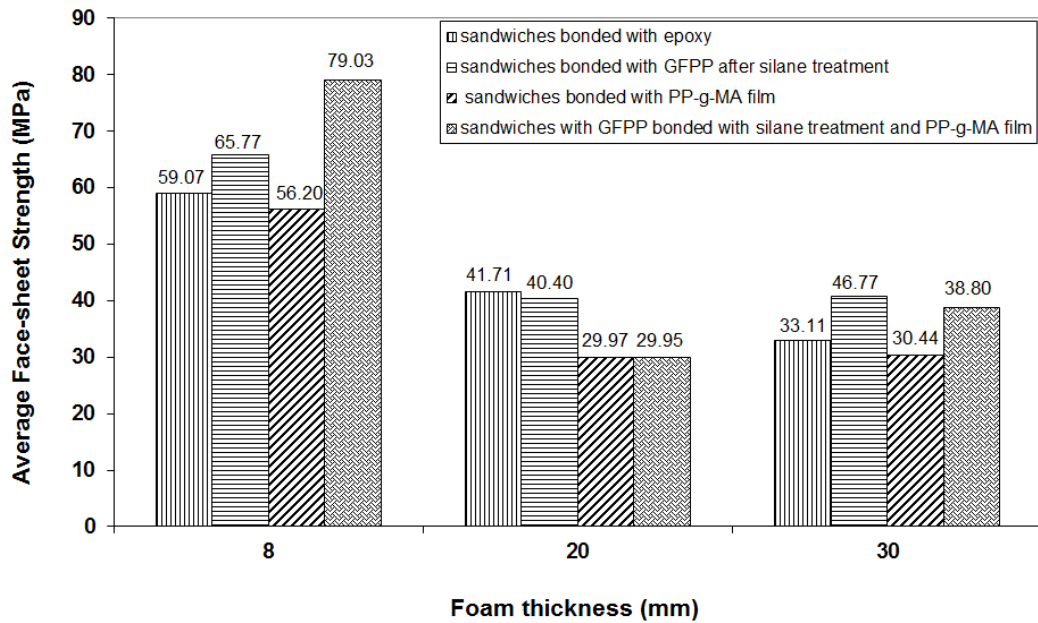
Figure 5.34. Average face-sheet strength versus foam thickness variation of sandwiches with various adhesives.

5.6.2.1. Failure Characterization of Al Foam Sandwiches under Flexural Loading

The main failure modes observed in the three point bending experiments (Figures 5.35 and 5.36) are the core shear yield and debonding of sandwich components, independent of core thickness. The concentrated load application to the sandwiches resulted in the localized bending of the upper face-sheet, as expected. Debonding occurred between FML face-sheet/Al foam core, Al layer/GFPP composite or Al layer/Al foam core probably due to the lower interfacial strength as compared to the core shear strength. In some samples, both core shear and debonding modes were observed sequentially. Indentation type of failure was also seen for the sample which had 30 mm thick core and integrated with epoxy. In terms of the core shear mechanism, shear cracks originated in the foam between the load and the support fixtures since the failure in the core started with cracking followed by some crushing of the cells. The core failed with about 45° angle showing a distinctive failure surface with crack propagation through the foam cells. The damage progression appeared to be steady and consistent with the increase of displacement. In spite of the debonding of the core from the FML face sheet after shear crack formation, the GFPP layer did not show any

delamination. Almost no debonding was observed between the GFPP and Al constituents in sandwiches integrated with PP based film indicating the strength of polymeric adhesive film. Other debonding cases among the components might be attributed to the insufficient adhesive effect. The geometrical variables in the test configuration such as span length, sandwich width or face-sheet thickness were not considered in this study in order to clearly observe the effect of core thickness and adhesive type. Therefore, other failure types like wrinkling or face-sheet yielding were not seen during the experiments.
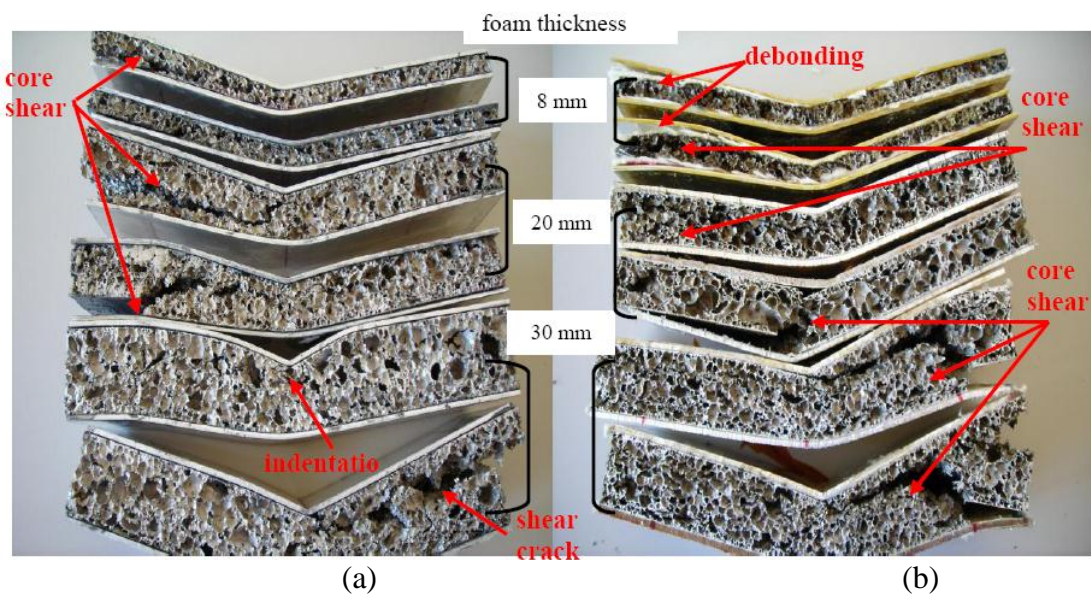
Figure 5.35. Failure modes observed during flexural testing of (a) Al sheet/Al foam sandwiches integrated with epoxy adhesive (b) Al sheet/GFPP/Al foam sandwiches bonded after silane surface treatment.
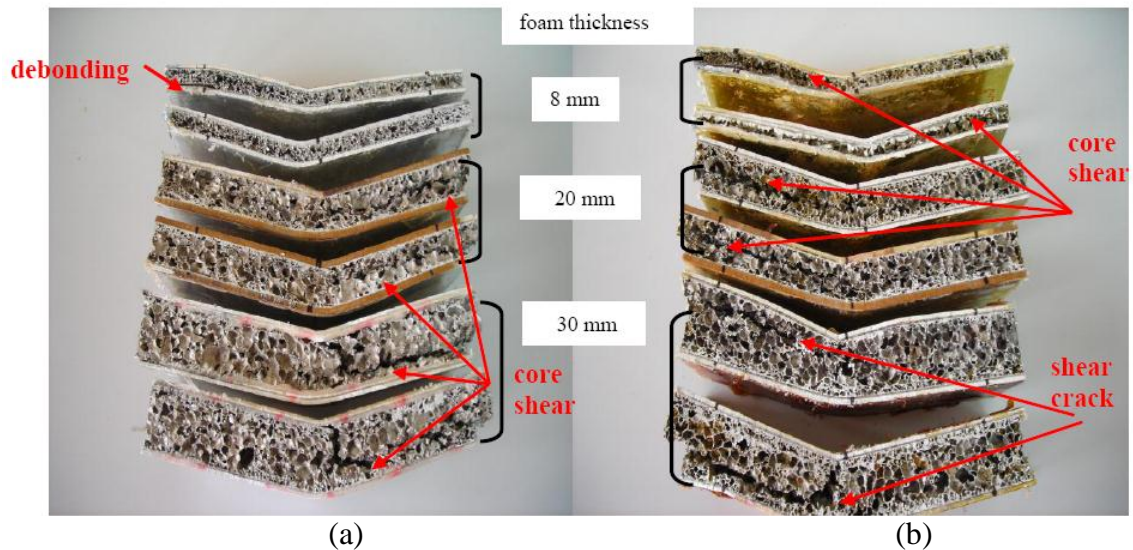
Figure 5.36. Failure modes observed during flexural testing of (a) Al sheet/GFPP/Al foam sandwiches bonded with PP-g-MA based film (b) Al sheet/GFPP/Al foam sandwiches integrated with PP-g-MA based film and silane surface treatment.

5.7. Energy Absorption Characteristics of Al Foams and Al Foam Sandwiches

In this thesis, the specific absorbed energies (SAE) of the Al foams and Al foam based sandwiches under compression were calculated with respect to strain as shown in the Figures from 5.37 to 5.41. It was found that the foam thickness increase resulted in the increase of absorbed energy. Table 5.10 gives the specific absorbed energy values of as-received Al foams and Al foam based sandwiches for various foam thickness. The specific energy absorption capacities of the sandwiches were calculated by averaging the SAE values of sandwiches for each thickness set of foam based sandwiches without considering the bonding type. The sandwiches consisted of 8 mm Al foam completed their densification at 30-60% deformation while the other sandwich samples containing thicker foams reached their highest SAEs at 50-70% strain. In general, the foam thickness increase resulted in the decrease of SAE for both monolithic Al foam and Al foam based sandwiches at 60% deformation.

Based on Table 5.10, sandwich structures exhibited highest specific absorbed energy values as compared to the as-received foams. This is attributed to the higher densities of sandwich samples which led to the shorter plateau part with higher stresses.

The area under the load-displacement curve became larger and thus, both absorbed energy values of the sandwiches and SAE parameter increased.
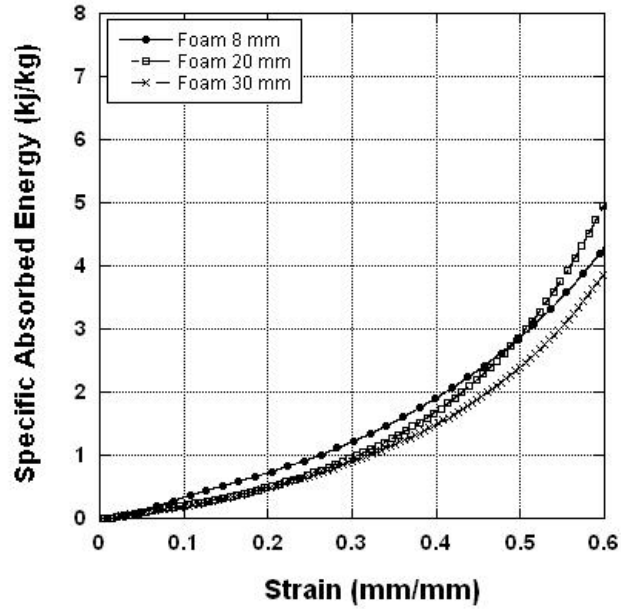
Figure 5.37. SAE versus strain of as-received Al foams.
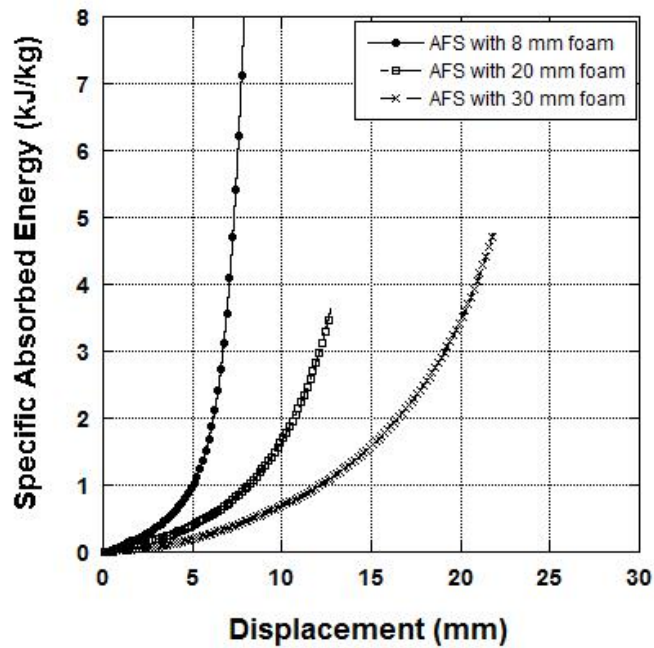
Figure 5.38. SAE versus displacement of Al sheet/Al foam sandwiches bonded with epoxy.
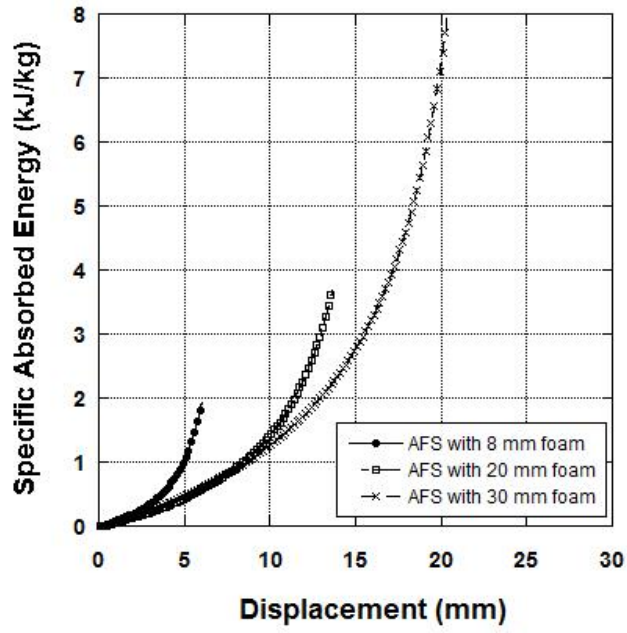
Figure 5.39. SAE versus displacement of Al sheet/Al foam sandwiches bonded with
GFPP after silane surface treatment.
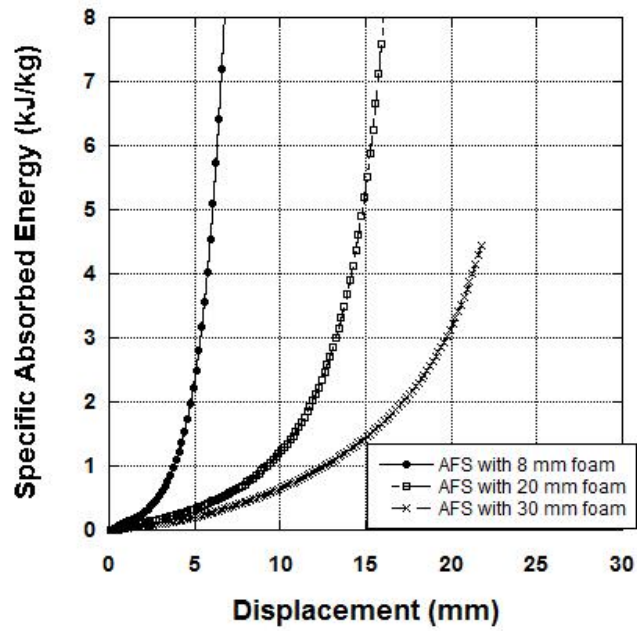
Figure 5.40. SAE versus displacement of Al sheet/GFPP/Al foam sandwiches bonded
with PP-g-MA based film.
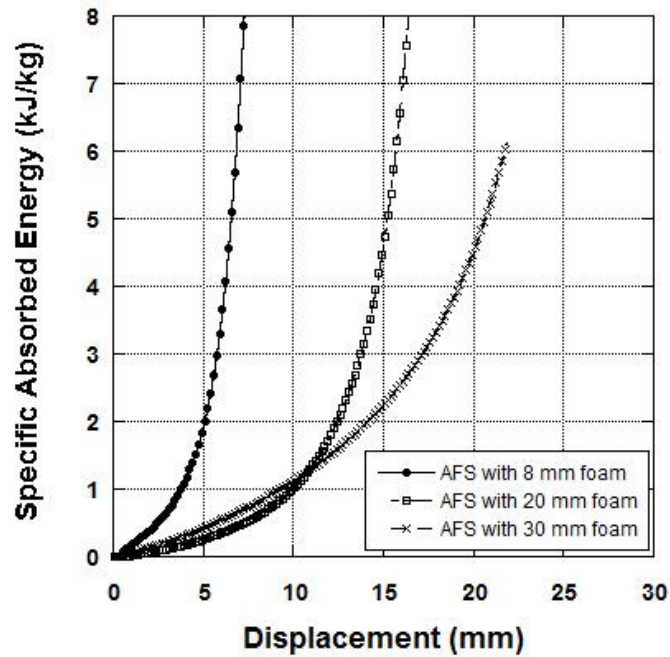
Figure 5.41. SAE versus displacement of Al sheet/Al foam sandwiches bonded with PP-g-MA based adhesive film after silane surface treatment of Al surfaces.

Table 5.10. Specific absorbed energy (SAE) comparison of as-received Al foams and Al foam sandwiches at 60% deformation. (The average values are given with standart deviations).

Sample Type	Foam Thickness (mm)	SAE (kJ/kg)
As-received Al foam	8	4.48 (0.66)
Al foam based sandwich		6.45 (2.35)
As-received Al foam	20	4.37 (0.56)
Al foam based sandwich		4.39 (0.99)
As-received Al foam	30	3.89 (0.18)
Al foam based sandwich		4.18 (0.83)

The dissipated energy under bending was calculated from the force-displacement curves of the specimens as shown in Figure 5.42 with respect to the foam thickness variation. Based on the three point bending test results, the increase of core thickness resulted in the increase of energy dissipation. Besides that, the GFPP

composite layer might have positive contribution in terms of the energy absorption of the sandwiches. The 30 mm thick foam sandwiches bonded with GFPP after silane surface modification exhibited the highest absorption capacity among the other samples. A significant jump is also observed for the sandwiches with the same thickness integrated with silane treatment and PP-g-MA based film addition.
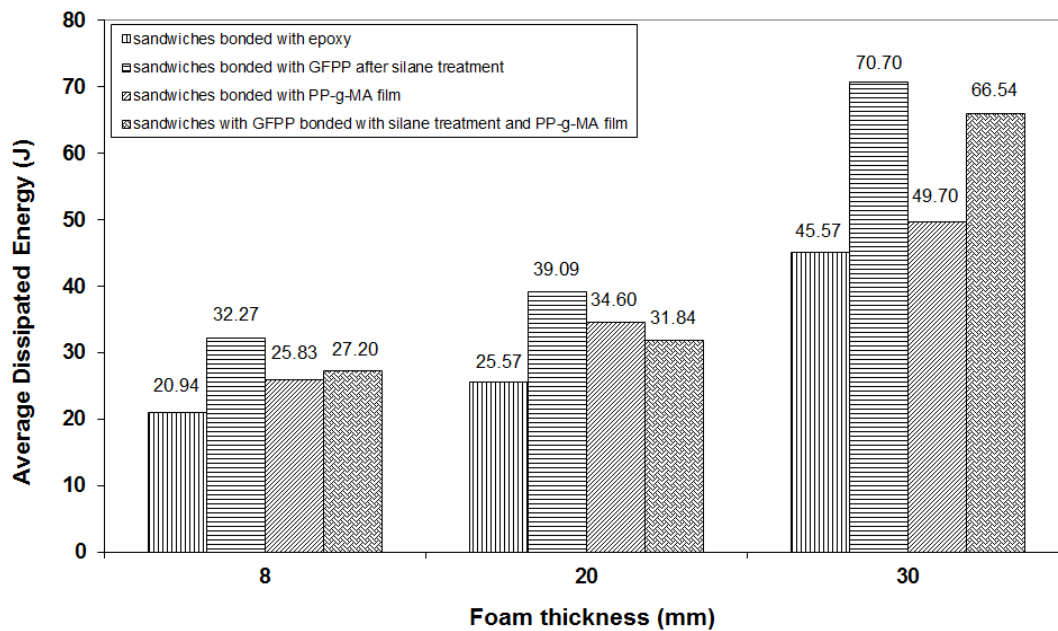
Figure 5.42. The energy dissipation versus foam thickness variation of sandwiches with various adhesives.

5.8. Blast Analysis of Sandwich Panel Under Simulated Blast Test

In the literature, the elastic behavior and plastic damage mechanisms of the core based sandwiches have been widely studied. The blast performance of the composite sandwich panels are generally evaluated by using equipments like ballistic pendulum and drop tower which apply dynamical forces to the structures. However, the presence of these equipments is not as common as quasi-static loading test machines. In this section of the study, our aim is to relate the quasi-static sandwich panel analysis to a dynamic blast load. Based on this idea, the lightweight sandwich composites were subjected to compression loading with a very special test apparatus and the corresponding test is called as "simulated blast test". The sandwiches were assumed as

single degree of freedom mass-spring systems in order to include the dynamic effect. The peak deflections of the panels under blast loading were predicted based on the procedure described below.

- Identification of the failure pressure (P_{fail}) and corresponding failure deflection (w_{fail}) under quasi-static compression test.
- Evaluation of the panel compliance (C_p) by means of LVDT measurements considering equation 4.13.
- Determination of panel natural frequency (ω) by using equation 4.11.
- Determination of maximum blast pressure (P_{blast}) and blast characteristic time (T) parameters by means of equation 4.14. The pressure-time $(P\text{-}t)$ histories of panels are presented in Figures 4.27 and 4.28 depending on the TNT amount and stand-off distance.
- Calculation of panel deflection (δ_{static}) under maximum blast pressure (P_{blast}) by considering panel compliance.
- Evaluation of $T\omega$ product and determination of peak deflection (δ_{peak}) under maximum blast pressure by using equation 4.15.
- Determination of failure index $(\delta_{peak}/ w_{fail})$.

The central deflection-force data of Al foam sandwich panels during quasi-static tests were recorded. The stress was calculated by considering the area acting over the support frame. The stress versus deflection behavior of Al foam sandwich panels are shown in Figures from 5.43 to 5.45. For 8 mm Al foam sandwiches, three distinct regions are visible on the graphs. In the first region, a linear deflection behavior is observed at low pressures. In the second zone, in spite of the stress increase, the central deflection is almost constant and in addition, thicker Al foam sandwich structures (20 mm and 30 mm foams) show extra regions. In the plots, the samples with 20 mm Al foams continue into 4th region at around 1.5 MPa pressure and the central deflection values are almost constant. Similarly, panels with 30 mm core exhibited five different zones during the test. In order to clearly identify the deformation modes and failure mechanisms of the panels; the loading was ended at specific load level and the image of the deformed panels were captured. As a typical representation, the shots of sandwiches with 20 mm Al foam after the first and second region loading are shown in Figures 5.46

and 5.47, respectively. Based on these images and stress-central deflection plots, in the first linear part (1st region), the panel approached to bladder under compressive loading. The reaction force produced from the bladder was transmitted to the panel and initial debonding at the interface of the back face-sheet components (Al and GFPP) was observed during this zone as seen in Figure 5.46. In the second region, the bladder was continued to push the sandwich sample and stress increase caused to the complete separation of Al face-sheet from the whole panel. The constant central deflection in the plots might be attributed to the detachment of Al layer. However, even at the final state of the second zone, GFPP composite currently bonded to the foam core as shown in Figure 5.47.
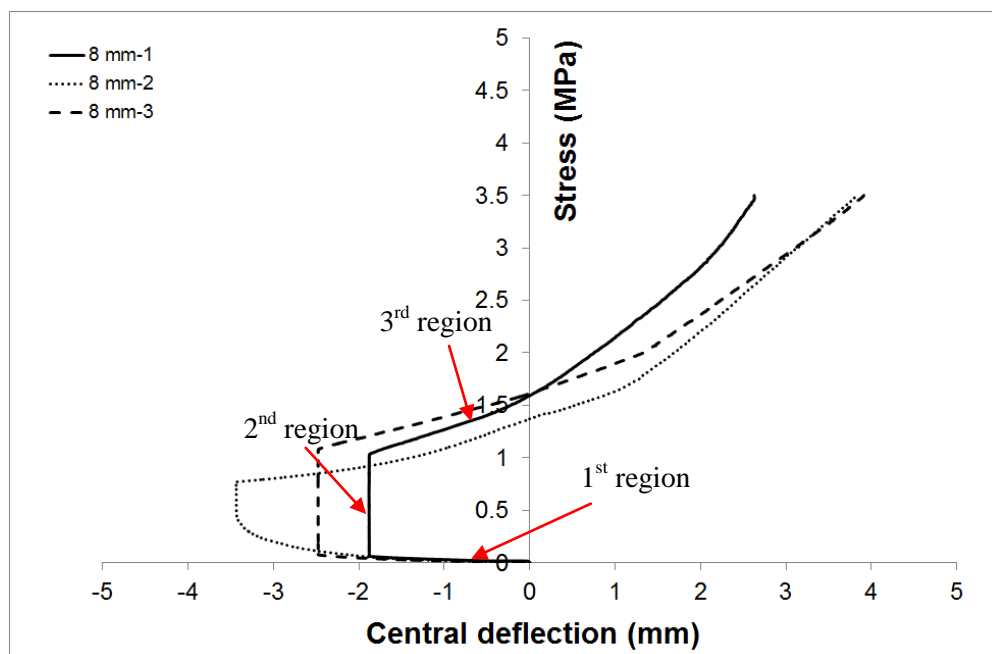
Figure 5.43. Stress vs. central deflection graph of Al sheet/GFPP/Al sandwiches with 8 mm Al foam during simulated blast test.
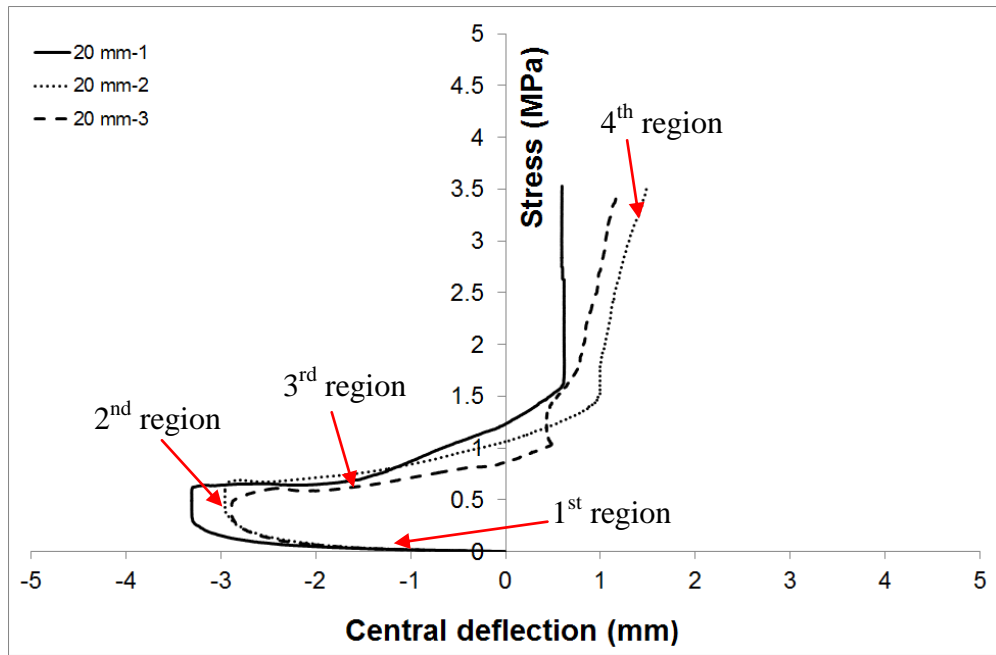
Figure 5.44. Stress vs. central deflection graph of Al sheet/GFPP/Al sandwiches with 20 mm Al foam during simulated blast test.
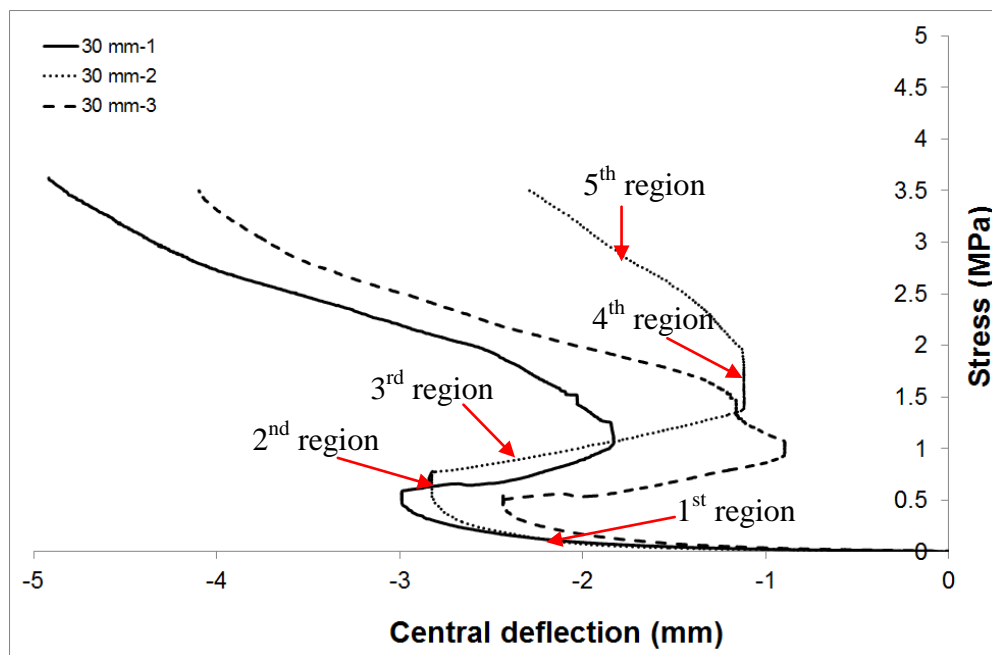
Figure 5.45. Stress vs. central deflection graph of Al sheet/GFPP/Al sandwiches with 30 mm Al foam during simulated blast test.
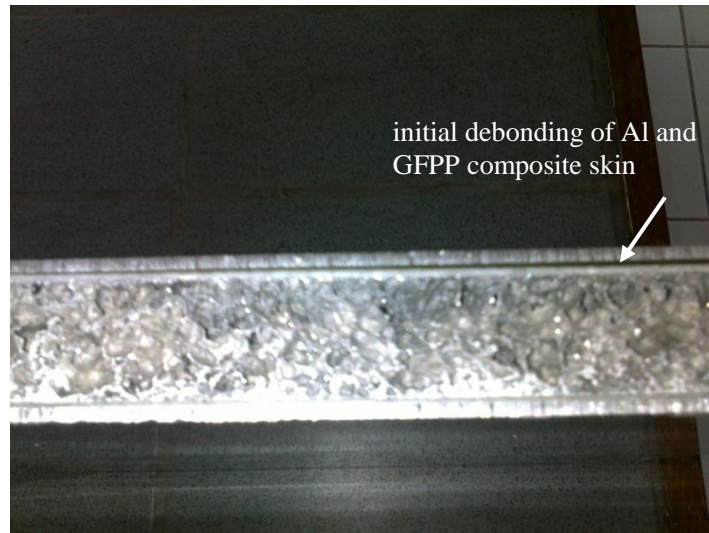
Figure 5.46. Side view of the sandwich test panel with 20 mm Al foam after loading up the end of 1st region with stress vs. central deflection plot.

Figure 5.47. Side view of the sandwich test panel with 20 mm Al foam after loading up the end of 2nd region with stress vs. central deflection plot.

Core shear or core crushing of Al foam was not observed during the 1st and 2nd regions and GFPP composite continued to protect the core material during these stages. The crushing of foam cells through the thickness of the panels started from the 3rd region and was not homogeneous during the compression. Therefore, the compaction of the whole sandwiches through the thickness did not occur and some variations in foam compaction for the different zones of the panel were observed. When the central part reached its maximum compaction capacity its deflection stopped, however, the zones around it continued to compact. Due to the collection of central deflection data, the graphs did not represent the whole sandwich structure deformation profile. As the core thickness increased, the repetition of this phenomenon was highly possible.

Core shear and core crushing were the main failure mechanisms observed in the panels after simulated blast tests. In spite of the debonding between the FML

components during the initial stages of the test, the protection of the core was performed by GFPP composite. Therefore, debonding of FML is not considered as a structural failure mechanisms such as skin wrinkling or core shear. Independent of core thickness, all the samples exhibited similar type of deformation patterns and images of the failed specimens as given in Figures from 5.48 to 5.50. Both front face and back face views are presented and 8 mm foam structures showed relatively uniform deformation profile. As expressed above, the compaction profiles through the thickness of the panels show disorderliness especially for thicker foam sandwiches. This non-uniformity is clearly seen in the figures. The back face of the samples exhibited dome-shaped deformation moving out from the center, changing a more quadrangular shape towards the supported edges. Both Al foam core and front face-sheet gained an inwardly curved shape. Along the panel plane the curvature extension was observed.

The identification of failure mechanisms has also great importance in terms of the compliance determination of the sandwich panels. The compliance (C_p) term of structures were calculated by considering the central deflection (w_t) and compressive stress (σ_{fail}) values associated with core-crushing failure. The average deflections of the panels after the simulated blast test were measured and given in Table 5.11. Based on the tabulated results, the final deflections of the samples are not similar to the values obtained from the stress-central deflection graphs. This is attributed to the compliance effect of the bladder. Besides that, in order to reveal the pure bending behavior of a sandwich panel, its compression compliance must be known. In this study, the compliance corrections of the bladder (including test frame) and sandwiches were done by compressive loading of the bladder and sandwich plates under the same test conditions. After compliance correction, the real deflections of the sandwich structures were obtained.

Table 5. 11. Average central deflection values measured after simulated blast test

Sample Type	Average Measured LVDT value (mm)
8 mm Al foam sandwich	17.36
20 mm Al foam sandwich	20.09
30 mm Al foam sandwich	19.45

core shear   debonding   core shear   core crushing   debonding of FML components

(a)

dome-shaped deformation profile

debonding of FML components

(b)
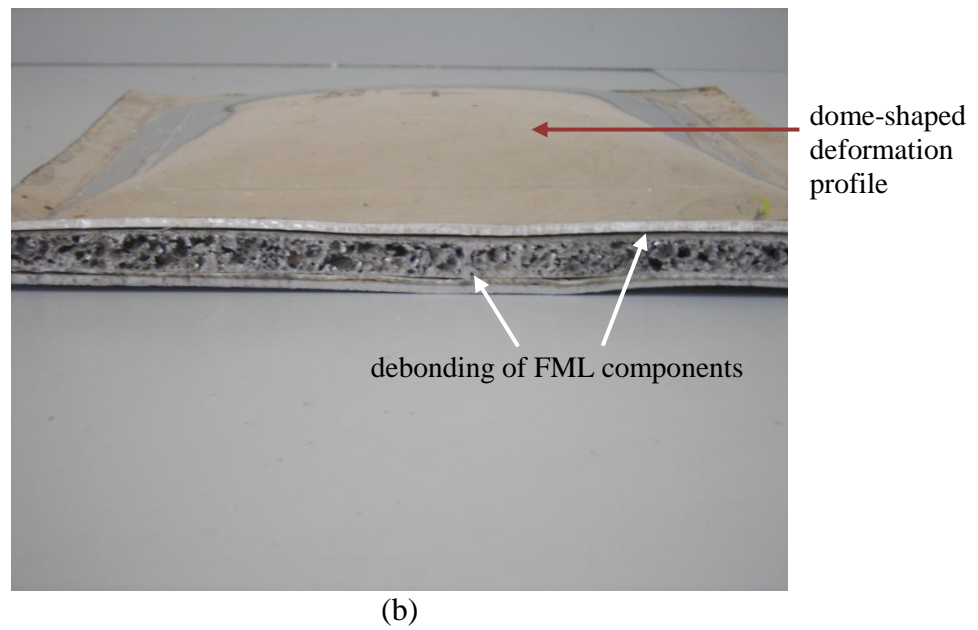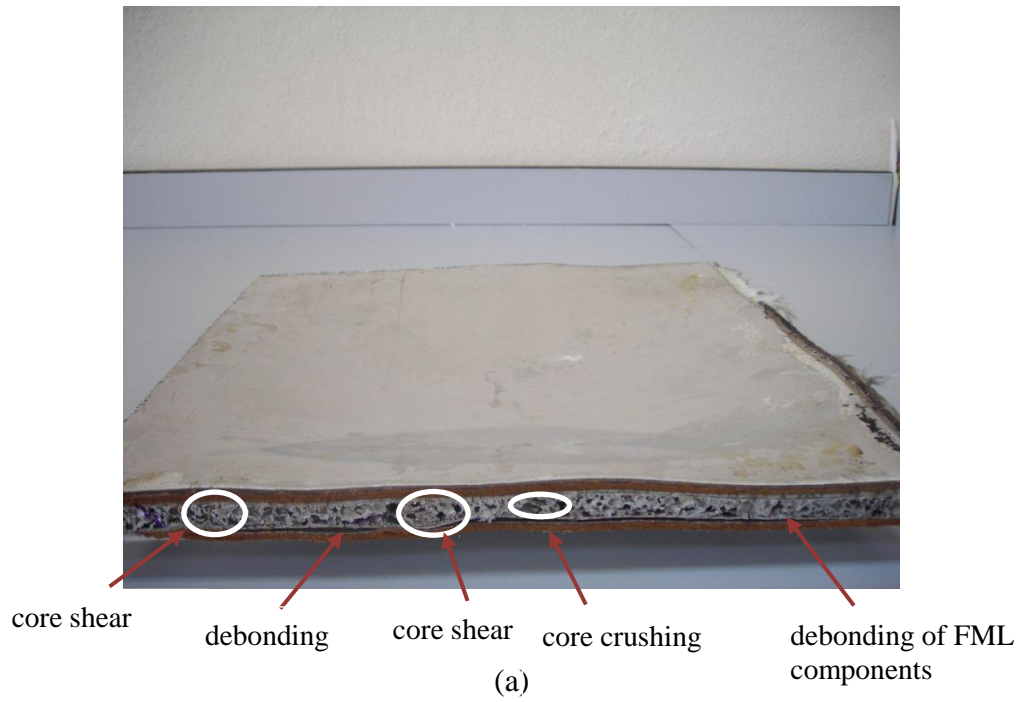
Figure 5.48. Deformation patterns of Al/GFPP/Al foam sandwich pane with 8 mm Al foam and loaded up to 200 kN: (a) front face view (b) back face view.
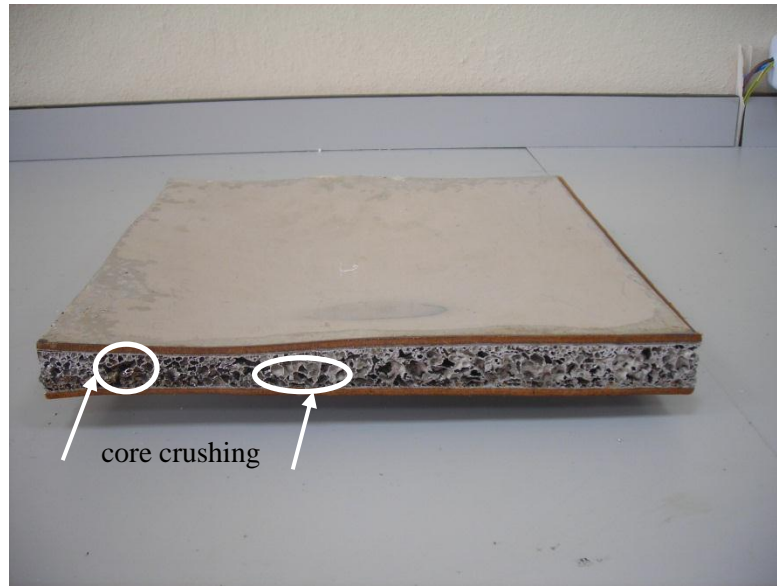
(a)
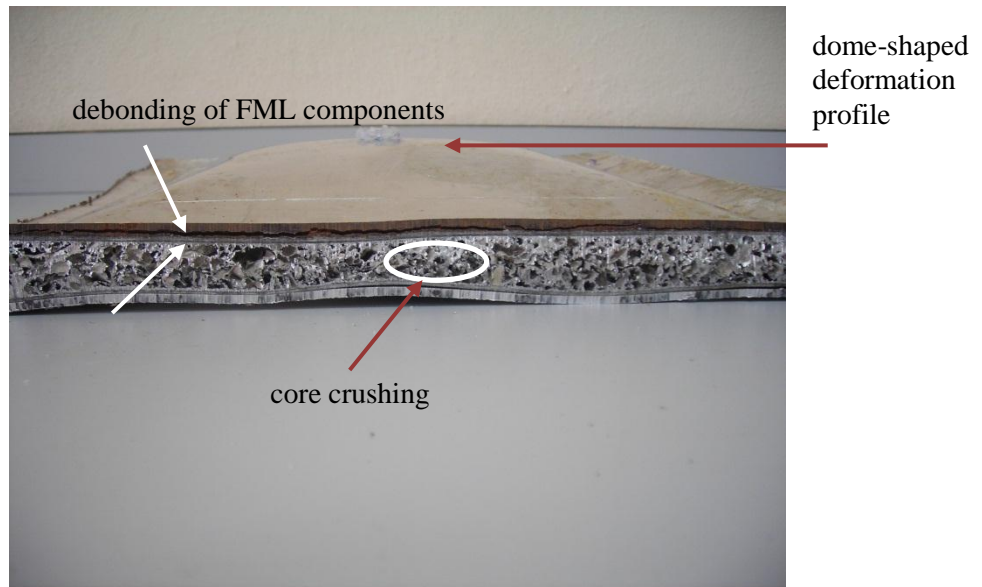
(b)

Figure 5.49. Deformation patterns of Al/GFPP/Al foam sandwich pane with 20 mm Al foam and loaded up to 200 kN: (a) front face view (b) back face view.
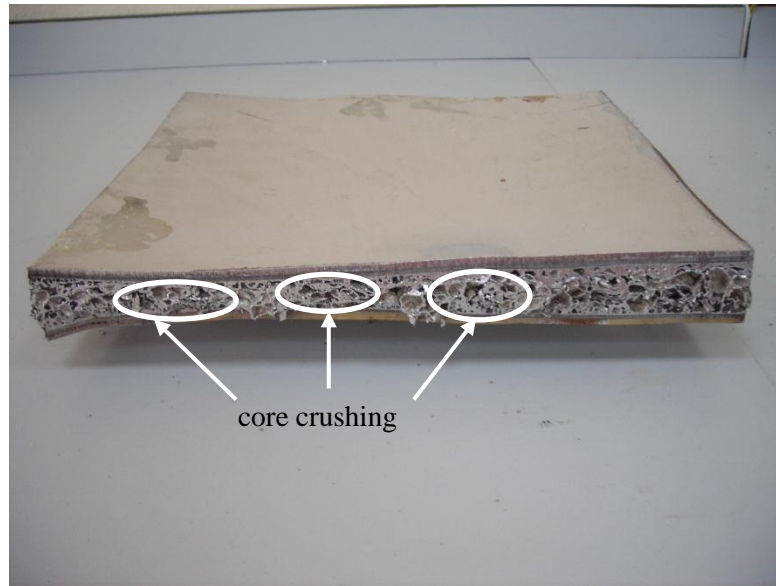
(a)
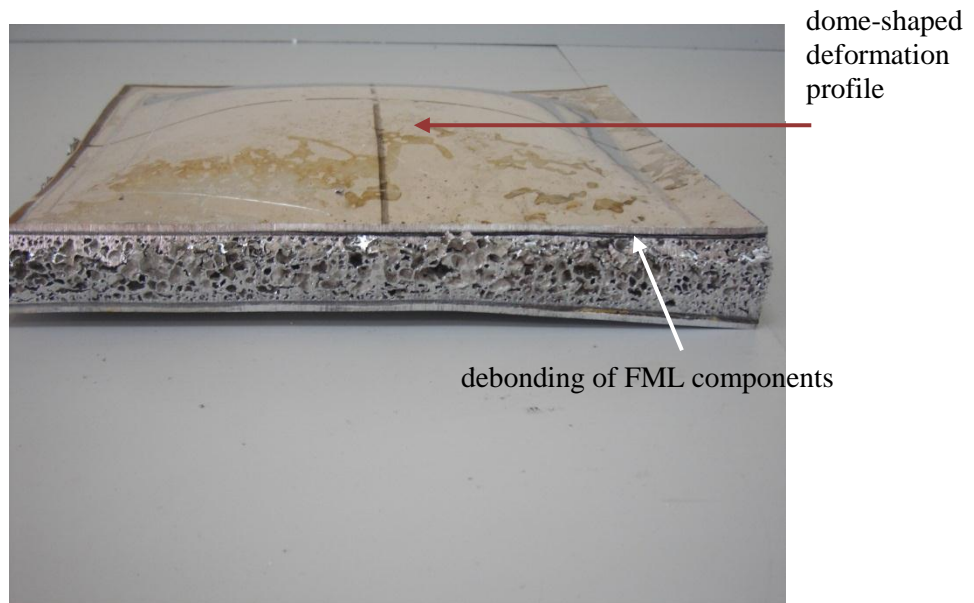
(b)

Figure 5.50. Deformation patterns of Al/GFPP/Al foam sandwich pane with 30 mm Al foam and loaded up to 200 kN: (a) front face view, (b) back face view.

The central deflection and stress graph of the bladder and sandwich panels during the compliance correction test are presented in Figures 5.51 and 5.52, respectively. The central deflection data was provided by LVDT measurement equipment located on the upper rigid plate. The same system was also adopted for the bladder and their characteristic curves were constructed. The images of sandwich panels

after the compliance test are seen in Figure 5.53. The real central deflection values of the samples were calculated by subtracting the compliance deflection values of individual bladder and sandwich system from the simulated blast test deflection values. The data numbers of the materials mentioned above were interpolated by means of curve fitting tool of the MATLAB software. The typical sandwich panels for each thickness set of foam based sandwiches were selected as representative cases. The Figures from 5.54 to 5.56 show both the compliance curves and simulated blast test results of selected panels.
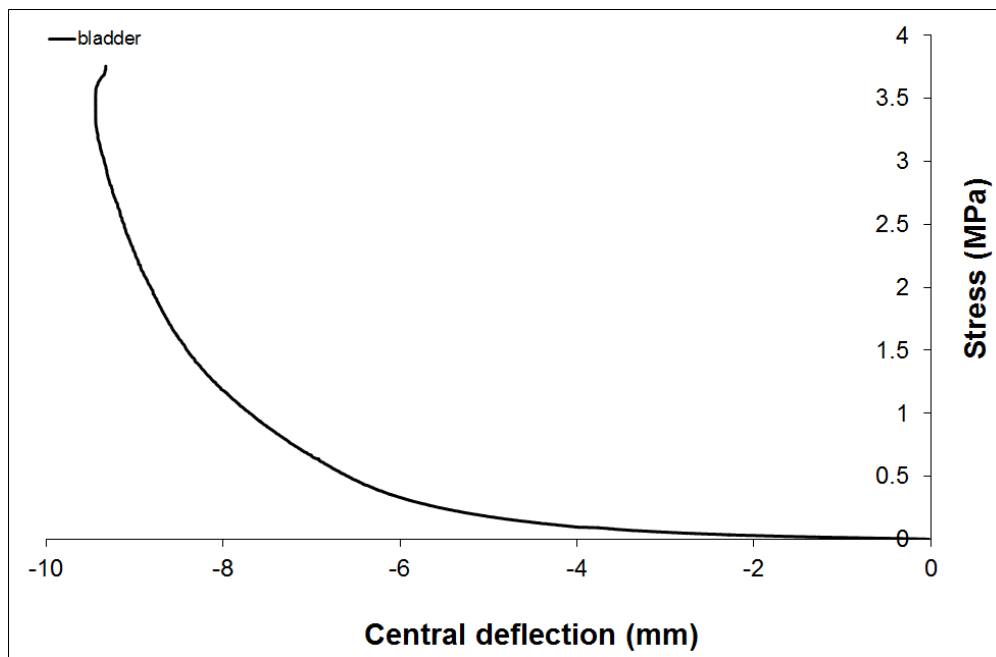
Figure 5.51. Compliance correction curve of the liquid soap filled bladder
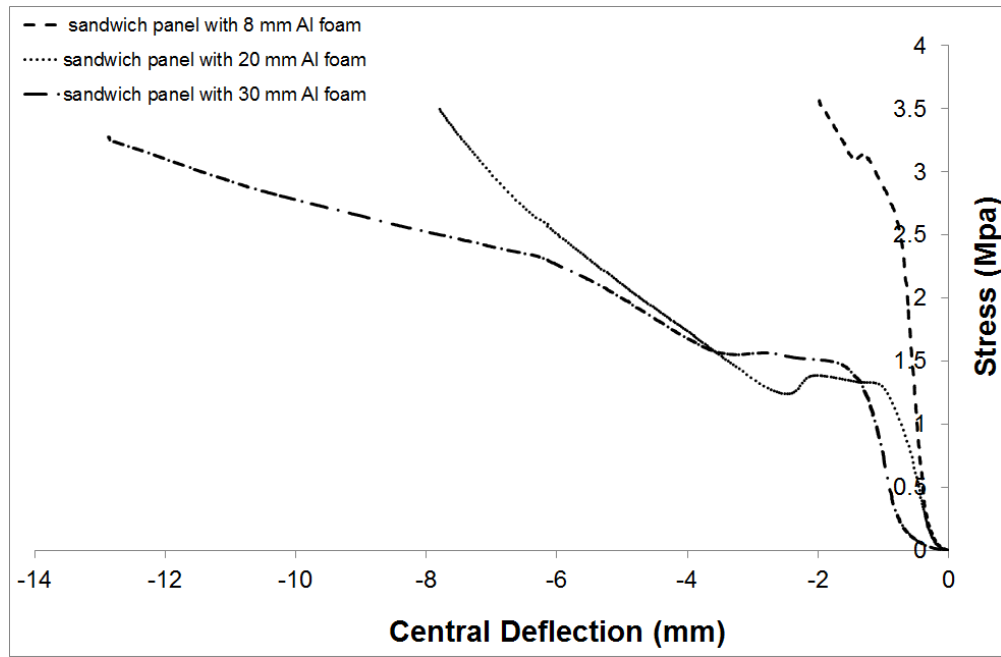
Figure 5.52. Compliance correction curve of the sandwich panels with various thicknesses of Al foams.

Figure 5.53. The sandwich panels after compliance test

138
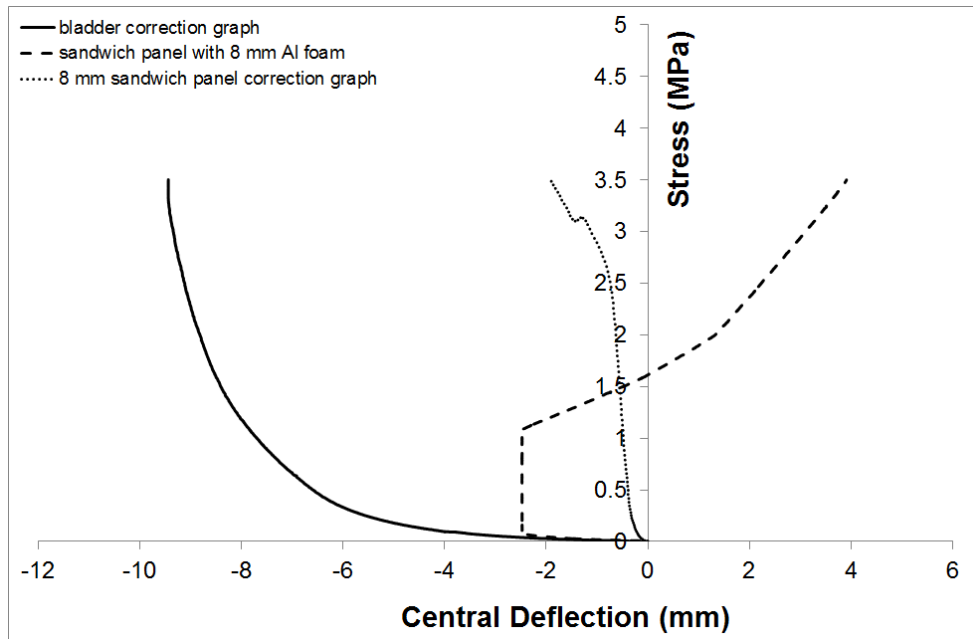
Figure 5.54. The compliance correction graphs of bladder, Al sheet/GFPP/Al foam sandwich panel with 8 mm Al foam and the response of same sandwich system during the simulated blast test.
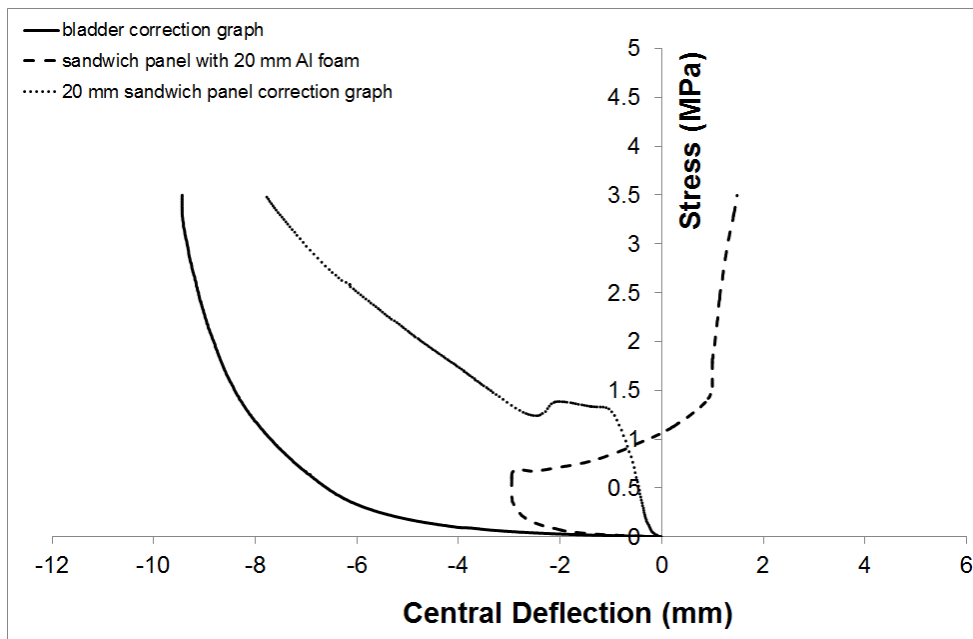
Figure 5.55. The compliance correction graphs of bladder, Al sheet/GFPP/Al foam sandwich panel with 20 mm Al foam and the response of same sandwich system during the simulated blast test.
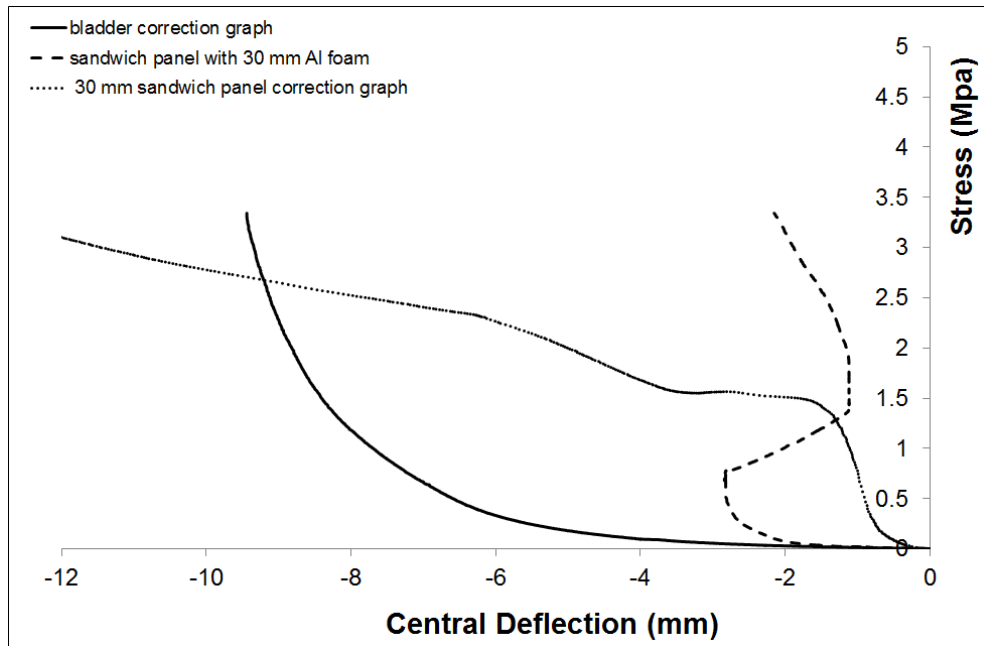
Figure 5.56. The compliance correction graphs of bladder, Al sheet/GFPP/Al foam sandwich panel with 30 mm Al foam and the response of same sandwich system during the simulated blast test.

After compliance correction, the compliance corrected stress vs. central deflection graphs of selected panels are shown in Figures from 5.57 to 5.59. In the literature, the compliance (C_p) of the sandwiches can be evaluated based on the failure points of the panels. For this study, the compliance of the sandwiches (C_p) was calculated by considering the central deflection at failure pressure as formulated in equation 4.13. The failure points of the panels were assigned as the starting of core crushing as indicated in the Figures. The natural frequencies (ω) of the sandwich specimens were approximated by using Equation 4.11. Both geometric and mechanical parameters required for this formulation are given in Tables 5.12 and 5.13. The poison ratio (v) of the Al/GFPP hybrid system was evaluated by using rule of mixtures. The total volume of an Al/GFPP specimen with rectangular cross-section was measured and volume of its constituents was calculated individually. Based on the known densities (ρ_{Al}: 2700 kg/m^3 and ρ_{GFPP}: 1579 kg/m^3) and Poison's ratios (v_{Al}: 0.33 and v_{GFPP}: 0.293) values of the materials, the Poison ratio value of the FML skin was calculated. The mechanical test results given in the previous sections of this thesis were used in order to calculate the natural frequency of the sandwich panels.
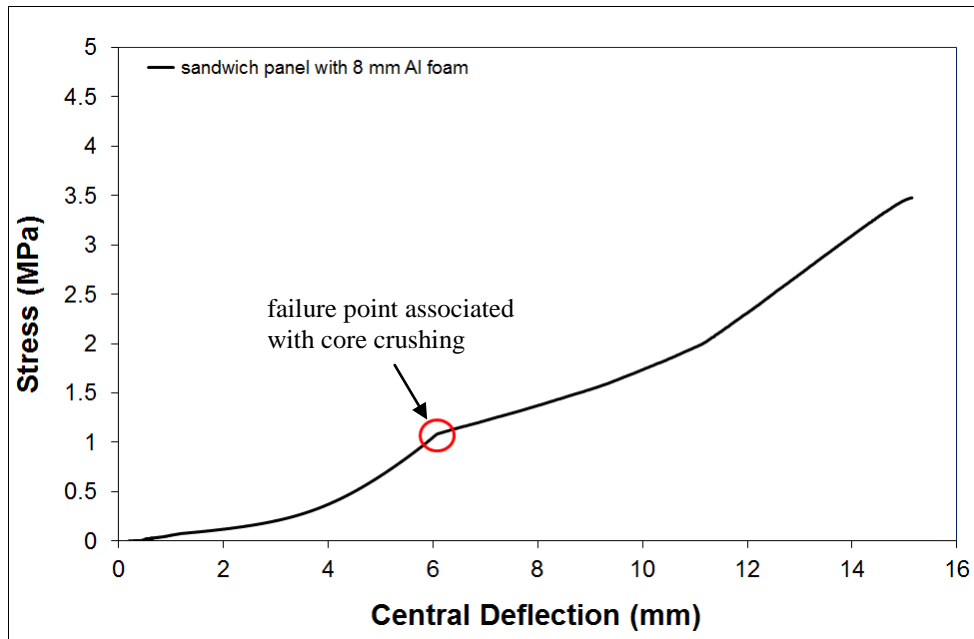
Figure 5.57. Stress vs. central deflection plot of Al sheet/GFPP/Al foam sandwich panel with 8 mm Al foam after compliance correction.
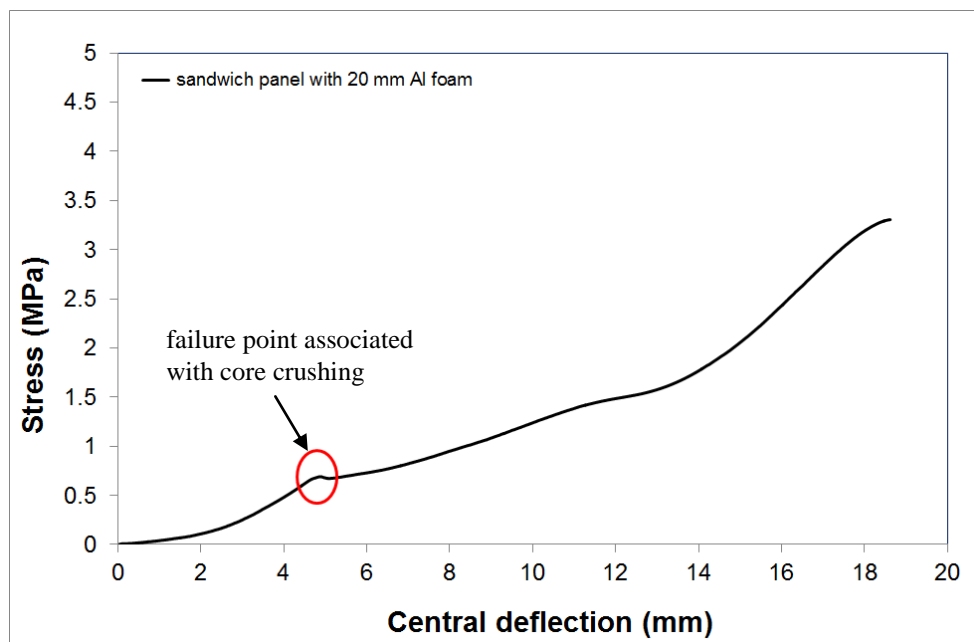
Figure 5.58. Stress vs. central deflection plot of Al sheet/GFPP/Al foam sandwich panel with 20 mm Al foam after compliance correction.
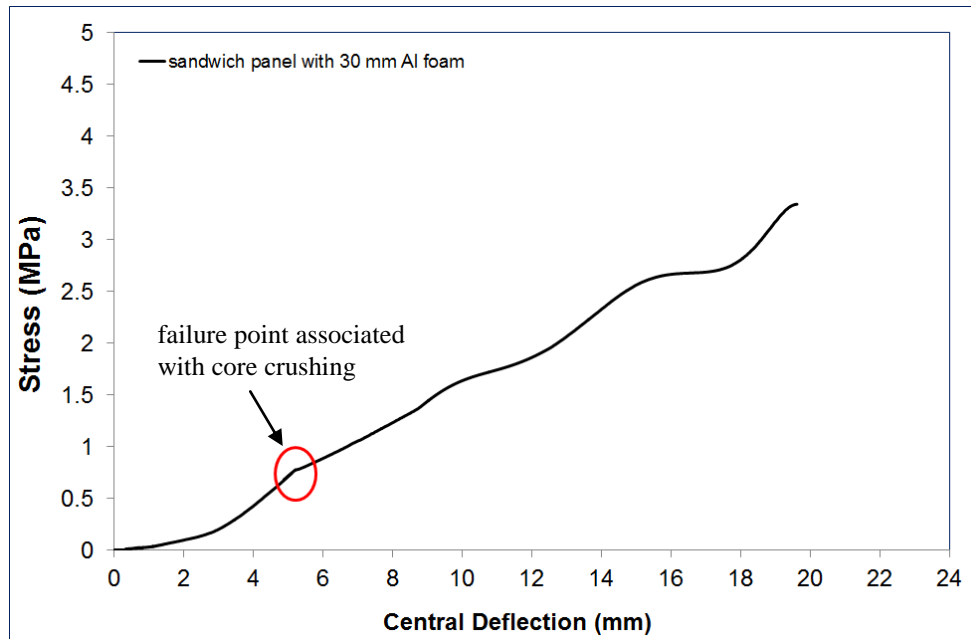
Figure 5.59. Stress vs. central deflection plot of Al sheet/GFPP/Al foam sandwich panel with 30 mm Al foam after compliance correction.

Table 5.12. Geometric parameters of sandwich panels

Sample Type	L_1/L_2	h_f (m)	h_c (m)	d (m)
8 mm Al foam sandwich			0.00795	0.0109
20 mm Al foam sandwich	1	0.0029	0.0179	0.0208
30 mm Al foam sandwich			0.0296	0.0325

Table 5.13. Mechanical parameters of sandwich panels

Sample Type	E_f (Pa)	G_c (Pa)	ρ_c (kg/m^3)	ρ_f (kg/m^3)	v_f	θ	ρ^* (kg/m^2)	ω (N/m.kg)
8 mm Al foam sandwich		51×10^6	361.7			0.168	17.445	3283.8
20 mm Al foam sandwich	4.006×10^9	18.5×10^6	330.4	2512	0.323	1.045	20.483	2616.6
30 mm Al foam sandwich		20.1×10^6	388.2			1.599	26.060	2954.6

The natural frequency of the panels depends on parameters tabulated in Tables 5.13 and 5.14. In this study, the length (L_1) and the width (L_2) of the panels were almost equal. Also, the properties related with FML face-sheet were the same. Hence, the core material properties significantly affected the natural frequency (ω) values of the structures. Based on equations 4.11 and 4.12, highest shear modulus and lowest foam thickness caused to minimum θ value and resulted in the maximum frequency as 3283.8 N/m.kg for 8 mm Al foam sandwich panel, as expected. Also, the core density markedly influences the planar density (ρ^*) and the natural frequencies of the structures highly dependent on this parameter.

Another important parameter used in this study is the blast characteristic time (T) to determine the peak deflection of the panel under blast pressure. Based on the pressure-time $(P\text{-}t)$ histories of panels, the characteristic time term was calculated by using equation 4.14. Figures 4.27 and 4.28 provided $P\text{-}t$ data for various TNT weights and stand-off distances, respectively. Eight different TNT weights and six stand-off distances were selected as representative cases for the determination of blast parameters. The maximum blast pressure (P_{blast}) values were clearly obtained from the same figures and minimum ten $P\text{-}t$ data was collected for the calculation of characteristic time parameter (T).

The sandwich panel deflection (δ_{static}) under maximum blast pressure was calculated by utilizing the C_p formulation. The compliance values of the samples were determined in the previous sections and for the required blast pressure, the corresponding δ_{static} values were calculated. The peak deflection (δ_{peak}) of the panel under blast pressure was evaluated by considering the dynamic effect of the system, $f(T\omega)$. The dimensionless deflection $(\delta_{peak}/\delta_{static})$ versus $f(T\omega)$ needs to be constructed by the differential equation governing to the system. Figure 5.60 is illustrated to clearly describe the dynamic effect of blast loading. The simple mechanical system loaded by a quasi-static force is shown in Figure 5.60 (a). However, the problem in our case is a single degree of freedom (SDOF) elastic oscillator loaded with a blast wave or impact excitation as seen in Figure 5.60 (b). During the analysis, the air blast wave is assumed as an exponentially decaying forcing function. The applied impulse parameter, I, is calculated by taking the time integral from the area under the $P\text{-}t$ curve. In general, the T is located where half of the impulse falls between time equal to zero and T. The other half of the impulse falls between time T and infinity. This mathematical discrepancy

occurs because the exponential decay never comes back to zero pressure; therefore, no definable duration *(T)* of loading exists. (Source: Baker, 1983)
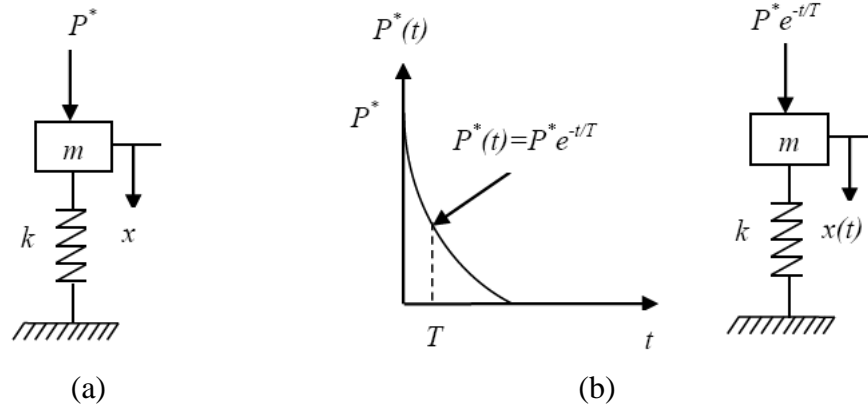
Figure 5.60. (a) The simple mechanical system under static loading, (b) linear oscillator loaded by a blast wave (Source: Baker, 1983).

For the system shown in Figure 5.60 (b), the equation of motion (Newton's second law) is

$$m\frac{d^2x}{dt^2} + kx = P^* e^{-t/T} \tag{5.1}$$

Based on Baker (1983), the initial conditions of no displacement and no velocity at time $t=0$, $x(0) = 0$ and $x'(0) = 0$, respectively. The complete solution of Eq. (5.1) is the summation of homogeneous $x_h(t)$ and particular $x_p(t)$ solutions:

$$x(t) = x_h(t) + x_p(t) \tag{5.2}$$

The homogeneous solution steps are given below:

$$x_h(t) = e^{st} \tag{5.3}$$

$$ms^2 e^{st} + ke^{st} = 0 \tag{5.4}$$

$$ms^2 + k = 0 \tag{5.5}$$

$$s = \mp \sqrt{-\frac{k}{m}} = \mp i \sqrt{\frac{k}{m}} \qquad (5.6)$$

$$x_h(t) = c_1 \sin \sqrt{\frac{k}{m}} t + c_2 \cos \sqrt{\frac{k}{m}} t \qquad (5.7)$$

After obtaining homogeneous solution, particular solution can be obtained following the steps given below.

$$x_p(t) = Ae^{bt} \qquad (5.8)$$

$$mAb^2 e^{bt} + kAe^{bt} = e^{bt}\left(mAb^2 + kA\right) = P^* e^{-t/T} \qquad (5.9)$$

$$e^{bt} = e^{-t/T} \qquad (5.10)$$

$$b = -\frac{1}{T} \qquad (5.11)$$

$$A\left(mb^2 + k\right) = P^* \qquad (5.12)$$

$$x_p(t) = \frac{P^*}{\dfrac{m}{T^2} + k} e^{-t/T} \qquad (5.13)$$

Therefore, the unknowns appearing in complete solution can be determined using the initial conditions;

$$x(0)=0 \qquad (5.14)$$

$$c_2 = -\frac{P^*}{\dfrac{m}{T^2} + k} \qquad (5.15)$$

$$x'(0)=0 \; ; \qquad (5.16)$$

$$c_1 = -\frac{\frac{1}{T}P^*}{\left(\frac{m}{T^2}+k\right)\sqrt{\frac{k}{m}}} \qquad (5.17)$$

The analytical solution of the system can be converted to the expression below after introducing the $\sqrt{k/m}$ as the natural frequency of the system (ω) in $x(t)$.

$$\frac{x(t)}{P^*/k} = \frac{1}{\frac{1}{\omega^2 T^2}+1}\left[\frac{\sin\omega t}{\omega T} - \cos\omega t + e^{-\frac{\omega t}{\omega T}}\right] \qquad (5.18)$$

$$= \frac{1}{\frac{\omega^2 T^2 + 1}{\omega^2 T^2}}\left[\frac{\sin\omega t}{\omega T} - \cos\omega t + e^{-\frac{\omega t}{\omega T}}\right] \qquad (5.19)$$

After some manipulations, final form of the equation of motion can be given as:

$$\frac{x(t)}{P^*/k} = \frac{(\omega T)^2}{1+(\omega T)^2}\left[\frac{\sin\omega t}{\omega T} - \cos\omega t + e^{-\frac{\omega t}{\omega T}}\right] \qquad (5.20)$$

The expression given in 5.20 must be differentiated with respect to time t, and the resulting velocity set equal to zero to obtain the scaled time (ωt_{max}) when $x(t)$ is maximum:

$$\underbrace{\frac{(\omega T)^2}{1+(\omega T)^2}\omega}_{\neq 0}\underbrace{\left[\frac{\cos\omega t}{\omega T} + \sin\omega t - \frac{1}{\omega T}e^{-\frac{\omega t}{\omega T}}\right]}_{=0} = 0 \qquad (5.21)$$

146

To have nontrivial solution to Eq. 5.21, the terms in the paranthesis must equal to zero, i.e.,

$$\frac{\cos \omega t_{max}}{\omega T} + \sin \omega t_{max} - \frac{1}{\omega T} e^{-\frac{\omega t_{max}}{\omega T}} = 0 \tag{5.22}$$

Eq. 5.22 in functional format can be expressed as

$$\omega t_{max} = \psi(\omega T) \tag{5.23}$$

Equation 5.22 is a transcendental equation and cannot be solved explicitly for ωt_{max}; however, it can be solved numerically. Once ωt_{max} is obtained for specific values of ωT, then ωt_{max} can be substituted into Eq.(5.20) to obtain resulting $\frac{x_{max}}{P^*/k}$ as a function of ωT. In functional format, the solution given by Equation 5.20 is reduced to;

$$X^-_{max} = \frac{x_{max}}{P^*/k} = \psi(\omega T) \tag{5.24}$$

In our study, both blast characteristic time *(T)* and maximum blast pressure *(P*)* parameters were obtained based on *P-t* analysis. The natural frequencies of the sandwich panels with three different thicknesses were also calculated. Based on equation 5.22, the ωt values for each *Tω* product were calculated and the computed ωt was added into the equation 5.20 with corresponding *Tω* value. Hence, the *f (Tω)* was plotted and the resultant X^-_{max} values can be determined. According to Figure 5.60 (a), the deflection *(δ_{static})* of the mass-spring system under *P** loading is equal to *P*/k*. When the same system is subjected to dynamic blast loading, *P*e$^{-t/T}$*, the deflection *x(t)* becomes δ_{peak} and the ratio between them equals to the X^-_{max}. Therefore, equation 5.24 can be represented as shown below:

$$X_{\max}^{-} = \frac{\delta_{peak}}{\delta_{static}} \qquad\qquad (5.25)$$
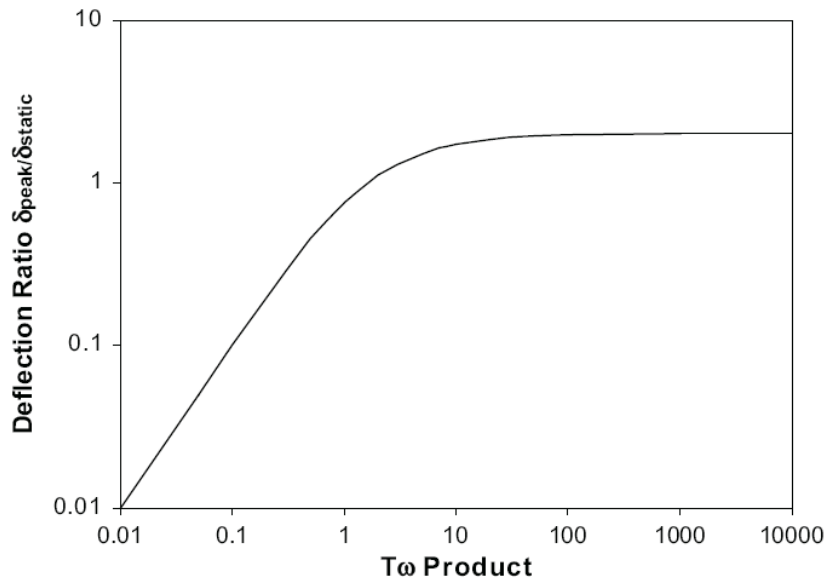
Figure 5.61. Characteristic curve of SDOF system under blast loading
(Source: Andrews, 2009)

Figure 5.61 shows a blast loaded oscillator which is familiar to sinusoidal driven excitation (Andrews, et al. 2009). The original form of this figure is given in Figure 3.21. Based on this figure, the solution presented in Figure 5.61 can be approximated by two straight line asymptotes. For very large values of $T\omega$ (greater than 40) and for very small values of $T\omega$ (less than 0.4), these asymptotes show very accurate approximations to the general solutions. The tables from 5.14 to 5.19 show the blast parameters of sandwich panels for various explosive weights and stand-off distances. As seen in Table 5.14, the maximum blast pressure was calculated as 15.645 MPa for 12 kg TNT explosive. The increase of TNT amount led to the increase of blast pressure, static and peak deflection parameters, as expected. The decaying characteristics of the blast pressure-time variation curve significantly affected the characteristic time term, T. Based on the tabulated results, the increase of T was not always proportional to TNT amount and showed its maximum and minimum values for 10 kg and 1 kg explosive weights, respectively. The $T\omega$ product is constructed as a function of X_{max}^{-} ($\delta_{peak}/\delta_{static}$) and called as "dimensionless deflection" obtained from Figure 5.61. This critical term was also given in the tables below. Although the dimensionless deflection of sandwich

148

panels showed close similarities, the average $\delta_{peak}/\delta_{static}$ ratio of 8 mm Al foam sandwich specimen exhibited the maximum value. The peak deflections of the samples were calculated based on this ratio and given in the same tables. As compared with the static and peak deflections of the panels for the same explosive weights, the 8 mm foam sandwich panel showed minimum values while the panel with 20 mm foam exhibited maximum deflections. The 20 mm and 30 mm Al foam sandwich panels showed the highest peak deflections of 241.049 mm and 219.720 mm for 12 kg TNT explosive, respectively. However, the deflection of 8 mm sandwich structure for the same weight was calculated as 181.546 mm. This situation is closely related with the natural frequency and compliance values of the sandwich structures. maximum deflections. The 20 mm and 30 mm Al foam sandwich panels showed the highest peak deflections of 241.049 mm and 219.720 mm for 12 kg TNT explosive, respectively. However, the deflection of 8 mm sandwich structure for the same weight was calculated as 181.546 mm. This situation is closely related with the natural frequency and compliance values of the sandwich structures.

Table 5.14. The variation of blast parameters of 8 mm Al foam sandwich with respect to TNT explosive amount for 45 cm stand-off distance

Sample Type	C_p (mm/MPa)	TNT amount (kg)	T (msec)	P_{blast} (MPa)	$T\omega$ (N.msec/m.kg)	δ_{static} (mm)	X_{max}	δ_{peak} (mm)
8 mm Al foam sandwich	5.8775	12	0.0367	15.645	120.515	91.953	1.974	181.516
		10	0.0384	14.431	126.097	84.818	1.976	167.600
		8	0.0333	13.112	109.350	77.065	1.972	151.973
		6	0.0322	11.387	105.738	66.927	1.971	131.913
		4	0.0285	9.637	93.588	56.641	1.967	111.413
		2	0.0288	6.880	94.573	40.437	1.968	79.580
		1.37	0.0345	5.450	113.291	32.032	1.973	63.199
		1	0.0292	4.886	95.886	28.717	1.968	56.515

Table 5.15. The variation of blast parameters of 20 mm Al foam sandwich with respect to TNT explosive amount for 45 cm stand-off distance.

Sample Type	C_p (mm/MPa)	TNT amount (kg)	T (msec)	P_{blast} (MPa)	$T\omega$ (N.msec/m.kg)	δ_{static} (mm)	X_{max}	δ_{peak} (mm)
20 mm Al foam sandwich	7.8290	12	0.0367	15.645	96.029	122.484	1.968	241.049
		10	0.0384	14.431	100.477	112.98	1.969	222.458
		8	0.0333	13.112	87.132	102.653	1.965	201.714
		6	0.0322	11.387	84.254	89.148	1.963	174.999
		4	0.0285	9.637	74.573	75.448	1.959	147.802
		2	0.0288	6.880	75.358	53.863	1.959	105.518
		1.37	0.0345	5.450	90.272	42.668	1.966	83.885
		1	0.0292	4.886	76.404	38.252	1.960	74.974

Table 5.16. The variation of blast parameters of 30 mm Al foam sandwich with respect to TNT explosive amount for 45 cm stand-off distance.

Sample Type	C_p (mm/MPa)	TNT amount (kg)	T (msec)	P_{blast} (MPa)	$T\omega$ (N.msec/m.kg)	δ_{static} (mm)	X_{max}	δ_{peak} (mm)
30 mm Al foam sandwich	7.1254	12	0.0367	15.645	108.433	111.476	1.971	219.720
		10	0.0384	14.431	113.456	102.826	1.973	202.876
		8	0.0333	13.112	98.388	93.428	1.969	183.960
		6	0.0322	11.387	95.138	81.136	1.968	159.677
		4	0.0285	9.637	84.206	68.667	1.963	134.794
		2	0.0288	6.880	85.092	49.022	1.964	96.280
		1.37	0.0345	5.450	101.933	38.833	1.970	76.501
		1	0.0292	4.886	86.274	34.814	1.964	68.376

Tables from 5.17 to 5.19 show the variation of blast parameters with respect to different stand-off distances for 1.37 kg TNT. The maximum blast pressure was calculated as 14.89 MPa when the distance between the panel and the explosive center was 0.2 m. Based on the tabulated results, the increase of stand-off distance resulted in the decrease of blast pressure. Except for the 0.3 m distance, the blast characteristic time exhibited higher values for longer stand-off distances. By considering Figure 5.61, the f $(T\omega)$ products were evaluated and the resultant dimensionless deflections of the panels were determined. As in the tables given for different TNT amounts, the 8 mm Al foam

sandwich showed the maximum average dimensionless deflection compared to the thicker foam structures. The 20 mm Al foam panel exhibited highest peak deflection of 226.619 mm when the stand-off distance was 0.2 m. The minimum deflection was calculated as 24.163 mm for 8 mm foam structure at 0.7 m stand-off distance.

Table 5.17. The variation of blast parameters of 8 mm Al foam sandwich with respect to stand-off distance for 1.37 kg TNT explosive.

Sample Type	C_p (mm/MPa)	Stand-off distance (m)	T (msec)	P_{blast} (MPa)	$T\omega$ (N.msec/m.kg)	δ_{static} (mm)	X_{max}^-	δ_{peak} (mm)
8 mm Al foam sandwich	5.8775	0.2	0.02098	14.89	69.410	87.515	1.956	171.18
		0.3	0.0196	7.806	64.844	45.879	1.953	89.603
		0.4	0.0287	6.01	94.951	35.323	1.967	69.481
		0.5	0.0386	3.707	127.704	21.787	1.976	43.052
		0.6	0.06013	2.907	198.934	17.085	1.984	33.898
		0.7	0.0788	2.068	260.701	12.154	1.988	24.163

Table 5.18 The variation of blast parameters of 20 mm Al foam sandwich with respect to stand-off distance for 1.37 kg TNT explosive

Sample Type	C_p (mm/MPa)	Stand-off distance (m)	T (msec)	P_{blast} (MPa)	$T\omega$ (N.msec/m.kg)	δ_{static} (mm)	X_{max}^-	δ_{peak} (mm)
20 mm Al foam sandwich	7.8290	0.2	0.02098	14.89	54.896	116.573	1.944	226.62
		0.3	0.0196	7.806	51.285	61.113	1.941	118.62
		0.4	0.0287	6.01	75.096	47.052	1.959	92.175
		0.5	0.0386	3.707	101.008	29.022	1.969	57.144
		0.6	0.06013	2.907	157.336	22.758	1.980	45.062
		0.7	0.0788	2.068	260.188	16.190	1.988	32.186

Table 5.19. The variation of blast parameters of 30 mm Al foam sandwich with respect to stand-off distance for 1.37 kg TNT explosive.

Sample Type	C_p (mm/MPa)	Stand-off distance (m)	T (msec)	P_{blast} (MPa)	$T\omega$ (N.msec/m.kg)	δ_{static} (mm)	X_{max}^-	δ_{peak} (mm)
30 mm Al foam sandwich	7.1254	0.2	0.0209	14.89	61.987	106.097	1.951	206.995
		0.3	0.0196	7.806	57.910	55.620	1.947	108.293
		0.4	0.0287	6.01	84.797	42.823	1.964	84.105
		0.5	0.0386	3.707	114.047	26.413	1.973	52.114
		0.6	0.0601	2.907	177.660	20.713	1.982	41.054
		0.7	0.0788	2.068	232.822	14.735	1.987	29.279

Independent of TNT amount or stand-off distance, the 8 mm foam panel showed the minimum deflection while the 20 mm foam structure exhibited the highest deflection. This situation is attributed to the minimum δ_{static} value of the thinner panel because of its lower C_p. For the same blast pressures, the static deflection parameter showed a direct relationship with the compliance term. As this terms decrease, the δ_{static} value also decreases. The final step of the simulated blast test is the determination of failure index. This index represents the ratio of peak deflection of the panel (δ_{peak}) under blast pressure to the deflection of the same panel under quasi-static compression loading (w_{fail}). If the failure index is greater than or equal to one, the panel is predicted to fail. Otherwise, the panel is assumed to survive. The tables from 5.20 to 5.25 show the failure index values of the structures. The failure index aligned from the highest to lowest values by considering the corresponding blast pressures. Based on the table results, none of the panels can survive. This is attributed to the high blast pressure values used in our analysis. In the literature, Andrews et al. (2009) evaluated some quasi-static test results under blast loading conditions and in their study the blast pressure was selected as 0.279 MPa. In our analysis, the minimum pressure was 2.068 MPa and corresponding peak deflection was 24.163 mm with 4.09 failure index. Both TNT weights and stand-off distance parameters were selected based on the real threats; therefore the present results represent the dynamic deflections under real conditions.

Table 5.20. The failure index values of 8 mm Al foam sandwich panel with respect to TNT amount for 45 cm stand-off distance.

Sample Type	w_{fail} (mm)	TNT amount (kg)	Failure Index (δ_{peak}/w_{fail})
8 mm Al foam sandwich	5.894	12	30.796
		10	28.435
		8	25.784
		6	22.380
		4	18.902
		2	13.501
		1.37	10.722
		1	9.588

Table 5.21. The failure index values of 20 mm Al foam sandwich panel with respect to TNT amount for 45 cm stand-off distance

Sample Type	w_{fail} (mm)	TNT amount (kg)	Failure Index (δ_{peak}/w_{fail})
20 mm Al foam sandwich	4.496	12	53.614
		10	49.479
		8	44.865
		6	38.923
		4	32.874
		2	23.469
		1.37	18.657
		1	16.675

Table 5.22. The failure index values of 30 mm Al foam sandwich panel with respect to TNT amount for 45 cm stand-off distance.

Sample Type	w_{fail} (mm)	TNT amount (kg)	Failure Index (δ_{peak}/w_{fail})
30 mm Al foam sandwich	4.892	12	44.911
		10	41.468
		8	37.601
		6	32.638
		4	27.552
		2	19.680
		1.37	15.637
		1	13.976

Table 5.23. The failure index values of 8 mm Al foam sandwich panel with respect to stand-off distances for 1.37 kg TNT.

Sample Type	w_{fail} (mm)	Stand-off Distance (m)	Failure Index (δ_{peak}/w_{fail})
8 mm Al foam sandwich	5.894	0.2	29.043
		0.3	15.202
		0.4	11.788
		0.5	7.304
		0.6	5.751
		0.7	4.099

Table 5.24. The failure index values of 20 mm Al foam sandwich panel with respect to stand- off distances for 1.37 kg TNT.

Sample Type	w_{fail} (mm)	Stand-off Distance (m)	Failure Index (δ_{peak}/w_{fail})
20 mm Al foam sandwich	4.496	0.2	50.404
		0.3	26.383
		0.4	20.501
		0.5	12.710
		0.6	10.022
		0.7	7.1589

Table 5.25. The failure index values of 30 mm Al foam sandwich panel with respect to stand-off distances for 1.37 kg TNT.

Sample Type	w_{fail} (mm)	Stand-off Distance (m)	Failure Index (δ_{peak}/w_{fail})
30 mm Al foam sandwich	4.892	0.2	42.313
		0.3	22.136
		0.4	17.192
		0.5	10.653
		0.6	8.392
		0.7	5.985

Based on the simulated test results, the $f(T\omega)$ product has vital importance in terms of the failure of the panels. It can be concluded from Figure 5.61 that, for long blast durations (large $T\omega$ values) compared to the natural period of the system, the peak deflections arrive at a constant value equal to twice of the static deflection, δ_{static}. However, for short durations (small $T\omega$ values), the dimensionless deflection ($\delta_{peak}/\delta_{static}$)becomes equal to the $T\omega$ product and can be much lower than the constant value seen for large $T\omega$ values. Therefore, the variation of T and ω significantly influence the dynamic deflection of the structure. Both blast pressure and impulse parameters directly affect the characteristic time of the blast wave. Similarly, the parameters related with the natural frequency of the panel such as L_1/L_2 ratio, E_f, h_f, d,θ, G_c and ρ^* indirectly operate the dynamic response of the system. The increase of difference between the static failure pressure and blast pressure markedly change the δ_{static} of the sandwich structure. Under higher blast pressures, this difference becomes higher and when the $f(T\omega)$ is larger than one, the δ_{peak} will be greater than w_{fail} which leads to the increase of failure index. Thus, the survivability of the panel highly dependent on these parameters mentioned above.

5.9. Dynamic Response of Material Systems Under Blast Loading

In this study, both monolithic materials and layered structures were subjected to blast loading by C4 explosive. As explained in the experimental section of this thesis, the composites fabricated with both commercial fabrics and developed structures were tested and compared in terms of their performance under real blast test conditions. The tested material systems were classified in five groups and their images after blast loadings are given in the photos below. Figure 5.62 shows the deformation of monolithic armor steel and Al sheets after blast testing. As seen from the figure, Al exhibited dome like deformation in its center part with a large inelastic deformation, however, armor steel showed relatively smaller deformation compared to the Al sheet under the same blast conditions.
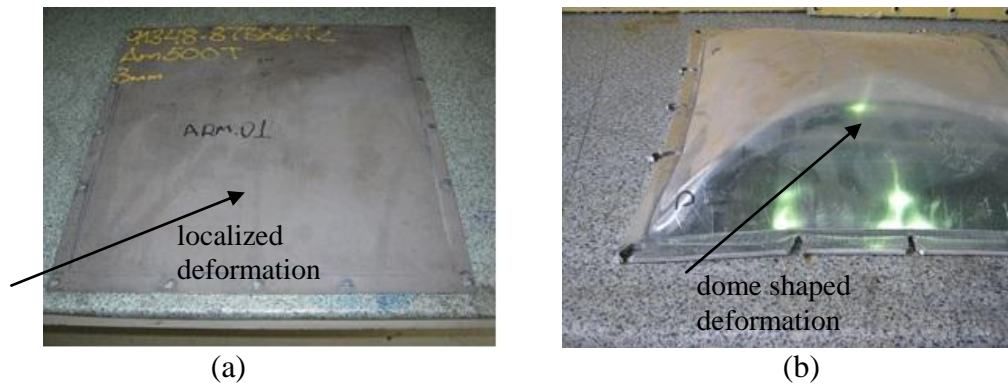
Figure 5.62. Deformation views of monolithic materials (a) armor steel (b) Al sheet after blast loading of C4 explosive.
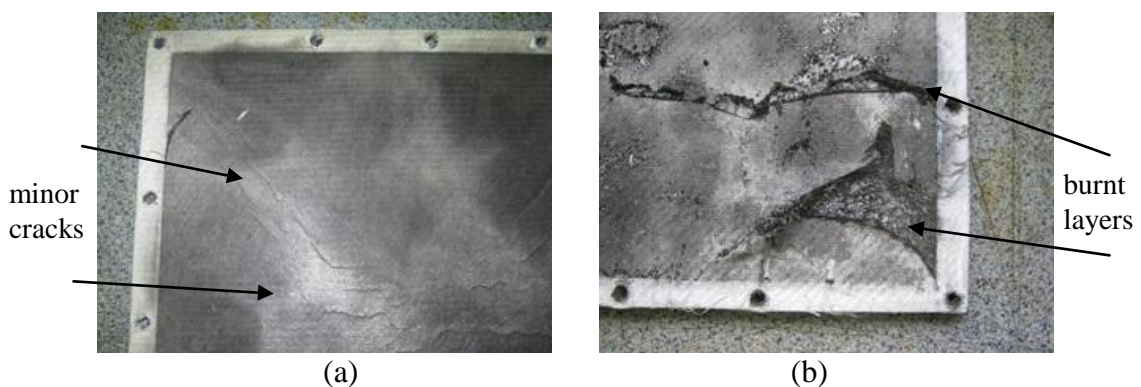
Figure 5.63. Deformation views of thermoplastic based composites (a) GFPP composite (b) PP based Miliken Tegris composite after blast loading of C4 explosive.
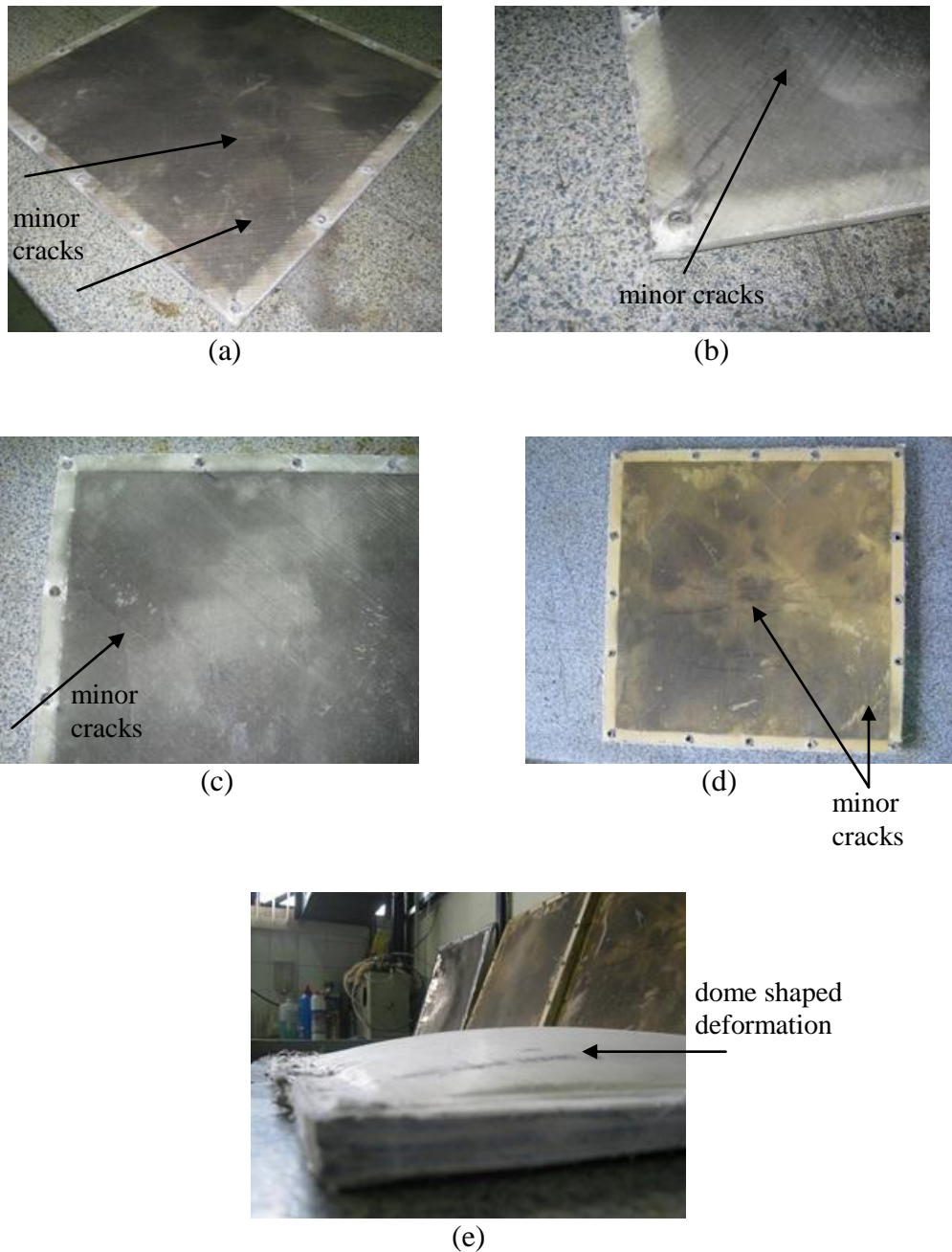
Figure 5.64. Deformation views of thermoset based composites: (a) GFVE (glass fiber reinforced vinyl-ester) composite, (b) GFPE (glass fiber reinforced polyethylene) composite (c) GFE (glass fiber reinforced epoxy) composite (d) Aramid based composite (e) Polyethylene based Dyneema™ composite.

The deformation patterns of hybrid material systems are seen in figures from 5.63 to 5.65. The thermoplastic based composites are shown in Figure 5.63. A relatively slight deformation was observed for the GFPP composite as compared to the monolithic materials. Small localized deformation was observed in the center part of the GFPP

plates with minor cracks along the edges. However, Miliken tegris™ based composite showed larger deformation and some burnt layers were seen as a result of blast effect.

The structural responses of thermoset based composites after blast test are exhibited in Figure 5.64. As seen from the pictures, minor cracks existed in some regions between sample and apparatus connection. Localized deformation opposite to the blast direction was observed for both GFVE and GFE composites. Also, positive swelling pattern outward to the apparatus direction was seen for GFPE composite. The extent of localized deformation was smaller in the center zone of the Dyneema plate as compared to the Aramid based composite.

Figure 5.65 shows the deformation effects of blast loading in FML systems. Delamination among the Dyneema layers was observed as a result of blast phenomenon. Debonding of Al and GFPP components was also seen after the tests. A uniform dome was present in the center parts of the two hybrid FML plates while a more quadrangular shape was observed towards the clamped edges. Almost no significant deformation was existent in the GFPP composite as can be seen from the photos.

Figure 5.66 exhibits the photos of Aramid/Al foam sandwich after blast testing. Core crushing damage was significantly observed with a cavity between the front face and crushed foam. Delamination of aramid layers and debonding of foam and composite material were also present as a result of blast effect. Regardless of the hybrid material system type, the adhesion between samples and apparatus was protected after blast testing.

delamination   dome shaped deformation

inelastic deformation with quadrangular shape

(a)

debonding

dome shaped deformation

(b)
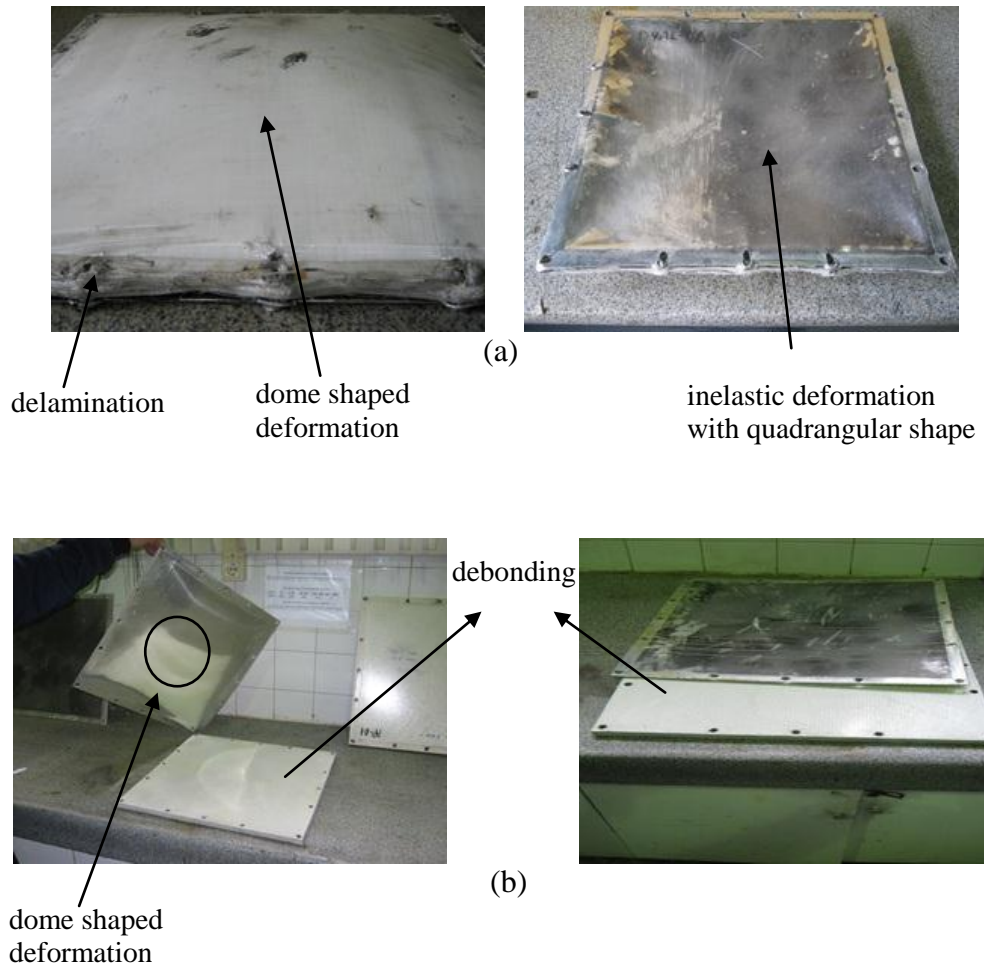
Figure 5.65. Deformation views of, (a) Al/Dyneema FML system (b) Al/GFPP FML system.

(a)

(b)

inwardly curved shape of front face

cavity due to the foam fragmentation and core crushing
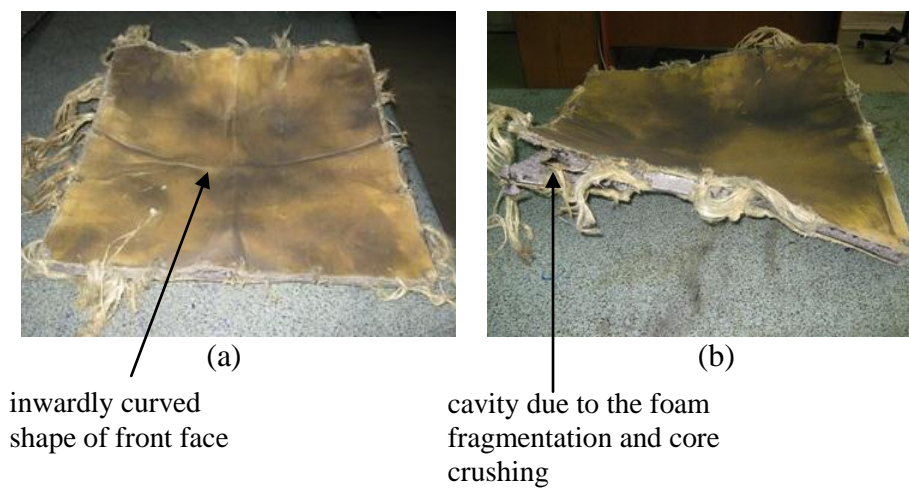
Figure 5.66. Deformation views of Al foam based sandwich structures.

(Cont. on next page)

158

delamination within (c) aramid layers

(d) debonding between foam and composite
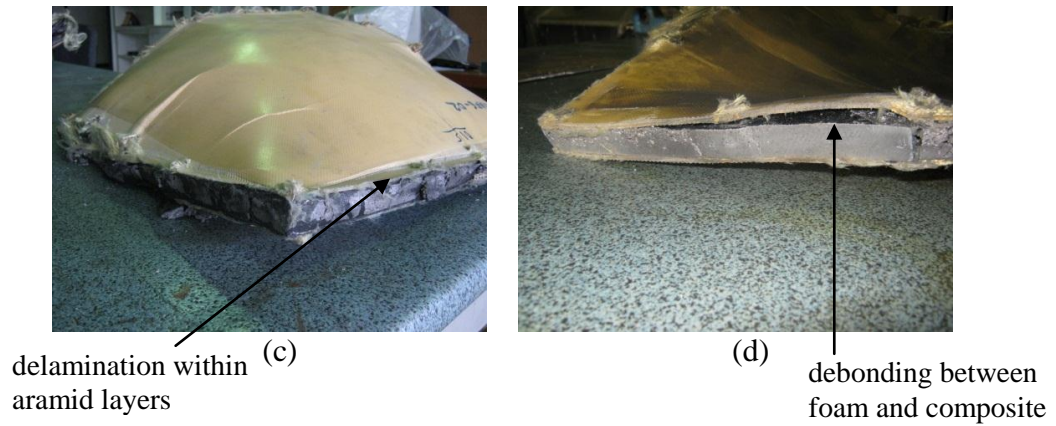
Figure 5.66. (Cont.)

Table 5.26. Comparison of central part deformations of hybrid material systems and monolithic materials after air blast testing.

Sample Type	Thickness (mm)	Areal Density (kg/m^2)	Deformation in the Central Region (mm)	Deformation in Central Region/Areal Density (m^3/kg)x10^3
Aramid/Al foam Sandwich System	26.90	16.85	110.70	6.5697
Aluminum	5.03	13.40	69.50	5.1865
Al/Dyneema FML System	13.20	16.30	51.60	3.1216
Polyethlyene Based Dyneema Composite	16	15.68	33.20	2.1173
Armor Steel	3.50	28.80	7.66	0.2659
Glass Fiber/Polyester (GFPE) Composite	10.24	17.23	4.50	0.2611
Polypropylene based Miliken Tegris	22.20	16.60	4.10	0.2469
Aramid Composite	21.30	26.00	2.70	0.1038
Al/GFPP FML system	16.90	26.50	2.10	0.0792
Glass fiber/Polypropylene (GFPP) Composite	21.80	30.26	0.30	0.0099
Glass Fiber/Vinylester (GFVE) Composite	10.64	16.20	-0.90	-0.0555
Glass Fiber/Epoxy (GFE) Composite	10.10	17.13	-1.60	-0.0934

The central deformation values of both monolithic materials and hybrid material systems are given in Table.5.26. GFPP composite, Al/GFPP FML system and Al foam with aramid composite were tested under blast loading conditions. Based on the tabulated results, the highest deformation was observed for the foam sandwich under dynamic loading, as expected. The GFPP and GFVE composited showed minimum deformation among the structures and the performance of GFVE and GFE was better than GFPE composite. By considering the areal densities of the materials, composite samples exhibited lower deformations as compared to the monolithic materials. Aluminum, Dyneema and their combination (Al/Dyneema FML system) exhibited the highest plastic deformation as a result of blast effect.

CHAPTER 6

CONCLUSIONS

In this study, aluminum (Al) foams were incorporated into the fiber/metal laminates (FML) sandwich systems to improve the energy absorption behaviors of the composites. The microstructural characterization of as-received Al foams with various thicknesses (8, 20 and 30 mm) was completed. Compression, tension and shear properties of these foams were evaluated according to the corresponding standards. The FML systems including Al metal layer and glass fiber reinforced polypropylene (GFPP) composite were integrated with Al foams to manufacture the sandwich panels. Interfacial bonding of the components was performed with various integration techniques such as silane surface modification, PP-g-MA/PP based film introduction and the combination of silane surface modification with PP-g-MA/PP based film addition. Interfacial adhesion properties of Al/GFPP FML bonded with various treatments was evaluated. In addition, tension test was applied to both Al/GFPP FML system and its constituents individually. The Al sheet/Al foam sandwich specimens were also produced in order to compare the effect of GFPP composite layer on the mechanical performance of the sandwich structures. Both compression and flexural behavior of Al foam based sandwiches were investigated and their energy absorption capacities were determined.

In this thesis, blast responses of sandwich panels integrated with PP-g-MA/PP film introduction were predicted by the application of simulated blast test. The principle of this test allows us to simulate the blast loading effects on the panels. For the air blast analysis, the applied force shows dynamic characteristics, however, in the simulated blast test the sandwich panel was assumed as a single-degree of freedom mass spring system to include the dynamic effect. Based on this approach, the light-weight sandwich composites were subjected to compression loading with a very special test apparatus. Liquid soap filled rubber bladder below the sandwich panels simulated the characteristics of blast loading with simply supported boundary conditions under quasi-static compressive forces. Based on the pressure-time graphs of the blast waves depending on the explosive amount and stand-off distance, the blast characteristic time

(*T*) was determined. By the calculation of natural frequency (*ω*) of the panel and characteristic time parameters, the *f (Tω)* product was determined. The peak deflection (δ_{peak}) of the sandwich structure under blast loading was predicted by considering the dimensionless deflection ($\delta_{peak}/\delta_{static}$) - *f (Tω)* graph. The blast performance of different material systems such as monolithic metals, composite structures, FML systems and sandwich panels were evaluated under real air blast loading test.

Following conclusions can be made based on results of experimental and simulation results;

- Based on the compression test results of as-received Al foams, the specimens with higher elastic modulus usually exhibited higher collapse strength for each thickness set of foams. It was found that the foam thickness increase generally resulted in collapse strength decrease. As the thickness increases, the structural defect probably increases and the lower strength values of thicker foams are attributed to this. Similar trend was also observed for the tension and shear test results and 8 mm foams showed the highest strength values.

- The tension test results of Al/GFPP FML system and its components were determined. The GFPP composite showed maximum ultimate tensile strength (243.37 ±26.9 MPa) while the Al specimens exhibited the minimum strength (148.03±10.41). The same parameter was calculated as 169.9±2.36 MPa for the Al/GFPP hybrid system. The interfacial adhesion properties of the FML system were evaluated by the application of lap-shear and peel tests. The Al and GFPP was bonded with the combination of silane treatment and PP-g-MA/PP film introduction, however, the experimental results showed that this combination does not yield the desired high bending strength. This may be due to the insufficient bonding of silane groups with PP-g-MA/PP film.

- The compression test results of Al foam based sandwiches integrated with various techniques were determined. It was found that the core thickness increase generally led to the collapse strength decrease. Based on the experimental results that the sandwiches with higher elastic modulus showed higher collapse strength for each thickness set of foam based structures, as observed in monolithic Al foams.

- The flexural behaviors of Al foam based sandwiches integrated with various techniques were characterized by three point bending test. Skin thickness,

162

sample and span length parameters were selected as the same in order to compare the effect of core thickness on the flexural response of sandwich structures. The core thickness increase led to the increase of overall collapse load according to the experimental results. The sandwiches with 8 mm foams showed the highest core shear and face-sheet strength values when the core thickness increase caused to the decrease of the parameters referred above. The GFPP composite presence also promoted these values and the samples modified with silane coupling agent and consolidated with PP based film layer showed the highest performance among all the bonding types. The damage progression appeared to be steady and consistent with the increase of displacement and the core shear and debonding were found to be the major failure mechanisms observed during the flexural tests.

- Based on the energy absorption capacity curves of the sandwiches, the foam thickness increase led to the increase of energy absorption capabilities, as expected. Considering the compression test results, higher core thickness resulted in the decrease of specific absorbed energy (SAE) values for both monolithic Al foams and Al foam based sandwich samples. Also, the layered foam structures exhibited higher SAE values as compared to the Al foams.

- The responses of sandwich panels under simulated blast loading were evaluated. Core shear and core crushing were the main failure mechanisms observed in the panels after simulated blast tests. In spite of the debonding between the FML components during the initial stages of the test, the protection of the core was performed by GFPP composite. Therefore, debonding of FML is not considered as a structural failure mechanisms such as skin wrinkling or core shear. Independent of core thickness, all the samples exhibited similar type of deformation patterns. The back face of the samples exhibited dome-shaped deformation moving out from the center, changing a more quadrangular shape towards the supported edges. Both Al foam core and front face-sheet gained an inwardly curved shape. Along the panel plane the curvature extension was observed.

- The effective compliance (C_p) term of structures were determined by considering the central deflection (w_t) and compressive stress (σ_{fail}) values associated with core-crushing failure. The real central deflection values of the

samples were calculated by subtracting the compliance deflection values of individual bladder and sandwich system from the simulated blast test deflection values. Core material properties significantly affected the natural frequency of the structures. The maximum natural frequency was calculated as 3283.8 N/m.kg for 8 mm Al foam sandwich panel.

- The static sandwich panel deflection (δ_{static}) under maximum blast pressure was calculated by utilizing the C_p formulation. The numerical analyses performed by LS Dyna CONWEP module were used to determine the pressure-time $(P\text{-}t)$ history of the blast loading according to the explosive amount and stand-off distance parameters. Eight different TNT weights (12, 10, 8, 6, 4, 2, 1.37 and 1 kg) and six stand-off distances (0.2, 0.3, 0.4, 0.5, 0.6 and 0.7 m) were selected as representative cases for the determination of blast parameters. Both blast characteristic time (T) and maximum blast pressure (P^*) were obtained based on these analyses and the maximum blast pressure was calculated as 15.645 MPa for 12 kg TNT explosive. The increase of TNT amount led to the increase of blast pressure, static and peak deflection parameters, as expected.

- The peak deflection (δ_{peak}) of the panel under blast pressure was evaluated by considering the dynamic effect of the system, $f\,(T\omega)$. The dimensionless deflection $(\delta_{peak}/\delta_{static})$ versus $f\,(T\omega)$ was constructed by the differential equation governing to the system. As compared with the static and peak deflections of the panels for the same explosive weights, the 8 mm foam sandwich panel showed minimum values while the panel with 20 mm foam exhibited maximum deflections. The 20 mm and 30 mm Al foam sandwich panels showed the highest peak deflections of 241.049 mm and 219.720 mm for 12 kg TNT explosive, respectively. However, the deflection of 8 mm sandwich structure for the same weight was calculated as 181.546 mm. This situation is closely related with the natural frequency and compliance values of the sandwich structures.

- By considering the $P\text{-}t$ graphs of the blast loading according to the various stand-off distances, the maximum blast pressure was calculated as 14.89 MPa when the distance between the panel and the explosive center was 0.2 m. The increase of stand-off distance resulted in the decrease of blast pressure, as expected. The 20 mm Al foam panel exhibited highest peak deflection of 226.619 mm when

the stand-off distance was 0.2 m. The minimum deflection was calculated as 24.163 mm for 8 mm foam structure at 0.7 m stand-off distance.

- The failure index is the ratio of peak deflection of the panel (δ_{peak}) under blast pressure to the deflection of the same panel under quasi-static compression loading (w_{fail}). If the failure index is greater than or equal to one, the panel is predicted to fail. Otherwise, the panel is assumed to survive. Based on the test results, none of the panels can survive and this is attributed to the high blast pressure values used in the analysis. According to the simulated blast test results, the minimum pressure was 2.068 MPa and corresponding peak deflection was 24.163 mm with 4.09 failure index. Both TNT weights and stand-off distance parameters were selected based on the real threats; therefore the present results represent the dynamic deflections under real conditions.

- The variation of T and ω significantly influence the dynamic deflection of the structure. Both blast pressure and impulse parameters directly affect the characteristic time of the blast wave. Similarly, the parameters related with the natural frequency of the panel such as panel length/width ratio, core elastic modulus, skin thickness, core thickness, shear modulus of core and planar density indirectly operate the dynamic response of the system. Thus, the survivability of the panel highly dependent on these parameters mentioned above.

- The central deformation values of both monolithic metals and hybrid material systems under real air blast loading were evaluated. The glass fiber reinforced polypropylene (GFPP) and glass fiber reinforced vinyl-ester (GFVE) composited showed minimum deformation among the structures and the performance of GFVE and glass fiber reinforced epoxy (GFE) was better than glass fiber reinforced polyethylene (GFPE) composite. By considering the areal densities of the materials, composite samples exhibited lower deformations as compared to the monolithic materials. Aluminum, Dyneema and their combination (Al/Dyneema FML system) exhibited the highest plastic deformation as a result of blast effect.

REFERENCES

Abdullah, M. R., & Cantwell, W. J. (2006). The Impact resistance of polypropylene-based fibre/metal laminates. *Composites Science and Technology,* 66, 1682–1693.

Aboudzadeh, M. A., Mirabedini, S. M., & Atai, M. (2007). Effect of silane-based treatment on the adhesion strength of acrylic lacquers on the PP surfaces. *International Journal of Adhesion & Adhesives,* 27**,** 519-526.

Adams, R.D. (2005). *Adhesive Bonding: Science, Technology and Applications*. Cambridge Woodhead.

Andrews, E. W., & Moussa, N.A. (2009). Failure mode maps for composite sandwich panels subjected to air blast loading. *International Journal of Impact Engineering*, 36, 418-425.

Alulight Foams, *http://.alulight.com/en/al foam*, 2011.

Ashby, M. F., & Gibson, L. J. (2000). *Metal Foams: A Design Guide*. USA: Butterworth-Heinemann.

Wikipedia, Metal Foams, *http://ask.com/wiki/Metal_foam*, 2011.

Asundi, A., & Choi, Y. N. (1997). Fiber metal laminates: An advanced material for future aircraft. *Journal of Materials Processing Technolog,* 63, 384-394.

Baker, A. A., Rose, L. R. F., & Jones, R. (2002). *Advances in the Bonded Composite Repair of Metallic Aircraft Structure*. Boston: Elsevier.

Baker, W., Cox, P., Westine, P., Kulesz, J., & Strehlow, R. (1983). *Explosion Hazards and Evaluation*. New York: Elsevier.

Bastawros, A. F., Barth-Simith, H., & Evans, A. G. (2000). Experimental analysis of deformation mechanisms in a closed-cell aluminum alloy foam, *Journal of the Mechanics and Physics of Solids,* 48, 301-322.

Bikiaris, D., Matzinos, P., Larena, A., Flaris, V., & Panayiotou, C. (2000). Use of silane agents and (PP-g-MA) copolymer as adhesion promoters in glass fiber/polypropylene composites. Journal of Applied Polymer Science, 81, 701-709.

Briskham, P., & Smith, G. (2000). Cyclic stress durability testing of lap shear joints exposed to hot-wet conditions. International Journal of Adhesion & Adhesives, 20, 33-43.

Carrillo, J. G., & Cantwell, W. J. (2009). Mechanical properties of a novel fiber/metal laminate based on a polypropylene composite. *Mechanics of Materials*, 41, 828– 838.

Chen, C., Harte, A. N., & Fleck, N. A. (2001). The plastic collapse of sandwich beams with a metallic foam core. *International Journal of Mechanical Sciences.* 43, 1483-1506.

Chen, M. A., Li, H. Z., & Zhang, X. M. (2007). Improvement of shear strength of aluminium/polypropylene lap joints by grafting maleic-anhydride onto polypropylene. *International Journal of Adhesion & Adhesives,* 2**7,** 175–187.

Compston, P., & Cantwell, W. J. (2001). The interfacial fracture toughness of a polyamide-based fiber/metal laminate bonded with an ionomer resin. *Journal of Materials Science Letters,* 2**0**, 509– 512.

Compston, P., Styles, M., & Kalyanasundaram, S. (2005). A comparison of low energy impact behaviour in aluminium foam and polymer foam sandwich structures. *Sandwich Structures 7: Advancing with Sandwich Structures and Materials*.45, 643-652.

Corigliano, A., Rizzi, A., & Papa, E. (2000). Experimental characterization and numerical simulations of a syntactic-foam/glass-fibre composite sandwich. *Composite Science and Technology*, 60, 2169-2180.

Cortes, P., & Cantwell, W. J. (2004). The tensile and fatigue properties of carbon fiber reinforced PRRK-Titanium fiber/metal laminates. *Journal of Reinforced Plastics and Composites,* 23, 1615-1623.

Daniel, I.M., & Abot, J. L. (2000). Fabrication, testing and analysis of composite sandwich beams. *Composite Science and Technology*, 60, 2455-2463.

Demjen, Z. (1999). Possible coupling reactions of functional silanes and polypropylene. *Polymer,* 40, 1763–1773.

Demjen, Z., & Pukanszky, B. (1997). Effect of Surface Coverage of Silane treated CaCO, on the tensile properties of polypropylene composites. *Polymer Composites,* 18, 741-747.

Demjen, Z., Pukanszky, B., & Nagy, J. (1998). Evaluation of interfacial interaction in polypropylene/surface treated $CaCO_3$ composites. *Composite Part A,* 29A, 323-329.

Deqing, W., Weiwei, X., Xiangjun, M., & Ziyuan, S. (2005). Cell structure and compressive behavior of aluminum foam. *Journal of Material Science,* 40, 3475-3480.

Dolce, F., Meo, M., Wright, A., & French, M. (2010). Structural response of laminated composite plates to blast loads. *Plastics, Rubber and Composites*, 39**,** 180-188.

Element6composites, *http://element6composites.com/technical-cf.asp*, 2011.

Franz, T., Nurick, G. N., & Perry, M. J. (2002). Experimental investigation into the response of chopped strand mat glass fFiber laminates to blast loading. *International Journal of Impact Engineering*, 27, 639-667.

Green, M. D., Guild, F. J., & Adams R. D. (2002). Characterisation and comparison of industrially pre-treated homopolymer polypropylene, HF 135M. *International Journal of Adhesion & Adhesives,* 22, 81-90.

Gupta, N., 2003, Characterization of syntatic foams and their sandwich composites: modeling and experimental approach", *Phd, Louisiana State University*, USA.

Guruşcu, A., 2009. Joining and interfacial properties of aluminum/glass fibre reinforced polypropylene sandwich composites", MS.Thesis, *Graduate School of Engineering and Science, İzmir Institute of Technology.*

Hamada, H., Fujihara K., & Harada, A. (2000). The influence of sizing conditions on bending properties of continuous glass fiber reinforced polypropylene composites. *Composites: Part A,* 31, 979–990.

Hanssen, A. G., Enstock, L., & Langseth, M. (2002). Close range blast loading of aluminum foam panels. *International Journal of Impact Engineering,* 27, 593-618.

Harte, A.N., Fleck, N. A. & Ashby, M. F. (2000) Sandwich panel design using aluminum alloy foam. *Advanced Engineering Materials*, 4, 219-222.

Idris, M. I., Vodenitcharova, T., & Hoffman, M. (2009). Mechanical behavior and energy absorption of closed cell aluminum foam panels in uniaxial compression. *Materials Science and Engineering A,* 517, 37-45.

Koza, E., Leonowicza, M., Wojciechowski, S., & Simancik F. (2003).Compressive strength of aluminum foams. *Materials Letters,* 58, 132-135.

Kulkarni, R. R., Chawla, K. K., & Vaidya, E. (2008). Characterization of long fiber thermoplastic/metal laminates. *Journal of Material Science,* 43, 4391–4398.

Langdon, G. S., Cantwell, W. J., & Nurick, G. N. (2005). The blast response of novel thermoplastic based fiber-metal laminates-some preliminary results and observations. *Composite Science and Technology,* 65**,** 861-872.

Langdon, G. S., Cantwell, W. J., & Nurick, G. N. (2007). Localised blast loading of fibre/metal laminates with a polyamide matrix. *Composites: Part B*, 38, 902–913.

Langdon, G. S., Lemanski, S. L., Nurick, G. N., Simmons, M. C., Cantwell, W. L., Schleyer, G. K. (2000). Behavior of fiber-metal laminates subjected to localised blast loading: Part 1-experimental observations. *International Journal of Impact Engineering,* 34**,**1202-1222.

Langdon, G. S., Nurick, G. N., & Cantwell, W. J. (2008). The Response of fibre-metal laminate panels subjected to uniformly distributed blast loading. *European Journal of Mechanics A/Solids*, 27, 107–115.

Langdon, G. S., Nurick, G. N., Lemanski, S. L., Simmons, M. C., Cantwell, W. J., & Schleyer, G.K. (2006). Failure characterisation of blast loaded fibre/metal laminate panels based on aluminium and glass fibre reinforced polypropylene. *Composites Science and Technology*, 27, 103-106.

Langdon, G. S., Yuen, S. C. K., & Nurick, G. N. (2005). Experimental and numerical studies on the response of quadrangular stiffened plates. Part II: Localised blast loading. *International Journal of Impact Engineering,* 31**,** 85-111.

Lawcock, G., Ye, L., Mai, Y. W., Sun, C. T. (1997). The effect of adhesive bonding between aluminum and composite prepreg on the mechanical properties of carbon-fiber-reinforced metal laminates. *Composites Science and Technology*, 57, 35-45.

Lee, N., J. Jang J. (1997). The use of mixed coupling agent system to improve the performance of polypropylene-based composites reinforced with short-glass-fibre mat. *Composite Science and Technology,* 57,1559-1569.

Lemanski, S. L., Nurick, G. N., Langdon, G. S., Simmons, M. S., Cantwell, W. J., & Schleyer, G. K. (2006). Understanding the behaviour of fibre-metal laminates subjected to localised blast loading. *Composite Structures*, 76, 82–87.

Lim, T. S., Lee, C. S., & Lee, D. G. (2004). Failure modes of foam core sandwich beams under static and impact loads. *Journal of Composite Materials*, 38, 1639-1662.

McCormack, T. M., Miller, R., Kesler, O., & Gibson. L. J. (2001). Failure of sandwich beams with metallic foam cores". *Interntional Journal of Solids and Structures*, 38, 4901-4920.

McCullough, K. Y. G., Fleck, N. A., & Ashby, M. F. (1999). Uniaxial stress-strain behavior of aluminum alloy foams. *Acta Materials*, 47(8), 2323-2330.

McKnight, S. T., Gillespie, J. W., & Lambing, J. L. T. (1993). Durability evaluation of non-chromate-based aluminum surface treatments for bonding with polypropylene.

Menkes, S. B., & Opat, H. J. 1973. Tearing and shear failures in explosively loaded clamped beams. *Experimental Mechanics*, 13, 480-486.

Michelle, S., Fatt, H., Lin, C, Revilock., D. M., & Hopkins, D. A. (2003). Ballistic impact of GLARE fiber-metal laminates. *Composite Structures*, 61, 73-88.

Motz, C., & Pippan, R. (2001). Deformation behavior of closed-cell aluminum foams in tension. *Acta Materials*, 49, 2463-2470.

Mukundan, S. 2003. Structural design and analysis of lightweight composite sandwich space radiator panel", MSC, *Texas A&M University, USA*.

Jones, N. 1999. Recent studies on the dynamic plastic behaviour of structures, *Mechanics Review,* 42 (4), 95-115.

Ngo, T., Mendis, P., & Gupta, A. (2007). Blast loading and blast effects on structures: an Overview, *EJSE Special Issue*, 76-90.

Norlin, P. & S. Reuterlöv. (2002). The role of sandwich composites in turbine blades. *Reinforced Plastics*, 3, 32-34.

Nurick, G. N,. & Martin, J. B. (1998). Deformation of thin plates subjected to impulsive loading-A review, Part II: Experimental studies. *International Journal of Impact Engineering,* 8(2), 171.186.

Nurick, G. N., & Shave, G. C. (1996). The deformation and tearing of thin square plates subjected to impulsive loads-an experimental study. *International Journal of Impact Engineering,* 18(1), 99-116.

Nurick, G. N., Gelman, M. E., & Marshall, N. S. (1996). Tearing of blast loaded plates with clamped boundary conditions. *International Journal of Impact Engineering*, 18(7-8), 803-827.

Nurick, G. N., Langdon, G. S., Chi, Y., & Jacob, N. (2009). Behavior of sandwich panels subjected to intense air blast-Part 1: Experiments. *Composite Structures*, 91, 433-441.

Petrie E. (2000). *Handbook of Adhesives and Sealants.* New York: McGraw-Hill.

Radford, D. D., McShene, V. S., Desphande, V. S., & Fleck, N. A. (2006). The response of clamped sandwich plates with metallic foam cores to simulate blast loading. *International Journal of Solids and Structures,* 43, 2243-2259.

Reyes G., & Kang H. (2007). Mechanical behavior of lightweight thermoplastic fiber–metal laminates. *Journal of Materials Processing Technology,* 186, 84–290.

Reyes, G., & Cantwell, W. J. (2000). The mechanical properties of fiber/metal laminates based on glass fibre reinforced polypropylene. *Composites Science and Technology,* 60, 1085-1094.

Russo, A., & Zuccarello, B. (2007). Experimental and numerical evaluation of the mechanical behavior of GFRP sandwich panels. *Composite Structures*, 81, 575-586.

Sarzynski, M. D. (2003). Carbon foam characterization: sandwich flexure, tensile and shear Response", *MSC., Texas A&M University, USA.*

Sezgin, F. E. (2008). "Mechanical behaviour of honeycomb cored laminated Composite sandwich structures", MS.Thesis, *Graduate School of Engineering and Science, İzmir Institute of Technology*.

Sriram, R., & Vaidya, U. (2006). Blast impact response of aluminium foam sandwich composites. *Journal of Material Science, 41*, 4023-4039.

Steeves, C. A., & Fleck, N. A. (2004). Collapse mechanisms of sandwich beams with composite faces and a foam core, loaded in three-point bending. Part 2: Experimental investigation and numerical modeling. *International Journal of Mechanical Siences*, 46, 585-608.

Styles, M. 2008. Characterization of the flexural behavior of aluminum foam Composite sandwich structures", *Phd, FacultyAustralian National University, Australia.*

Styles, M., Compston, P., & Kalyanasundaram, S. (2007). The effect of core thickness on the flexural behavior of aluminium foam sandwich strucrures. *Composite Structures*, 80, 532-538.

Tekalur, S. A., Shivakumar, K., & Shukla, A. (2008). Mechanical behavior and damage evolution in e-glass vinylester and carbon composites subjected to static and blast loads. *Composites: Part B*, 39, 57-65.

Vinson, Jack R. (1999). *The Behavior of Sandwich Structures of Isotropic and Composite Materials*. Kluwer Academic Publishers.

Vogel, J., Keller, J., Sviridov, A., Feige, H. J., Kreyssig, K., Auersperg, J., & Plass, P. (2011). Characterization of strength behavior of aluminum foam sandwiches under static load. *Strain*, 47, e234-242.

Vogelesang, L. B., & Vlot, A. (2000). Development of fibre/metal laminates for advanced aerospace structures. *Journal of Materials Processing Technology, 103*, 1-5.

Zenkert, Dan. (1995). *An Introduction to Sandwich Construction*. Emas Publishing.

Zhu, F. (2008). Impulsive loading of sandwich panels with cellular core, *Phd, Swinburne University of Technology, Australia.*

VITA

Suat Bahar Baştürk
26-03-1980, İzmir/TURKEY

EXPERIENCES

2002-2005 : Research Assistant, Materials Science and Engineering Programme, İzmir Institute of Technology.

2005-2011 : Research Assistant, Department of Mechanical Engineering, İzmir Institute of Technology.

EDUCATION

Ph.D. (2005-2011) : Mechanical Engineering, İzmir Institute of Technology

M.Sc. (2002-2005) : Materials Science and Engineering, İzmir Institute of Technology

B.Sc (1998-2002) : Mechanical Engineering, Celal Bayar University

ACADEMIC FIELDS OF INTERESTS

Sandwich Composite Materials
Processings, mechanical testing, characterization and finite element modeling of sandwich composite materials.

Polymer Matrix Composite Materials
Processing, mechanical testing, characterization and finite element modeling of composite materials.

Fiber/Metal Laminates (FMLs)
Processing, mechanical testing, characterization and finite element modeling of FML systems with ANSYS.

Ceramic Matrix Composite Materials
Processing and characterization of HA whisker/HA powder composites.

SCI EXPANDED JOURNAL PAPERS

- Baştürk S.B., Tanoğlu M., "Mechanical and Energy Absorption Behavior of Metal/Polymer Layered Sandwich Structures", Journal of Reinforced Plastics and Composites (JRPC), 2011, DOI Numarası: 10.1177/0731684411421844

- Baştürk S.B., Tanoğlu M., "Development and Mechanical Behavior of FML/Aluminum Foam Sandwiches" Journal of Reinforced Plastics and Composites (JRPC) (Under Review).

- Baştürk S.B, Guruşcu A, Tanoğlu M, "Interfacial Properties of Metal/Polymer Layered Sandwich Structures" (in preparation).

- Baştürk S.B, Tanoğlu M, "Dynamic Behavior Analysis of FML/Aluminum Foam Sandwich Structures under Simulated Blast Test" (in preparation).